JOURNAL OF CAVE AND KARST STUDIES

April 2008
Volume 70, Number 1
ISSN 1090-6924
A Publication of the National Speleological Society

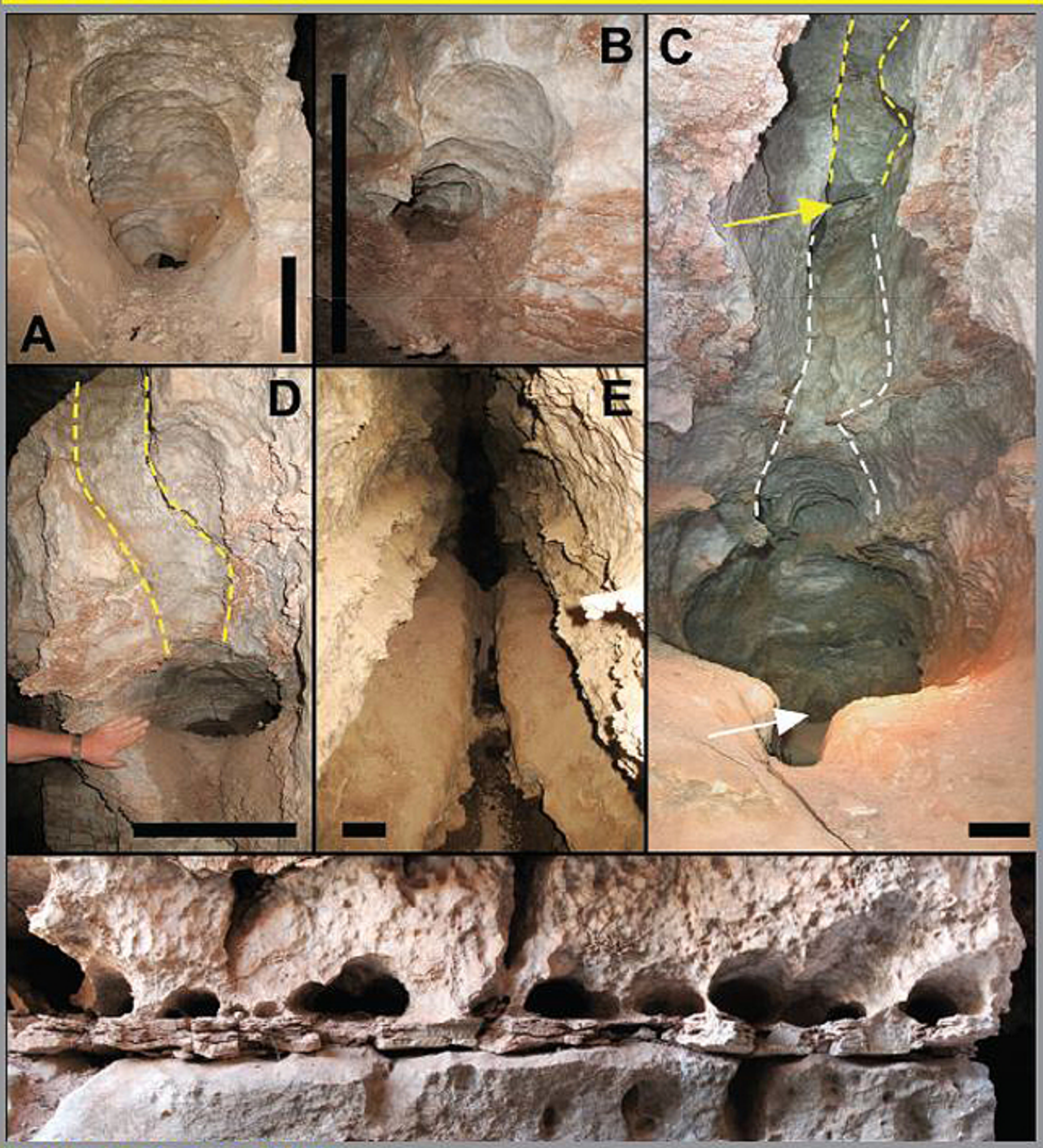

IN THIS ISSUE:

Published By
The National Speleological Society

The *Journal of Cave and Karst Studies* (ISSN 1090-6924, CPM Number #40065056) is a multi-disciplinary, refereed journal published three times a year by the National Speleological Society, 2813 Cave Avenue, Huntsville, Alabama 35810-4431 USA; Phone (256) 852-1300; Fax (256) 851-9241, email: nss@caves.org; World Wide Web: http://www.caves.org/pub/journal/. The annual subscription fee is $23 US, $44 US for 2 years, and $65 US for 3 years. Check the *Journal* website for international rates. Back issues and cumulative indices are available from the NSS office.
POSTMASTER: send address changes to the *Journal of Cave and Karst Studies*, 2813 Cave Avenue, Huntsville, Alabama 35810-4431 USA.

The *Journal of Cave and Karst Studies* is covered by the following ISI Thomson Services Science Citation Index Expanded, ISI Alerting Services, and Current Contents/ Physical, Chemical, and Earth Sciences.

Front cover: Feeder feature in Coffee Cave, New Mexico, see article by Stafford et.al. beginning on page 47.

EDITORIAL
Journal of Cave and Karst Studies Listing in the *Journal of Citation Report*: What Does it Mean?

MALCOLM S. FIELD
U.S. Environmental Protection Agency, National Center for Environmental Assessment (8623P), 1200 Pennsylvania Ave., N.W., Washington, D.C. 20460, USA, tel: (703) 347-8601, fax: (703) 347-8692, email: field.malcolm@epa.gov

THOMSON ISI LISTING

Several years ago the *Journal of Cave and Karst Studies* achieved a listing in the distinguished Thomson Institute for Scientific Information (ISI) which included Science Citation Index Expanded, ISI Alerting Services, and Current Contents Physical, Chemical, and Earth Sciences. A significant aspect of an ISI listing is a measure of the influence a listed journal has on scientific research. This is where the Thomson ISI *Journal Citation Reports* (JCR) becomes important.

JOURNAL CITATION REPORTS

The JCR currently covers more than 7,500 of the world's most highly cited, peer-reviewed journals in approximately 200 disciplines; the Science Edition covers over 5,900 leading international science journals from the Thomson Science Citation Index (SCI) database. It is the recognized authority for evaluating journals (Thomson, 2008).

After a journal is accepted for listing by Thomson ISI and has been in the system for a minimum of three years, the journal becomes eligible for an additional listing in the JCR, which is a multidisciplinary journal evaluation tool and is the only evaluation resource that provides statistical information based on citation data. By compiling cited references, a measure of research influence and impact at the journal level is obtained and illustrates the relationships between citing and cited journals (Thomson, 2005a).

The importance of a journal's influence on scientific research is evident by the importance university administrators and federal research institutions have placed on SCI data, which are now being used as a measure of faculty productivity and faculty productivity quality. It is no longer enough to publish in refereed journals, now they must be SCI journals as well. To avoid U.S. karst work going to foreign karst journals that are listed in the SCI, it is critical that the *Journal* continue to be published regularly and voluminously with high-quality peer-reviewed articles.

CITATION STATISTICS

The JCR lists the total cites, which represents the number of times that the *Journal* has been cited by all journals included in the product database within the current product year and the total number of articles published in a journal in the current product year. It also provides four basic statistics to measure a particular journal's influence. These statistics are impact factor, immediacy index, cited half-life, and citing half-life and are explained below (Thomson, 2005a,b).

IMPACT FACTOR

The impact factor is a measure of the frequency that an article in the *Journal* is cited in a particular year. It is calculated by dividing the number of current citations to items published in the two previous years by the total numbers of articles and reviews published in the two previous years.

IMMEDIACY INDEX

The immediacy index is a measure of how quickly the average article in the *Journal* is cited. It tells a user how often articles in a journal are cited within the same year. It is calculated by dividing the number of citations to articles published in a given year by the number of articles published in that year.

CITED HALF-LIFE AND CITING HALF-LIFE

The cited half-life represents the median age of *Journal* articles cited in the current JCR year. It is useful for evaluating the age range of the articles from the journal and may be used for making archiving and retention decisions. The citing half-life represents the median age of the articles cited by the *Journal* in the current JCR year. It is useful for evaluating the age of the majority of articles referenced by a journal.

JOURNAL OF CAVE AND KARST STUDIES STATISTICS

So how does the *Journal of Cave and Karst Studies* measure up? Figure 1 shows the JCR statistics for 2005 and 2006, the only two years available as of this writing. The *Journal* impact factor increased from 0.357 in 2005 to 0.576 in 2006 suggesting that the impact that articles have on scientific research increased in 2006. Unfortunately, the *Journal* immediacy index decreased from 0.235 in 2005 to 0.000 in 2006 suggesting articles published in 2006 were not being cited very quickly. However, a more realistic explanation may be the small number of articles actually published in that year. This statistic is somewhat misleading because it is dependent on the number of articles published in 2006, which the JCR accurately lists as nine

2005

Mark	Journal Title	ISSN	Total Cites	Impact Factor	Immediacy Index	Articles	Cited Half-Life	Citing Half-Life
☐	J CAVE KARST STUD	1090-6924	77	0.352	0.235	17		> 10.0

2006

Mark	Journal Title	ISSN	Total Cites	Impact Factor	Immediacy Index	Articles	Cited Half-Life	Citing Half-Life
☐	J CAVE KARST STUD	1090-6924	103	0.576	0.000	9	6.3	9.2

Figure 1. *Journal Citation Reports* statistics for the *Journal of Cave and Karst Studies* for 2005 and 2006.

because the December 2006 issue came out in 2007. Had the December 2006 issue been included in the counting, a total of 16 articles would have been listed. In addition, because the *Journal* has only been included in the Thomson ISI database for a short time, categories such as the immediacy index are going to lag for a while.

The *Journal* cited half-life increased from no data in 2005 to 6.3 yr in 2006 which suggests that there were no published articles in the *Journal* cited in 2005 but some cited works in 2006. The *Journal* citing half-life decreased from >10.0 yr in to 2005 to 9.2 yr in 2006 suggesting that the number of articles cited in the *Journal* decreased from 2005 to 2006. By comparison, the only other karst journal in the Thomson ISI database had no listing for 2006.

When the JCR statistics for the *Journal of Cave and Karst Studies* are compared with other journals (e.g., *Science*) it doesn't appear to rate very well. However, other journals have been included in JCR for a much longer time than the *Journal of Cave and Karst Studies* and are not nearly so specialized. The extremely parochial nature of the *Journal of Cave and Karst Studies* limits the number of papers that will get submitted for publication which then limits the number of papers that get cited.

Overall, the *Journal* is on an upswing as evidenced by the improved 2006 *Journal* impact factor over the 2005 *Journal* impact factor[1]. As the *Journal* continues to expand because more and more papers are being submitted, it is very probable that the *Journal* statistics listed in the JCR will also continue to increase. For example, for 2007 it is expected that ~20 articles to be listed in the JCR because it includes the December 2006 issue, but not the December 2007 issue due to the lateness associated with these two issues[2]. While 30+ published articles per year in the *Journal* have not been common in the past, it is very likely to become common in the not too distant future. This increase in published articles in the *Journal* will almost definitely lead to higher ratings for the *Journal*.

REFERENCES

Thomson, 2005a, Journal Citation Reports on the Web v. 4.0: Thomson ISI, URL http://scientific.thomson.com/media/scpdf/jcr4_sem_0305.pdf, [accessed January 10, 2008].

Thomson, 2005b, Journal Citation Reports Tutorial (v. 4.0): Thomson ISI, URL http://scientific.thomson.com/tutorials/jcr4/jcr4tut6.html, [accessed January 14, 2008].

Thomson, 2008, Journal Citation Reports on the Web v. 2.0: Thomson ISI, URL http://scientific.thomson.com/products/jcr/, [accessed January 10, 2008].

[1] The JCR report released just prior to press of this issue reports an impact factor for the *Journal of Cave and Karst Studies* = 1.000.

[2] Note that we expect to be returning to our publishing schedule shortly.

J. Mulec, G. Kosi, and D. Vrhovšek – Characterization of cave aerophytic algal communities and effects of irradiance levels on production of pigments. *Journal of Cave and Karst Studies,* v. 70, no. 1, p. 3–12.

CHARACTERIZATION OF CAVE AEROPHYTIC ALGAL COMMUNITIES AND EFFECTS OF IRRADIANCE LEVELS ON PRODUCTION OF PIGMENTS

JANEZ MULEC*[1], GORAZD KOSI[2], AND DANIJEL VRHOVŠEK[3]

Abstract: Aerophytic algae grow on various substrata under favourable ecological conditions. In the illuminated parts of caves, where relative humidity reaches 100%, they colonize sediments, rocky surfaces, and artificial materials. An aerophytic algal community from the cave entrance is composed almost exclusively of cyanobacteria, in contrast to lampenflora where green algae become more dominant. In the later stage of species succession in the lampenflora community, cyanobacteria are more abundant and thus community structure becomes more similar to the community from the cave entrance. Absence of correlation between photon flux density and chlorophyll *a* concentration indicates that substratum characteristics at the micro level notably influence algal growth. Chl *a* concentration per surface unit in the case of the epilithic algae from the cave entrance is lower (max. 1.71 μg cm^{-2}) compared to that for the lampenflora algae (max. 2.44 μg cm^{-2}). At cave temperatures, the light saturation point is quickly reached. At 9.0 °C and frequent low photon flux densities in a cave entrance and around lamps in show caves, biosynthesis of accessory photosynthetic pigments for two typical cave aerophytic organisms, cyanobacterium *Chroococcus minutus* and green alga *Chlorella* sp., is considerably elevated.

INTRODUCTION

Caves are one of the extreme environments generally characterized by low nutrient input (Pedersen, 2000). Low nutrient input is a limiting factor for many groups of organisms, although some species, like algae, find this environment still suitable for colonization and growth. In caves, algae can be found in bodies of water (Kuehn et al., 1992; Sanchez et al., 2002) and aerophytic habitats (Golubić, 1967; Dobat, 1970). In caves, many surfaces serve for algal colonization including: sediments, rocky surfaces and artificial material. We recently published the composition of algal communities from another two interesting cave aerophytic habitats, from stromatolitic stalagmites and from stalactites, where growth is enhanced by carbonate deposition promoted by cyanobacteria towards sun light (Mulec et al., 2007). Development of aerophytic vegetation is influenced by light, temperature, high relative humidity (reaching 100%) and/or seeping water, and substratum characteristics (Golubić, 1967; Martinčič et al., 1981; Chang and Chang-Schneider, 1991). Aerophytic algae are easily observed in the cave entrance illuminated by direct or indirect sunlight and, in show caves equipped with artificial illumination, as a part of a lampenflora community around lamps (Mulec, 2005). Several approaches have been tested to control growth of this alien lampenflora vegetation (Olson, 2006). Illuminated spots in a generally nutrient-poor cave environment are quickly colonized by aerophytic algae. The large amount of energy and consequent biomass introduced into the cave ecosystem indirectly influence cave fauna, as well as affecting the survival and transport of organisms entering the cave, either actively or passively. Higher nutrient input enables new comers to be more competitive in the cave environment than specialized troglomorphic organisms. Consequently, obligate cave-dwelling organisms are threatened and may become extirpated or extinct without restoration of previous natural conditions (Pipan, 2005).

Caves are generally not considered to be isolated habitats; however, there is an example of the spatially isolated Movile cave where the existence of complex animal communities is based only on bacterial chemolithotrophy (Sarbu et al., 1996; Kinkle and Kane, 2000). Three key modes of transport of viable algal propagules into the karst underground can be distinguished: air currents, water flow, and introduction by animals and humans (Dobat, 1970). The existence of lampenflora deep in show caves proves the efficient transport of propagules from sources above caves, which is more or less constant. Species composition of aerophytic algal communities from cave entrances differs compared to lampenflora. In illuminated cave entrances cyanobacteria prevail (Palik, 1964a; Golubić, 1967; Buczkó and Rajczy, 1989; Vinogradova et al., 1995, 1998; Asencio and Aboal, 2000). Vinogradova et al. (1998) established that light is a key factor that influences zonation of cyanobacteria in the cave entrance.

[1] Karst Research Institute, Scientific Research Centre of the Slovenian Academy of Sciences and Arts, Titov trg 2, SI-6230 Postojna, SLOVENIA, janez.mulec@guest.arnes.si
[2] National Institute of Biology, Večna pot 111, SI-1000 Ljubljana, SLOVENIA, gorazd.kosi@nib.si
[3] LIMNOS, Podlimbarskega 31, SI-1000 Ljubljana, SLOVENIA, dani@limnos.si

Table 1. Location and characterization of the caves and mines in this study.

Cave / mine	Municipality	Altitude (m)	Length (m)	Depth (m)	Orientation of cave entrance	Lithology
Postojnska jama	Postojna	529	19555	115	NW	Cretaceous limestones
Kostanjeviška jama	Krško	170	1726	47	S	Cretaceous limestones and dolomites
Pekel pri Zalogu	Žalec	314	1159	40	NE	Triassic limestones and dolomites
Pivka jama cave	Postojna	540	794	77	E	Cretaceous limestones
Lead and zinc mine Mežica	Ravne na Koroškem	500	3500	300	S	Carnian limestones, Triassic dolomites, shales
Mercury mine Idrija	Idrija	330	1000	22	S	Permocarbonian shales and dolomites
Škocjanske jame	Sežana	425	5800	250	NW	Cretaceous and Paleogene limestones
Županova jama	Grosuplje	468	682	70	NW	Jurassic limestones

In caves, new algal species were identified (Jones, 1964; Palik, 1964b; Van Landingham, 1966a,b; Sant'Anna et al., 1991; Hernandéz-Mariné and Canals, 1994). Beyond taxonomy, ecophysiological studies on cave algae are rare, although caves represent an almost ideal natural laboratory for algological studies with practically constant ecological parameters. The purpose of this study was to ascertain how different irradiance levels influence quantity and quality change in the algal community, how low irradiances affects the ratio of photosynthetic pigments in algae, and to compare floristic analysis from the same caves conducted 22 years ago by Martinčič et al. (1981).

Study Area

Six caves (Postojnska jama, Kostanjeviška jama, Pekel pri Zalogu, Pivka jama, Škocjanske jame, Županova jama) and two mines (Idrija, Mežica) were studied in the karst region of Slovenia (Table 1). Škocjanske jame is, due to its importance from the speleological and ecological point of view, listed in the UNESCO World heritage list and as important underground wetlands (Ramsar convention). Sampling was performed in the summer of 2003. Where lampenflora were sampled in show caves, lamps are periodically turned on due to tourist visits or maintenance of the tourist infrastructure. Only in the Mežica lead and zinc mine are lamps on 24 hours due to the constant monitoring of underground water flow. Sampling sites for lampenflora were selected randomly. Sampling of aerophytic algae in the cave entrance of Škocjanske jame was performed in one of the entrances named Schmidlova dvorana, which is a cave space of huge dimensions, 22 m wide, 25 m high and 100 m deep. This large shady area in the cave mouth is directly illuminated by sunlight in the morning. Due to the orientation and position of the cave entrance, in the early spring and late autumn, an even wider area is directly illuminated. Growth experiments were carried out in the part of Postojnska jama that is not open to the public.

Materials and Methods

Samples for floristic analysis were taken from eight caves and mines. Prior to taking specimens photon flux density at the sites was measured using a LICOR LI−1000 DataLogger (USA). In the cave entrance several measurements of photon irradiance were made; the most representative ones were used for statistical analysis. We inoculated Jaworski medium (Warren et al., 1997) at the sampling sites using sterile scrapes of the algal mat. In the case of lampenflora, if confluent growth was observed around a lamp, up to seven samples were taken around the same lamp at different distances to observe differences in the community composition. Mixed and pure algal cultures were isolated in Jaworski liquid and on solid 1% Jaworski agar media. Jaworski medium is frequently used in algology as it supports growth a variety of groups of algae. Cyanobacteria were selectively isolated when the medium was supplemented with 100 $\mu g\ ml^{-1}$ of DCMU (diuron, N-3, 4-dichlorophenyl-N′-dimetil urea). Cultivation conditions were: 20 °C, 8:16 light/dark period with a photon flux density of 100 $\mu mol\ m^{-2}\ s^{-1}$ for several weeks. Cultures were regularly screened using a magnifying glass and light microscope (Nikon Eclipse TE300). Floristic data obtained from culture material were supplemented with microscopic data of the same field material fixed with 4% formalin solution. Diatom samples were processed and identified as described by Clesceri et al. (1998). Sputtered gold specimens were screened using a SEM microscope (JSM-840, JEOL, USA). Several keys and articles were used to identify algal species: Abdelahad (1985, 1989), Asencio and Aboal (2000), Couté (1982), Ettl and Gärtner (1995), Garbacki et al. (1999), Geitler (1932), Golubić (1967), Hindak (1996), Hoffmann (1986), Komárek and

Anagnostidis (2000, 2005), Krammer and Lange-Bertalot (1986, 1988, 1991), Lemmermann et al. (1915), Sulek (1969).

Cyanobacterium *Chroococcus minutus* and green alga *Chlorella* sp., isolated in pure culture from the lampenflora community, which frequently inhabit aerophytic habitats including the cave entrance, were used in growth experiments in that part of Postojnska jama that is not open to the public (9.0 °C, RH 95%). Cultures in liquid Jaworski medium were cultivated in triplicate using a photon flux gradient of 100, 50, 20, 10, 5, 2.5 and 0 μmol m^{-2} s^{-1} with the same lighting period (8:16 light/dark period) and regular mixed. The inoculum was 10^4 cells per ml. After 25 days of incubation, cells were counted, harvested, and the concentration of photosynthetic pigments established: Chl *a*, Chl *b* and carotenoids for *Chlorella* sp. after Wetzel and Likens (1995) and phycocyanin after Lee et al., (1994) and Chl *a* after Vollenweider et al. (1974) for *C. minutus*.

Sites for ascertainment of Chl *a* levels of epilithic cave algae were carefully selected. Known flat rocky surfaces with minor substratum irregularities with confluent overgrowth of algae were scraped off with an alcohol flame sterilized pocket knife and collected in a test tube. The concentration of Chl *a* was established using the procedure described by Vollenweider et al. (1974). At each site photon flux density was measured.

Results

In the aerophytic algal community from the cave entrance of Škocjanske jame cyanobacteria prevailed (69% of identified taxa) while Chlorophyta (19%) and Chrysophyta (12%) represented the minor part of the community (Table 2). Samples were also taken at the same sites to determine Chl *a* levels of epilithic algae, which ranged from 0.14 to 1.71 μg cm^{-2} (Table 2). There is no correlation ($r = 0.04$, $p > 0.05$) between irradiance and Chl *a* as well as between the number of algal taxa and Chl *a* concentration ($r = 0.19$, $p > 0.05$). Taking into account only the cyanobacterial component, we established that with increasing irradiance the number of coccoid cyanobacteria lowers ($r = -0.42$, $p < 0.05$).

Lampenflora can be observed in the immediate vicinity of artificial lighting. In Slovenian caves zonation of vegetation is not observed. We identified 60 algal taxa in the lampenflora community from eight show caves (Table 3). Cyanobacteria were the most abundant (47%) followed by Chlorophyta (30%) and Chrysophyta (23%).

In Pekel pri Zalogu cave, samples were taken around one selected lamp with an illumination gradient and confluent phototrophic growth to determine Chl *a* levels of epilithic algae. Concentrations ranged from 0.57 to 2.45 μg cm^{-2} (data not shown). As in the case of aerophtytic algae from Schmidlova dvorana, lampenflora showed no correlation between irradiance and Chl *a* levels ($r = -0.19$ $p > 0.05$).

Irradiances used in our growth experiment were similar to the measurements of irradiance experienced in caves around lamps and in the shady parts of cave entrances. From Figure 1, it is evident that in cyanobacterium *C. minutus* the concentration of Chl *a* increased up to a photon flux density of 50 μmol m^{-2} s^{-1} and at 100 μmol m^{-2} s^{-1} a slight decline is observed. Concentration of phycocyanin at low photon flux densities (e.g., 2.5, 5 and 10 μmol m^{-2} s^{-1}) were higher compared to 20 and 50 μmol m^{-2} s^{-1}. Kirk (1983) experienced a similar effect that at low irradiance the ratio of biliproteins to Chl *a* increases. At the highest photon flux density of 100 μmol m^{-2} s^{-1} phycocyanin concentration elevated a little more. With green alga *Chlorella* sp. at low photon flux densities (e.g., 2.5, 5 and 10 μmol m^{-2} s^{-1}) the concentration of accessory photosynthetic pigments is also elevated (Fig. 2). By gradually increasing from 20 to 100 μmol m^{-2} s^{-1}, the molar ratio of accessory pigments (i.e., Chl *b* and carotenoids) was lowered in favour of Chl *a*. At 100 μmol m^{-2} s^{-1} the ratio of Chl *a* vs. Chl *b* was 3:1, which is typical for green algae (Kirk, 1983).

Discussion

Algae frequently grow in the illuminated parts of caves. In caves, two distinct aerophytic microhabitats colonized by epilithic algae can be distinguished: (1) cave entrances illuminated by sunlight and (2) areas around lamps in show caves and mines. Cyanobacteria prevail in the algal community from cave entrances. They can colonize into the deepest parts of the cave entrance where biodiversity of phototrophic organisms is the lowest (Vinogradova et al., 1998). Many of the identified algae from poorly illuminated cave environments cannot be considered typical cave species (Hoffmann, 2002), although the presence of some of them (e.g., *Pediastrum boryanum*, Table 2) indicates not only efficient transport but also the existence of a suitable niche in water droplets for non-aerophytic algae.

As reported in other papers, the lampenflora community shows lower biodiversity compared to the algae from cave entrances. In 1981 Martinčič et al. published a floristic analysis of lampenflora from six Slovenian show caves: Črna jama, jama Pekel pri Zalogu, Pivka jama, Postojnska jama, Škocjanske jame and Taborska jama (now called Županova jama) where they identified a total of 44 algal species, with the highest portion of cyanobacteria. Comparing these results and the results of the present study 20 years later, we did not observe any major difference in the composition of the lampenflora community. The green alga *Trentenpohlia aurea* appears with the highest frequency in Slovenian show caves.

The key question here would be: What is species succession like in the case of lampenflora? Although cyanobacteria are the most adaptable phototrophs under stressed conditions, in microhabitats with less environmental stress, like illuminated spots around lamps, they are

Table 2. Composition of algal community with regard to concentrations of Chl *a* and photosynthetic active radiation at sampling sites in the Schmidlova dvorana cave entrance from Škocjanske jame.

	Sampling site																					
Chl *a* (µg cm^{-2})	0.14	0.20	0.49	0.56	0.94	0.61	0.37	1.71	1.34	0.54	0.51	0.93	0.37	0.32	0.57	0.14	0.95	0.81	1.87	0.93	0.21	0.50
Species\ Photosynthetic active radiation (µmol m^{-2} s^{-1})	0.30	0.27	0.28	0.24	0.21	0.31	0.11	0.90	0.10	0.80	0.40	0.70	0.20	0.06	0.57	0.45	0.51	0.48	0.11	0.75	0.41	1.96
PROKARYOTA																						
CYANOPHYTA																						
Aphanocapsa sp. Nägeli	·	·	·	·	·	·	·	+	+	+	·	·	+	·	·	·	·	+	·	·	·	·
Aphanocapsa muscicola (Meneghini) Wille	·	·	+	+	+	+	+	+	+	+	·	·	+	+	+	+	+	+	+	+	+	+
Aphanothece castagnei (Brébisson) Rabenhorst	·	·	·	+	·	·	·	·	·	·	·	·	+	·	·	·	·	·	·	·	·	·
Chondrocystis dermochroa (Nägeli) Komárek et Anagnostidis	·	·	·	·	·	+	·	·	·	·	·	·	·	·	+	+	+	·	·	+	·	·
Chroococcus sp. Nägeli	·	·	·	·	·	·	·	·	·	·	·	·	·	·	·	·	·	·	·	+	+	·
Chroococcus helveticus Nägeli	·	·	·	·	·	·	·	·	·	·	·	·	·	·	·	·	+	+	·	·	·	·
Chroococcus lithophilus Ercegović	·	·	·	·	·	·	·	·	·	·	·	·	·	·	·	·	·	+	+	·	·	·
Chroococcus minutus (Kützing) Nägeli	·	·	·	·	·	·	·	·	·	·	·	·	·	·	·	·	·	+	·	·	·	·
Chroococcus montanus Hansgirg	·	·	·	·	·	·	·	·	·	·	·	·	·	·	·	·	·	+	·	·	·	·
Chroococcus varius A. Braun in Rabenhorst	·	·	·	+	·	·	·	·	·	·	·	·	·	·	·	·	·	·	·	·	·	·
Chroococcus turgidus (Kützing) Nägeli	·	·	·	·	·	·	·	·	·	·	·	·	·	·	·	·	·	+	·	·	·	·
Cyanothece aeruginosa (Nägeli) Komárek	·	·	·	+	·	·	·	+	·	+	·	+	·	·	·	·	·	·	·	·	·	·
Geitleria calcarea Friedmann	·	·	+	+	+	·	·	+	·	+	+	·	+	+	·	·	·	+	+	·	·	·
Gloeocapsa sp. Kützing	·	·	·	·	·	+	·	·	·	·	·	·	·	·	+	·	·	·	·	+	·	·
Gloeocapsa aeruginosa Kützing	·	·	·	·	·	+	·	·	·	·	·	·	·	·	+	·	·	·	+	+	·	+
Gloeocapsa atrata Kützing	·	·	·	·	·	+	·	·	·	·	·	·	+	·	·	·	+	·	+	·	+	·
Gloeocapsa kuetzigiana Nägeli	·	·	+	·	·	·	·	·	·	·	·	·	·	·	·	·	·	+	·	·	·	·
Gloeocapsa rupestris Kützing	·	·	·	·	·	·	·	·	·	·	·	·	·	·	·	·	·	+	·	·	+	·
Gloeocapsopsis sp. Geitler ex Komárek	·	+	+	·	·	·	·	·	·	·	·	·	·	·	·	·	·	·	·	·	+	·
Gloeocapsopsis pleurocapsoides (Nováček) Komárek et Anagnostidis	+	·	·	·	·	·	+	·	·	·	·	+	·	·	·	·	·	·	·	·	·	·
Gloeothece palea (Kützing) Rabenhorst	·	·	·	·	·	·	·	·	·	·	·	·	·	·	·	·	·	+	+	+	·	·
Gloeothece rupestris (Lyngbye) Bornet, in Wittrock et Nordstedt	·	·	·	·	·	·	·	·	·	·	·	·	·	·	+	·	·	+	·	·	·	·
Leptolyngbya foveolarum (Rabenhorst ex Gomont) Anagnostidis et Komárek	·	·	·	·	·	·	·	·	·	·	·	·	·	·	·	·	·	·	·	+	+	·
Leptolyngbya fragilis (Gomont) Anagnostidis et Komárek	·	·	·	·	+	+	·	+	·	+	+	+	·	+	+	·	+	+	+	·	·	·
Leptolyngbya gracillima (Zopf ex Hansgirg) Anagnostidis et Komárek	·	·	·	·	·	·	·	·	·	·	·	·	·	·	+	·	·	·	·	·	·	·
Leptolyngbya perelegans (Lemmermann) Anagnostidis et Komárek	·	·	·	·	·	·	·	·	·	·	·	·	·	·	·	·	·	·	·	+	+	·
Leptolyngbya schmidlei (Limanowska) Anagnostidis et Komárek	·	·	·	·	·	·	·	·	·	·	·	·	·	·	+	·	·	·	·	·	·	·
Leptolyngbya tenuis (Gomont) Anagnostidis et Komárek	·	·	·	·	·	·	·	·	·	·	·	·	·	·	·	·	·	·	·	·	+	·
Lyngbya sp. C. Agardh ex Gomont	+	·	+	+	·	·	+	+	+	+	+	+	+	+	·	+	+	+	+	+	+	+
Lyngbya attenuata Fritsch	·	·	·	+	·	·	·	·	·	·	·	·	·	·	·	·	·	·	·	·	·	·
Nostoc minutum Desmaz ex Born	·	·	·	·	·	·	·	·	·	·	·	·	·	·	·	·	·	·	·	+	·	·
Oscillatoria sp. Vaucher ex Gomont	·	·	·	·	·	·	·	·	·	·	+	·	+	+	·	·	·	+	·	·	·	+
Oscillatoria subbrevis Schmidle	·	·	·	+	·	·	·	·	+	·	·	·	·	·	·	·	·	·	·	·	·	·
Phormidium inundatum Kützing ex Gomont	·	·	·	+	·	·	·	·	·	+	·	·	·	·	·	·	·	·	·	·	·	·

Table 2. Continued.

Species\ Photosynthetic active radiation (µmol m^{-2} s^{-1})	Sampling site																					
Chl *a* (µg cm^{-2})	0.14	0.20	0.49	0.56	0.94	0.61	0.37	1.71	1.34	0.54	0.51	0.93	0.37	0.32	0.57	0.14	0.95	0.81	1.87	0.93	0.21	0.50
	0.30	0.27	0.28	0.24	0.21	0.31	0.11	0.90	0.10	0.80	0.40	0.70	0.20	0.06	0.57	0.45	0.51	0.48	0.11	0.75	0.41	1.96
Planktolyngbya limnetica (Lemmermann) Komárková-Legnerová et Cronberg	·	+	+	·	·	·	·	·	·	·	·	·	+	·	+	·	·	·	·	·	·	+
Plectonema sp. Thuret ex Gomont	·	·	·	·	·	·	·	·	·	·	·	·	·	·	+	·	+	·	·	·	+	·
Pseudophormidium tenue (Thuret ex Gomont) Anagnostidis et Komárek	·	·	·	·	·	·	·	·	·	·	·	·	·	·	·	·	·	·	·	·	·	+
Scytonema sp. Agardh	·	·	·	·	·	·	·	·	·	·	·	·	·	·	·	·	·	+	+	·	·	·
Scytonema hofmanni Agardh	·	·	·	·	·	·	·	·	·	·	·	·	·	·	·	·	+	·	·	·	·	·
Synechococcus elongatus Nägeli	·	·	·	·	·	·	·	·	·	·	·	·	·	·	·	·	+	·	·	·	·	·
Synechocystis sp. Sauvageau	+	+	·	+	+	+	+	+	+	·	+	·	+	·	·	·	·	·	+	·	·	·
EUKARYOTA																						
CHRYSOPHYTA																						
Eunotia argus (Ehrenberg) Kützing	·	·	·	·	·	·	·	·	·	·	·	·	·	·	·	·	·	+	·	·	·	·
Cymbella ehrenbergii Kützing	·	·	·	·	·	·	·	·	·	·	·	·	·	·	·	+	·	·	·	·	·	·
Navicula sp. Bory	·	·	·	·	·	·	·	·	·	·	·	·	·	·	·	+	·	·	·	·	+	·
Navicula contenta var. *biceps* (Arnott, Grunow in Van Heurck) Cleve	·	·	·	·	·	·	·	·	·	·	·	·	·	·	+	+	·	·	+	+	·	+
Navicula gallica var. *perpusilla* (Grun) Lange-Bertalot	·	·	·	·	·	·	·	·	·	·	·	·	·	·	+	·	·	·	·	·	·	·
Navicula mutica Kützing	+	·	·	·	·	·	·	·	·	·	·	·	·	·	·	+	·	·	·	·	·	·
Navicula stroemii Hustedt	·	·	·	·	·	·	·	·	·	·	·	·	·	·	·	·	+	·	·	·	·	·
CHLOROPHYTA																						
Chlorella sp. Beijerinck	·	+	·	·	·	+	+	·	·	·	·	·	+	·	·	+	·	+	+	+	·	+
Chlorosarcina sp. Gerneck	·	·	·	·	·	·	·	·	·	·	·	·	·	·	+	·	·	·	·	·	·	·
Gloeocystis polydermatica (Kützing) Hindák	·	·	·	·	·	·	·	·	·	·	·	·	·	·	·	·	·	·	+	·	·	·
Klebsormidium flaccidum Silva, Mattox et Blackwell	·	·	·	·	·	·	·	·	·	·	·	·	·	·	·	·	·	·	·	·	+	+
Muriella sp. J.B. Petersen	·	·	·	·	·	·	·	·	·	·	·	·	·	·	·	·	+	·	·	·	·	·
Pediastrum boryanum (Turpin) Meneghini	·	·	+	·	·	·	·	·	·	+	+	·	·	·	·	+	·	+	+	·	+	·
Pleurococcus sp. Meneghini	·	·	·	·	·	·	·	·	·	·	·	·	·	·	·	·	·	·	·	·	·	+
Scenedesmus sp. Meyen	·	·	·	·	·	·	·	·	·	·	·	·	·	·	·	·	·	·	·	·	·	+
Scenedesmus bijugatus (Turpin) Meneghini	·	·	·	·	·	·	·	·	·	·	·	·	·	·	+	·	·	·	·	·	·	·
Stichococcus bacillaris Nägeli	·	·	·	·	·	+	+	·	·	·	+	·	+	·	+	+	·	·	·	+	+	·
Trentepohlia aurea Martius	·	+	·	·	·	·	·	·	·	·	·	·	·	·	·	·	+	+	+	·	·	·

Table 3. Species composition of the lampenflora algae from 8 show caves and mines.

Species	Cave/Mine							
	Id	Ko	Me	Pe	Pi	Po	Šk	Žu
PROKARYOTA								
Cyanophyta								
Aphanocapsa biformis A. Brown in Rabenhorst	·	·	+	+	+	·	·	·
Aphanocapsa fusco-lutea Hansgirg	·	·	·	·	·	·	+	·
Aphanocapsa muscicola (Meneghini) Wille	+	+	+	+	+	+	+	+
Aphanocapsa parietina Nägeli	·	·	·	+	·	·	·	·
Chondrocystis dermochroa (Nägeli) Komárek et Anagnostidis	+	·	+	+	·	·	·	·
Chroococcus lithophilus Ercegović	·	·	·	·	·	·	+	·
Chroococcus minutus (Kützing) Nägeli	+	·	+	·	·	·	+	·
Chroococcus schizodermaticus W.West	·	·	·	·	·	·	+	·
Chroococcus varius A. Braun in Rabehorst	·	·	+	·	·	·	·	·
Chroococcus westii (W.West) Boye-Petersen	·	·	·	+	·	·	+	·
Gloeocapsa sp. Kützing	·	+	·	·	·	·	+	·
Gloeocapsa atrata Kützing	·	·	·	·	·	+	+	·
Gloeocapsa bituminosa (Bory) Kützing	·	·	·	·	·	·	+	·
Gloeocapsa punctata Nägeli	·	·	·	·	·	+	·	·
Gloeocapsa rupestris Kützing	·	+	·	·	·	·	·	·
Leptolyngbya foveolarum (Rabenhorst ex Gomont) Anagnostidis et Komárek	·	+	·	·	·	·	·	·
Leptolyngbya fragilis (Gomont) Anagnostidis et Komárek	·	·	·	+	·	+	·	·
Leptolyngbya perelegans (Lemmermann) Anagnostidis et Komárek	·	·	·	·	·	+	·	·
Leptolyngbya scytonemicola (Gardner) Anagnostidis et Komárek	·	·	·	+	·	·	·	·
Lyngbya sp. C. Agardh ex Gomont	+	·	+	+	·	+	+	·
Oscillatoria sp. Vaucher ex Gomont	·	·	·	+	·	·	·	·
Planktolyngbya bipunctata (Lemmermann) Anagnostidis et Komárek	·	·	·	·	·	+	·	·
Planktolyngbya limnetica (Lemmermann) Komárková-Legnerová et Cronberg	·	·	·	·	+	·	·	·
Plectonema cf. *puteale* Hansgirg	·	·	·	+	·	+	+	·
Pseudoanabaena catenata Lauterborn	·	+	·	·	·	·	·	·
Pseudocapsa sp. Ercegović	·	·	·	·	·	·	+	·
Scytonema hofmanni Agardh	·	·	·	+	·	·	·	·
Synechocystis sp. Sauvageau	+	+	+	+	+	+	·	+
EUKARYOTA								
Chrysophyta								
Chlorocloster sp. Pascher	·	+	+	+	·	+	·	+
Cymbella ehrenbergii Kützing	·	·	·	·	·	+	·	·
Elipsoidon sp. Pascher	·	+	·	·	·	·	·	·
Elipsoidon oocystoides Pascher	·	·	·	·	·	·	·	+
Fragilaria pinnata Ehrenberg	·	·	+	·	·	·	+	+
Heterococcus sp. Chodat	·	·	·	·	·	·	+	·

Table 3. Continued.

Species	Cave/Mine							
	Id	Ko	Me	Pe	Pi	Po	Šk	Žu
Heterococcus furcatus Pitschmann	·	·	·	·	·	·	+	·
Monodus sp. Chodat	·	·	+	+	·	·	·	+
Navicula sp. Bory	·	+	·	·	·	·	+	·
Navicula contenta var. *biceps* (Arnott, Grunow in Van Heurck) Cleve	+	+	·	+	·	·	+	+
Navicula gallica var. *perpusilla* (Grun) Lange-Bertalot	·	+	+	·	·	+	·	+
Navicula mutica Kützing	+	+	+	+	·	+	·	+
Nitzschia sp. Hassall	·	·	+	·	·	·	·	·
Pinnularia borealis Ehrenberg	·	·	·	·	·	·	+	·
Chlorophyta								
Apatococcus cf. *lobatus* (Chodat) J.B. Petersen	+	·	·	·	·	·	·	·
Chlorella sp. Beijerinck	+	+	+	+	+	+	+	+
Chlorotetraedron sp. MacEntee	+	·	·	·	·	·	·	·
Gloeocystis polydermatica (Kütz.) Hindák	·	·	·	+	·	·	·	·
Klebsormidium flaccidum Silva, Mattox et Blackwell	+	+	+	·	·	·	·	·
Microthamnion cf. *strictissimum* Rabenhorst	·	·	+	·	·	·	·	·
Muriella sp. J.B Petersen	+	·	·	+	·	·	·	·
Myrmecia sp. Printz	+	·	·	·	·	·	·	·
Pediastrum boryanum (Turpin) Meneghini	·	·	+	·	·	+	·	·
Pseudochlorella sp. Lund	·	·	·	·	·	·	+	·
Pseudoclonium cf. *basiliense* Vischer	+	·	+	+	·	·	·	·
Scenedesmus bijugatus (Turpin) Meneghini	·	·	·	·	+	·	·	·
Scenedesmus obliquus (Turpin) Kützing	·	·	·	·	+	·	·	·
Scotiellopsis sp. Vinatzer	·	+	+	·	·	·	·	+
Stichococcus bacillaris Nägeli	+	+	+	+	+	+	·	+
Stichococcus exiguous Gerneck	·	·	+	·	·	·	·	·
Stichococcus undulatus Vinatzer	+	·	·	·	·	·	·	·
Trentepohlia aurea Martius	·	+	+	+	+	+	+	+

Note: Id–mercury mine Idrija, Ko–Kostanjeviška jama, Me–lead and zinc mine Mežica, Pe–Pekel pri Zalogu, Pi–Pivka jama, Po–Postojnska jama, Šk–Škocjanske jame, Žu–Županova jama

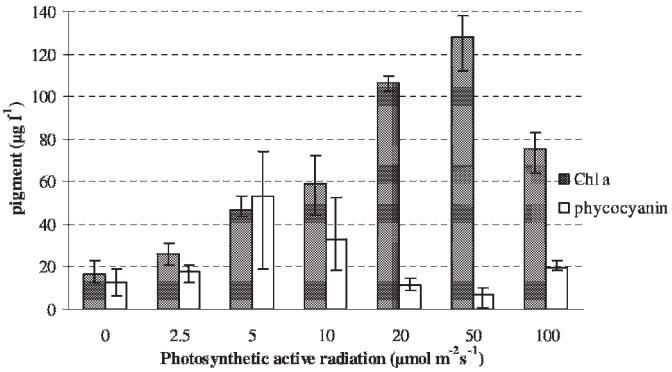

Figure 1. Chl *a* and phycocyanin concentrations at different photon flux densities after 25 days of cultivation of *Chroococcus minutus* in Postojnska jama.

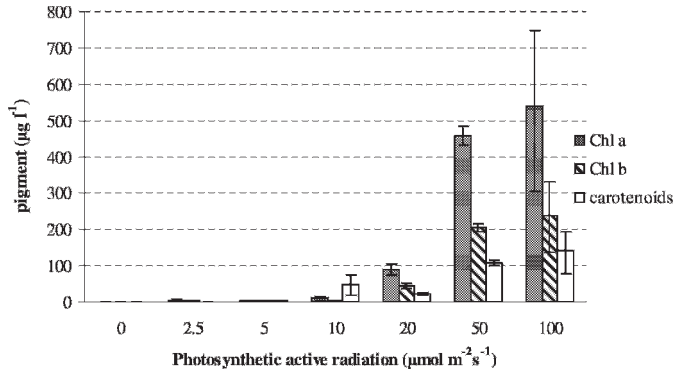

Figure 2. Concentrations of the Chl *a*, Chl *b* and carotenoids at different photon flux densities after 25 days of cultivation of *Chlorella* sp. in Postojnska jama.

overgrown by fast-growing eukaryotic algae. This observation is supported by a 10-times higher increase in cell count of *Chlorella* sp. after 25 days of cultivation under cave conditions compared to *C. minutus* (data not shown), which is similar to the findings of Gaylarde and Gaylarde (2000) who concluded that the first colonizers on the walls of buildings are eukaryotic algae, but cyanobacteria become predominant later in the species succession. This later stage does not develop if the biofilm is frequently removed from the buildings (Gaylarde and Gaylarde, 2000). The best similar example can be seen in the case of the lampenflora community from Škocjanske jame with one of the highest percentage of cyanobacteria (57%) we found, which could be due to the fact that lampenflora have not been removed since the establishment of electric illumination in 1959 (Mulec, 2005). Nevertheless lampenflora algae are usually ubiquitous, fast reproducing, and adaptable soil algae (Rajczy, 1989). Although some authors report lampenflora communities having more eukaryotic algae than cyanobacteria (Faimon et al., 2003), it could be that they sampled lampenflora in the early stage of species succession.

We identified 59 algal taxa from the Schmidlova dvorana cave entrance of Škocjanske jame. A higher number of identified taxa belonging to Oscillatoriales compared to Nostocales confirmed that this cave environment is exposed only to low photon flux density (Table 2). Namely cyanobacteria from the order Oscillatoriales are better adapted to constant low irradiance levels than Nostocales (Albertano et al., 2000). If we take into account that in the cave entrance relative air humidity is constant and only the photon irradiance lowers the deeper we go into the cave, a correlation between irradiance and Chl *a* concentration is expected. Our results showed there is no correlation that indicates a substratum and/or presence of seeping water with available nutrients on sites in karst caves play an important role in the colonization and growth of aerophytic algae. No correlation between irradiance and biomass (Chl *a*) was observed as in the case of lampenflora. However, there is a difference in Chl *a* concentration per surface unit between these two microhabitats. Lampenflora algae demonstrated higher values (max. 2.44 μg cm^{-2}) compared to the algae from cave entrance (max. 1.71 μg cm^{-2}). This difference can be explained due to the different light regime in both microhabitats (i.e., changing light quality and irradiance levels during the day in the cave entrance), different periods of illumination, different *in situ* moisture levels, and different species composition. Generally speaking, areas around lamps have more stable conditions since they are deeper into the constant zone of the cave. However, these values are a few magnitudes lower when compared with the concentrations from non-cave environments like the Niagara cliff where it was 7.3 μg cm^{-2} (Matthes-Sears et al., 1997).

Results presented here indicate that the light is not the only key factor for high or low algal biodiversity. Our results further show that, if we take into account only the cyanobacterial part of the community, coccoid forms tolerate low irradiance more easily; and thus, they represent the major part of the community. Aerophytic algae must develop an intimate interaction with substratum on which they are attached. Which component of the limestone substratum directs or limits algal colonization? In carbonate rocks, several different trace elements can be found in significant concentrations: Al, Ba, Cd, Co, Cu, Fe, K, Mg, Mn, Na, Si, Sr, Ti, U and Zn (Morse and MacKenzie, 1990). Some of these elements could also be lethal for algae or certain groups of algae. In caves, algae often colonize flowstone surfaces. Various minerals can be traced in flowstone in which Co, Cr, Cu, Fe, Mg, Mn, Ni and Zn are the most frequent elements deposited together with the flowstone (Hill and Forti, 1997). Tomaselli et al. (2000) determined that some algae have a preference for a specific substratum to colonize. Nevertheless, one should take into account that in caves various substances in seeping and dripping water can notably influence algal growth.

Physiological adaptations of algae in cave conditions are not well studied. When light is limiting for algal growth the Chl *a* content increases and it decreases when light is not limiting (Meeks, 1974). For cyanobacterium *C. minutus* at cave temperature (9.0 °C), the light saturation lies between 50 and 100 μmol m^{-2} s^{-1}. A similar trend is observed for green alga *Chlorella* sp. at photon flux densities slightly higher than 100 μmol m^{-2} s^{-1}. Based on our experiences from caves, the majority of algae grow generally at photon-flux density much lower than the saturation value and even lower than the compensation point. Diatoms and cyanobacteria have an average compensation point between 5 and 6 and green algae at 21 μmol m^{-2} s^{-1} (Hill, 1996). Algae in caves must include in their survival strategy other ways to obtain energy, like heterotrophy. Giordano et al. (2000) suggests that cells living in caves at low photon irradiance could have a better yield of available photons. To capture as many available photons as possible at low irradiance, cells synthesise accessory photosynthetic pigments. At 9.0 °C and below 10 μmol m^{-2} s^{-1}, the biosynthesis of accessory pigments in two typical aerophytic organisms (*C. minutus* and *Chlorella* sp.) was elevated. With *Chlorella* sp. at values higher than 10 μmol m^{-2} s^{-1}, the ratio of carotenoids to Chl *ab* approached 1:3, which is an expected ratio for green algae. At 100 μmol m^{-2} s^{-1}, a typical ratio Chl *a*: Chl *b* 3:1 for green algae was observed (Kirk, 1983). Different photon irradiance also influences the ratio of Chl *a* vs. phycocyanin in *C. minutus*. At the highest irradiance used in the experiment, the concentration of Chl *a* decreased, but phycocyanin slightly increased. Zilinskas Braun and Zilinskas Braun (1974) explained such a phenomenon with lowered efficiency of energy transfer from phycocyanin to Chl *a*. In the cave habitat, very adaptable algae can prosper if they can use low photon irradiance dosages.

ACKNOWLEDGEMENTS

This work was partly supported by the financial contribution of the Slovenian Research Agency Z6-7072, role and significance of microorganisms in karst processes.

REFERENCES

Abdelahad, N., 1985, Osservazioni su alcune cianoficee cavernicole rare e interesanti: Giornale Botanico Italiano, v. 119, no. 2, p. 45–46.

Abdelahad, N., 1989, On four *Myxosarcina*-like species (Cyanophyta) living in the Inferniglio cave (Italy): Archiv für Hydrobiologie: Supplementband, v. 82, Algological studies, no. 9, p. 3–13.

Albertano, P., Bruno, L., D'Ottavi, D., Moscone, D., and Palleschi, G., 2000, Effect of photosynthesis on pH variation in cyanobacterial biofilms from Roman catacombs: Journal of Applied Phycology, no. 12, p. 279–384.

Asencio, A.D., and Aboal, M., 2000, Algae from La Serreta cave (Murcia, SE Spain) and their environmental conditions: Archiv für Hydrobiologie: Supplementband, v. 131, Algological studies, no. 96, p. 59–78.

Buczkó, K., and Rajczy, M., 1989, Contributions to the flora of the Hungarian caves II. Flora of the three caves near Beremend, Hungary: Studia Botanica Hungarica (Antea: Fragmenta Botanica), v. 21, p. 13–26.

Chang, T.P., and Chang-Schneider, H., 1991, Algen in vier süddeutschen Höhlen: Berichte der Bayerischen Botanischhen Gesellschaft, v. 62, p. 221–229.

Clesceri, L.S., Greenberg, A.E., and Eaton, A.D., 1998, Standard methods for the examination of water and wastewater, 20th edition, Washington, American Public Health Association, p. 10–27.

Couté, A., 1982, Ultrastructure d'une cyanophycée aérienne calcifiée cavernicole: *Geitleria calcarea* Friedmann: Hydrobiologia, v. 97, p. 255–274.

Dobat, K., 1970, Considérations sur la végétation cryptogamique des grottes du Jura Souabe (sud-ouest de l'Allemagne): Annales de Spéléologie, v. 25, no. 4, p. 872–907.

Ettl, H., and Gärtner, G., 1995, Syllabus der Boden-, Luft- und Flechtenalgen, Stuttgart, Gustav Fischer Verlag, p. 721.

Faimon, J., Štelcl, J., Kubešová, S., and Zimák, J., 2003, Environmentally acceptable effect of hydrogen peroxide on cave lamp–flora, calcite speleothems and limestones: Environmental Pollution, v. 122, p. 417–422.

Garbacki, N., Ector, L., Kostikov, I., and Hoffmann, L., 1999, Contribution à l'étude de la flore des grottes de Belgique: Belgian Journal of Botany, v. 132, no. 1, p. 43–76.

Gaylarde, P.M., and Gaylarde, C.C., 2000, Algae and cyanobacteria on painted buildings in Latin America: International Biodeterioration and Biodegradation, v. 46, p. 93–97.

Geitler, L., 1932, Cyanophyceae, *in* Rabenhorst, L., ed., Kryptogamen-Flora, Akademische, Leipzig, Verlagsgesellschaft, p. 1196.

Giordano, M., Mobili, F., Pezzoni, V., Hein, M.K., and Davis, J.S., 2000, Photosynthesis in the caves of Frasassi (Italy): Phycologia, v. 39, no. 5, p. 384–389.

Golubić, S., 1967, Algenvegetation der Felsen: Eine ökologische Algenstudie im dinarischen Karstgebiet, *in* Elster, H.J., and Ohle, W., eds., Die Binnengewässer, Stuttgart, Band XXIII, E. Schweizerbart'sche Verlagsbuchhandlung, p. 183.

Hernandéz-Mariné, M., and Canals, T., 1994, *Herpyzonema pulverulentum* (Mastigocladaceae), a new cavernicolous atmophytic and lime-incrusted cyanophyte: Archiv für Hydrobiologie: Supplementband, v. 105, Algological studies, no. 75, p. 123–136.

Hill, C., and Forti, P., 1997, Cave minerals of the world, 2nd edition, Huntsville, National Speleological Society, p. 463.

Hill, W.R., 1996, Effects of light, *in* Stevenson, R.J., Bothwell, M.L., and Lowe, R.L., eds., Algal ecology: freshwater benthic ecosystems, San Diego, Academic Press, p. 121–144.

Hindak, F., 1996. Kľúč na určovanie nerozkonárených vláknitých zelených rias (Ulotrichineae, Ulotrichales, Chlorophyceae), Slovenská botanická spoločnost' pri SAV, Bratislava, p. 77.

Hoffmann, L., 1986, Cyanophycées aériennes et subaériennes du Grand-Duché de Luxembourg: Bulletin du Jardin Botanique National de Belgique, v. 56, p. 77–127.

Hoffmann, L., 2002, Caves and other low-light environments: aerophitic photoautotrophic microorganisms, *in* Bitton, G., ed., Encyclopedia of Environmental Microbiology, New York, John Wiley & Sons, p. 835–843.

Jones, H.J., 1964, Algological investigations in Mammoth cave, Kentucky: International Journal of Speleology, v. 1, no. 4, p. 491–516.

Kinkle, B.K., and Kane, T.C., 2000, Chemolithoautotrophic microorganisms and their potential role in subsurface environments, *in* Wilkens, H., Culver, D.C., and Humphreys, W., eds., Ecosystems of the World 30. Subterranean ecosystems, Amsterdam, Elsevier, p. 309–318.

Kirk, J.T.O., 1983, Light and photosynthesis in aquatic ecosystems, Cambridge, Cambridge University Press, p. 401.

Komárek, J., and Anagnostidis, K., 2000, Cyanoprokaryota 1. Teil: Chroococcales, *in* Ettl, H., Gärtner, G., Heying, H., and Mollenhauer, D., eds., Süβwasserflora von Mitteleuropa 19/1, Heidelberg, Spectrum Akademischer Verlag, p. 548.

Komárek, J., and Anagnostidis, K., 2005, Cyanoprokaryota 2. Teil: Oscillatoriales, *in* Büdel, B., Gärtner, G., Krienitz, L., and Schagerl, M., eds., Süsswasserflora von Mitteleuropa 19/2, Heidelberg, Elsevier, p. 759.

Krammer, K., and Lange-Bertalot, H., 1986, Bacillariophyceae 1. Teil: Naviculaceae, *in* Ettl, H., Gerloff, J., Heying, H., and Mollenhauer, D., eds., Süβwasserflora von Mitteleuropa 2/1, Stuttgart, Gustav Fischer Verlag, p. 876.

Krammer, K., and Lange-Bertalot, H., 1988, Bacillariophyceae 2. Teil: Bacillariaceae, Epithemiaceae, Surirellaceae, *in* Ettl, H., Gerloff, J., Heying, H., and Mollenhauer, D., eds., Süβwasserflora von Mitteleuropa 2/2, Stuttgart, Gustav Fischer Verlag, p. 596.

Krammer, K., and Lange-Bertalot, H., 1991, Bacillariophyceae 3. Teil: Centrales, Fragilariaceae, Eunotiaceae, *in* Ettl, H., Gerloff, J., Heying, H., and Mollenhauer, D., eds., Süβwasserflora von Mitteleuropa 2/3, Stuttgart, Gustav Fischer Verlag, p. 576.

Kuehn, K.A., Oneil, R.M., and Koehn, R.D., 1992, Viable photosynthetic microalgal isolates from aphotic environments of the Edwards aquifer (central Texas): Stygologia, v. 7, no. 3, p. 129–142.

Lee, T., Tsuzuki, M., Takeuchi, T., Yokoyama, K., and Karube, I., 1994, *In vivo* fluorimetric method for detection of cyanobacterial waterblooms: Journal of Applied Phycology, v. 6, p. 489–495.

Lemmermann, E., Brunnthaler, J., and Pascher, A., 1915, Heft 5: Chlorophyceae 2, *in* Pascher, A., ed., Die Süβwasserflora Deutschlands, Österreichs und der Schweiz, Gustav Fischer, Jena, p. 250.

Martinčič, A., Vrhovšek, D., and Batič, F., 1981, Flora v jamah z umetno osvetlitvijo: Biološki Vestnik, v. 29, no. 2, p. 27–56.

Matthes-Sears, U., Gerrath, J.A., and Larson, D.W., 1997, Abundance, biomass, and productivity of endolithic and epilithic lower plants on the temperate–zone of Niagara Escarpment, Canada: International Journal of Plant Sciences, v. 158, p. 451–460.

Meeks, J.C., 1974, Chlorophylls, *in* Stewart, W.D.P., ed., Algal physiology and biochemistry, Botanical monographs, Volume 10, Oxford, Blackwell scientific publications, p. 161–175.

Morse, J.W., and MacKenzie, F.T., 1990, Geochemisty of sedimentary carbonates. Developments in sedimentology 48: Amsterdam, Oxford, Elsevier, p. 707.

Mulec, J., 2005, Algae in the karst caves of Slovenia [Ph.D. thesis], Ljubljana, University of Ljubljana, p. 149.

Mulec, J., Kosi, G., and Vrhovšek, D., 2007, Algae promote growth of stalagmites and stalactites in karst caves (Škocjanske jame, Slovenia): Carbonates and Evaporites, v. 22, no. 3, p. 6–10.

Olson, R., 2006, Control of lamp flora in developed caves, *in* Hildreth-Werker, V., and Werker, J.C., eds., Cave conservation and restoration, Huntsville, National Speleological Society, p. 343–348.

Palik, P., 1964a, Über die Algenwelt der Höhlen in Ungarn: International Journal of Speleology, v. 1, no. 1–2, p. 35–44.

Palik, P., 1964b, Eine neue Aulakochloris–Art aus der Tropfsteinhöhle von Abaliget: International Journal of Speleology, v. 1, no. 1–2, p. 25–28.

Pedersen, K., 2000, Exploration of deep intraterrestrial microbial life: current perspective. MiniReview: FEMS Microbiology Letters, v. 185, p. 9–16.

Pipan, T., 2005, Epikarst - a promising habitat: copepod fauna, its diversity and ecology: a case study from Slovenia (Europe), Ljubljana, ZRC Publishing, p. 101.

Rajczy, M., 1989. The flora of Hungarian caves, Karszt és Barlang, Special issue, p. 69–72.

Sanchez, M., Alcocer, J., Escobar, E., and Lugo, A., 2002, Phytoplankton of cenotes and anchialine caves along a distance gradient from the northeastern coast of Quintana Roo, Yucatan Peninsula: Hydrobiologia, v. 467, no. 1–3, p. 79–89.

Sant'Ana, C.L., Branco, L.H.Z., and Silva, S.M.F., 1991, A new species of *Gloeothece* (Cyanophyceae, Microcystaceae) from São Paolo State, Brazil: Archiv für Hydrobiologie: Supplementband, v. 89, Algological studies, no. 89, p. 1–5.

Sarbu, S.M., Kane, T.C., and Kinkle, B.K., 1996, A chemoautotrophically based cave ecosystem: Science, v. 272, no. 5270, p. 1953–1955.

Sulek, J., 1969, Taxonomische Übersicht der Gattung *Pediastrum* Meyen, *in* Fott, B., and Komárek, J., eds., Studies in Phycology, Stuttgart, E. Schweizerbart'sche Verlagsbuchhandlung, p. 197–261.

Tomaselli, L., Lamenti, G., Bosco, M., and Tiano, P., 2000, Biodiversity of photosynthetic micro-organisms dwelling on stone monuments: International Biodeterioration and Biodegradation, v. 46, p. 251–258.

Van Landingham, S., 1966a, Three new species of *Cymbella* from Mammoth cave, Kentucky: International Journal of Speleology, v. 2, no. 1–2, p. 133–136.

Van Landingham, S., 1966b, A new species of *Gomphonema* (Bacillariophyta) from Mammoth cave, Kentucky: International Journal of Speleology, v. 2, no. 4, p. 405–406.

Vinogradova, O.N., Kovalenko, O.V., Wasser, S., Nevo, E., Tsarenko, P.M., Stupina, V.V., and Kondratiuk, E.S., 1995, Algae of the Mount Carmel National Park (Israel): Algologia, v. 5, no. 2, p. 178–192.

Vinogradova, O.N., Kovalenko, O.V., Wasser, S.P., Nevo, E., and Weinstein-Evron, M., 1998, Species diversity gradient to darkness stress in blue–green algae/cyanobacteria: a microscale test in a prehistoric cave, Mount Carmel, Israel: Israel Journal of Plant Sciences, v. 46, p. 229–238.

Vollenweider, R.A., Talling, J.F., and Westlake, D.F., 1974, A manual on methods for measuring primary production in aquatic environments, IBP Handbook No. 12. International biological programme, 2nd edition, Oxford, Blackwell scientific publications, p. 225.

Warren, A., Day, J.G., and Brown, S., 1997, Cultivation of algae and protozoa, *in* Hurst, C.J., Knudsen, G.R., McInerney, M.J., Stetzenbach, L.D., and Walter, M.V., eds., Manual of environmental microbiology, Washington, American Society for Microbiology, p. 61–71.

Wetzel, R.G., and Likens, G.E., 1995, Limnological analyses, 2nd edition, New York, Springer-Verlag, p. 139–165.

Zilinskas Braun, G., and Zilinskas Braun, B., 1974, Light absorption, emission and photosynthesis, *in* Stewart, W.D.P., ed., Algal physiology and biochemistry, Botanical monographs, Volume 10, Oxford, Blackwell scientific publications, p. 346–390.

D.A. Burney, N. Vasey, L.R. Godfrey, Ramilisonina, W.L. Jungers, M. Ramarolahy, and L. Raharivony – New Findings at Andrahomana Cave, Southeastern Madagascar. *Journal of Cave and Karst Studies,* v. 70, no. 1, p. 13–24.

NEW FINDINGS AT ANDRAHOMANA CAVE, SOUTHEASTERN MADAGASCAR

D.A. Burney[1,*], N. Vasey[2], L.R. Godfrey[3], Ramilisonina[4], W.L. Jungers[5], M. Ramarolahy[6], and L. Raharivony[6]

Abstract: A remote eolianite cave and sinkhole complex on the southeast coast of Madagascar has played a major role in the history of paleontology in Madagascar. Andrahomana Cave has yielded a rich fossil record of the extinct megafauna. Expeditions in 2000 and 2003 produced a wealth of new material and provided the first systematic information concerning the genesis, stratigraphy, and taphonomy of the site. Recovered bones of one of the most poorly understood extinct large lemurs, *Hadropithecus stenognathus*, include many skeletal elements previously unknown. Radiocarbon dates show that the site has sampled this disappeared fauna in the mid-to-late Holocene, but that bone-bearing layers are stratigraphically mixed, probably owing to the effects of reworking of the sediments by extreme marine events. The diverse biota recovered contains elements of both eastern rain forest and southwestern arid bushland, reflecting the cave's position in the zone of transition between wet and dry biomes. Bones of two unusual small mammals add to the previously long faunal list for the site: 1) the first fossil evidence for *Macrotarsomys petteri*, a large-bodied endemic nesomyid rodent previously known only from a single modern specimen; and 2) the type specimen and additional material of a newly described extinct shrew-tenrec (*Microgale macpheei*). Evidence for prehistoric and colonial-era humans includes artifacts, hearth deposits, and remains of human domesticates and other introduced species. Although previously protected by its extreme isolation, the unique site is vulnerable to exploitation. An incipient tourist industry is likely to bring more people to the cave, and there is currently no form of protection afforded to the site.

Introduction

Madagascar is noted for having many large and spectacular caves, and several of these have yielded troves of fossils of the extinct giant lemurs, huge elephant birds, pygmy hippos, and other elements of the island's lost Holocene subfossil biota (e.g., Simons et al., 1995; Burney et al., 1997, 2004). One of the richest of these, Andrahomana Cave on Madagascar's southeast coast, a remote collapsed-cave feature that has been visited by only a handful of outsiders, is both visually spectacular and scientifically important (see Appendix 1 for a chronological account of exploration).

The site is normally reached by climbing down gneissic cliffs to the east, then wading at low tide over exposed coral reefs. During the 2003 expedition, an alternative route was developed that was much faster and less dependent on the tides, consisting of direct approach to the northern, inland rim of the sinkhole, followed by a moderate rappel or cable-ladder descent down the vertical face. An approach along the rocky shoreline from the west was also used a few times, but proved to be too dangerous because the deep rills in the gneissic bedrock form deadly bore waves when the sea swell is very large.

The stony matrix from which the cave is sculpted is a roughly 100 m thick pile of eolianite, with at least three separate units of calcareous sandstones laid down by dune-forming winds. Current theory holds that these deposits are normally formed at the end of Pleistocene glacial cycles as sea level rises rapidly following deglaciation, grinding up coral reefs and other marine deposits (see Burney et al., 2001). These eolianite units lie exposed in a sheer south-facing cliff face cut by the rough seas that bring huge swells ashore from Antarctica. A gaping entrance near the base of this cliff leads into a double sinkhole, whose figure-eight-shaped footprint is partially roofed by a sweeping massive triple-arch shaped by multiple collapses. Beyond this complex natural bridge, with its large central pillar, is a small sunken rainforest thriving in the microhabitat provided inside the cave system. This moist refuge is surrounded above by a much drier landscape of spiny semiarid bushland.

* Corresponding author
[1] National Tropical Botanical Garden, 3530 Papalina Road, Kalaheo, HI 96741, USA, dburney@ntbg.org
[2] Department of Anthropology, Portland State University, Portland, OR 97207, USA
[3] Department of Anthropology, University of Massachusetts-Amherst, Amherst, MA 01003, USA
[4] Musée d'Art et d'Archéologie, 17 Rue du Docteur Villette, Antananarivo 101, Madagascar
[5] Department of Anatomical Sciences, Stony Brook University, Stony Brook, NY 11794, USA
[6] Département de Paléontologie et d'Anthropologie Biologique, Faculté des Sciences, B.P. 906, Université d'Antananarivo, Antananarivo 101, Madagascar

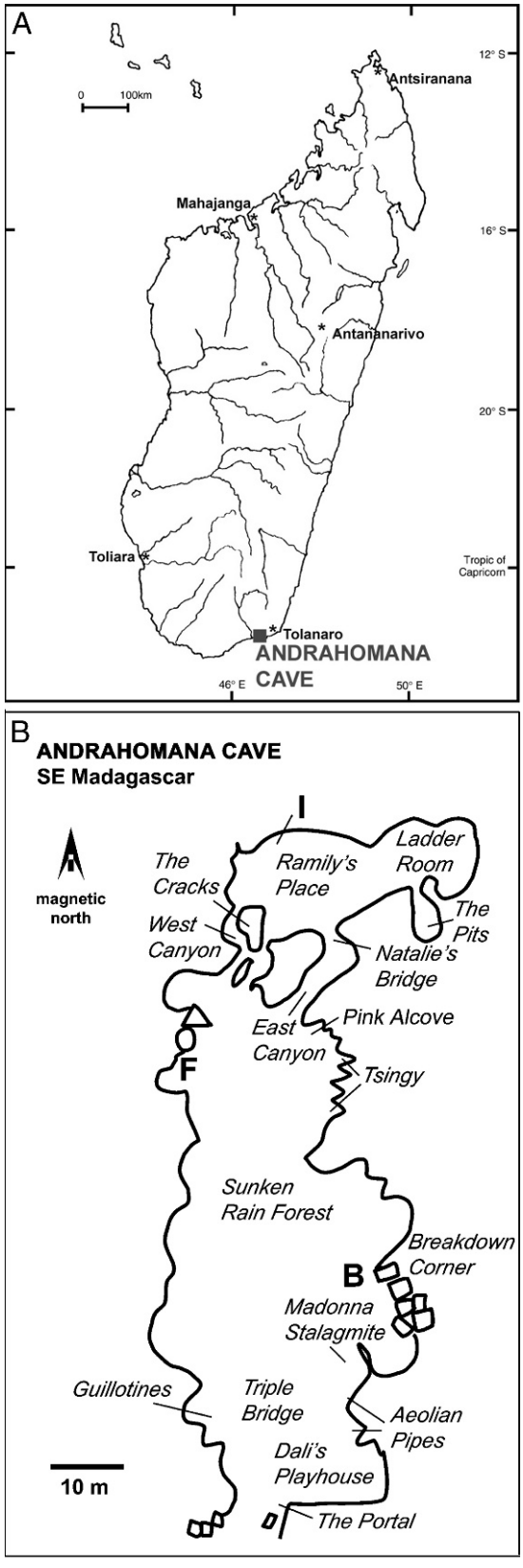

Figure 1. A. Location of Andrahomana Cave, on the southeast corner of Madagascar near Tolagnaro (formerly known as Ft. Dauphin). Entrance coordinates are S25°11′55″ E46°37′59″.

Around the edges of the collapsed areas, the remaining portions of the high vaulted ceiling are perforated by dozens of skylights and the walls are adorned with giant speleothems and unusual ruiniform features shaped like towers, fins, and buttresses. As interesting as these erosional and depositional features are, the great attraction for the sparse assemblage of paleontologists who have been coming here at long intervals since Franz Sikora's 1899 visit is the soft sandy sediments that mantle the floor, because these contain well-preserved bones of extinct megafauna, as well as a diverse collection of bones of smaller vertebrates and shells of large ornate land snails and other invertebrates. Remarkably, despite the proven potential of the site and the number of paleontologists who have visited, previous excavations have been largely undocumented and uncontrolled.

We report here the results of a brief survey in 2000 and a more extensive excavation program in 2003 that includes preliminary stratigraphic descriptions, faunal lists, radiometric dating, and paleoecological inferences. The goals of this work included not only recovering more complete material for rare taxa described previously from the site, but also the creation of a provisional chronostratigraphic context with which to interpret this material. These new details allow the first inferences regarding the paleoecology of the region, particularly the possible role of natural and human-induced changes in the history of the site.

SITE DESCRIPTION

Aside from the richness and preservation of its faunal remains, the site is also important because it is the only documented fossil vertebrate site from the entire southeastern portion of the island (S25°11′55″ E46°37′59″; Fig. 1A). Situated in an area of rapid transition from semiarid bushland to the west and humid rainforest to the east, the site potentially samples both types of environments.

The eolianite body here is complex and extensive, composed of three thick layers of calcareous sandstone that vary considerably in texture and color and in many places exhibit sharp zones of contact. The entire deposit lies unconformably on dense granitic and gneissic rocks that are exposed in the sea cliffs here and outcrop inland as a series of weathered hills, ridges, and inselbergs.

←

Figure 1. B. Survey map of the floor of Andrahomana Cave. Place names supplied by the authors. Capital letters B, F, and I indicate locations of excavations from the 2000 and 2003 expeditions. The cave roof is collapsed, except in the areas of Dali's Playhouse, the Triple Bridge, and Aeolian Pipes.

The overlying three-part eolianite in this area probably corresponds to, beginning at the bottom layer, Tatsimian, Karimbolian, and Aepyornian (Besairie, 1972). Although this material has not been dated, it is most likely mid- to late-Pleistocene in age; each unit probably reflects the depositional results of a post-glacial sea-level rise following a major ice-age cycle. These units are likely to have been deposited at least 100,000 years apart, reflecting the major component of glacial-interglacial cycles. Thus the cave's material would have been at least 200,000 years in the making, although it is not known whether these deposits are from the more recent, or earlier cycles.

In any case, these dune sands were consolidated through a process of recrystallization in which overlying acidic waters from the surface percolated through, dissolving highly soluble aragonitic calcium carbonate and replacing it, on drying, with harder and less soluble calcite. The addition of silica from overlying soils and atmospheric dust would have helped further harden this natural cement. This recrystallization phase was followed much later by dissolution, as ground water flowing between the porous eolianites and the relatively impervious basement rocks etched away the sandstone from below, producing a cavern. Further dissolution, probably aided by subsequent marine incursion, has led to the collapse of this cave in the central chamber. Considerable time, perhaps 100,000 years or more, passed before the cave collapsed, as the large inactive speleothems of up to 2 meters in diameter around the edge of the opening would have formed in the humid conditions of a more enclosed cave. Growth rates of similar-sized speleothems elsewhere in Madagascar and in similar climates in Africa have been measured by U-series techniques (Brook et al., 1990; Burney et al., 1994, 1997). These speleothems are likely to be at least as old if they formed at similar rates.

Since this collapse, Andrahomana has served as a natural trap for terrestrial sediments and biotic remains. Evidence in the lower parts of the cave shows that either high sea-stands or extreme marine events have brought the sea back into the cave on occasion, adding marine materials to these deposits as well.

Work from the 2000 and 2003 expeditions included mapping with compass, clinometer, and hip-chain, surface survey, sediment description from bucket-auger cores and test pits, and controlled excavation. Contrary to the claim of Alluaud (1900) that Sikora had excavated the entire place (*tout fouillé*) the year before, coupled with the digging efforts of subsequent visitors (see Appendix 1), a considerable amount of previously unexcavated sediments was located. Earlier excavations were easily recognized by the deranged nature of the sediment layers and lack of large bones in the old spoil piles. Fine-screening of this material rejected by earlier investigators, however, did provide a rich yield of smaller bones, teeth, and artifacts, and provided insight into the coarser methods of earlier investigators.

Controlled excavations were carried out at location B in 2000, and locations F and I in 2003 (Fig. 1B). Each showed a similar pattern: an upper unit, generally 10–20 cm thick, of brown humic silty sand, containing primarily bones of the present fauna, and a much thicker lower unit, of ca. 1 m to <3 m thickness, of coarser, lighter-colored sands, including a larger component of remains of extinct fauna. Artifacts of post-European colonization provenance, including glass and spent cartridges, occur near the top of the upper unit, with no definite evidence of humans deeper in the unit. Dates on bones from this unit are late Holocene, but are not in stratigraphic order (Table 1).

The lower unit lacks human artifacts and contains bones dating to the mid-Holocene that are not in consistent stratigraphic order. This suggests that late Holocene sediments here have been disturbed and perhaps largely eroded by extreme marine events, perhaps one or more tsunami or storm overwashes. Recent evidence for the Burckle Impact Crater, between southern Madagascar and Antarctica (Masse et al., 2006) suggests that at least one mega-tsunami of far greater magnitude than any recorded historically was generated in this area in the Holocene, as supported by the occurrence of chevron dune deposits in the coastal regions of extreme southern Madagascar.

Fauna

Table 2 provides a full list of taxa found in the subfossil deposits at Andrahomana in 2003 and additional occurrences in prior collections. Certain species are represented in both collections, but a few are represented in small numbers only in earlier collections, and many other species (especially non-mammals) are reported here for the first time.

Taxa typically confined to either dry or humid habitats are found in the collection, as might be expected given that Andrahomana is situated in an area of abrupt transition from semiarid spiny bushland to the west and humid rainforest to the east, a divide created in large part by the Anosyenne Mountains. Extant taxa typical of drier habitats include *Numida meleagris* among the birds, *Geogale aurita* and *Echinops telfairi* among the afrosoricidans, *Triaenops furculus* among the bats, *Lemur catta* among the primates, and *Macrotarsomys bastardi* among the rodents. These taxa are found in western dry deciduous forests and southern spiny bush areas of Madagascar (Carleton and Goodman, 2003; Eger and Mitchell, 2003; Goodman, 2003). *Lemur catta* regularly frequents the premises of the cave today and it is likely the other taxa do as well. In addition to these extant taxa, several extinct taxa recovered from Andrahomana also likely occupied drier habitats, including the primates *Megaladapis edwardsi* and *Hadropithecus stenognathus*, which are dominant elements of the subfossil fauna of the extreme south and southwest, but not elsewhere (see Godfrey and Jungers, 2002, for a review), and the rodent *Hypogeomys australis*, although the

Table 1. Acceleration mass spectrometer ^{14}C purified collagen dates from Andrahomana Cave.

Material/Method	Age B.P. ± 1σ	Calibrated 2σ Range[a]	Sample I.D. Provenance or Accession No.	Lab. Number	$\delta^{13}C$	Comments/Other
Hadropithecus stenognathus bone	6724 ± 54	B.P. 7660–7490	BJ-HS-1	AA-45963 T-16044A	−9.1	Humeral fragment
Hypogeomys australis bone	4440 ± 60	B.P. 5840–4420	Not Given	Beta-73370	…	In Goodman and Rakotondravony (2006)
Hypogeomys australis tooth	1536 ± 35	A.D. 428–618 B.P. 1522–1332	AHA-I-L1-CD1,2 AHA-03-1	NZA-18996 R-28421/1	−20.0	…
Macrotarsomys petteri bone	2480 ± 40	B.C. 790–410 B.P. 2740–2360	AHA-I-L1-CD3	Beta-212739	…	Demi-mandible; too small for ^{13}C
Macrotarsomys petteri bone	1760 ± 40	A.D. 150–390 B.P. 1800–1560	AHA-I-L6-CD1,2	Beta-212738	…	Demi-mandible; too small for ^{13}C
Megaladapis sp. bone	4566 ± 25	B.P. 5436–5059	AHA-03-7	NZA-18997 R-28421/7	−20.1	Infant femur

[a] Calibrations from Stuiver et al. (1998).

natural history and distribution of the latter species is still poorly known (Goodman and Rakotondravony, 1996).

Extant taxa confined to more humid habitats include *Microgale principula* among the afrosoricida, *Avahi laniger* among the primates, and *Nesomys rufus* among the rodents (Jenkins, 2003; Ryan, 2003; Thalmann, 2003). These species are found only in earlier collections; none were recovered from our excavations in 2003 despite deliberate effort not to bias our collection in favor of larger-bodied taxa. *Avahi laniger* and *Nesomys rufus* no longer live in the region and their occurrence in the subfossil deposits of Andrahomana has not been previously published. *Avahi laniger* is represented by a single skull apparently found by Sikora and currently housed in the British Museum (Natural History) (BMNH ZD.1960.2103), and a number of skulls collected by Sikora and housed in the BMNH were attributed to *Nesomys rufus*. The subfossil occurrence of another locally extinct species, *Macrotarsomys petteri*, further suggests at least slightly more humid climatic regimes in this region of Madagascar in recent millennia (Goodman et al., 2006). *Macrotarsomys petteri* was only recently described and named, known from a single specimen collected 450 km northwest of Andrahomana in the Mikea forest north of Toliara (Goodman and Soarimalala, 2005).

Among the vertebrates recovered at Andrahomana, the largest taxa are extinct, as are the largest species in several smaller-bodied orders. Elephant birds (*Aepyornis*, *Mullerornis*), giant lemurs (*Hadropithecus stenognathus*, *Archaeolemur majori*, *Megaladapis edwardsi*, and *Pachylemur insignis*), the carnivore, *Cryptoprocta spelea*, the pygmy hippo, *Hippopotamus lemerlei*, the giant jumping rat, *Hypogeomys australis*, and the giant land tortoise, *Geochelone grandidieri*, are gone, known only from fossils. Ostensibly smaller taxa fared better. Nevertheless, analyses underway on the minifauna of Andrahomana demonstrate that smaller taxa were not immune to anthropogenic and climatic changes occurring in recent millennia. In a recent publication, we describe a new subfossil shrew-tenrec from Andrahomana, *Microgale macpheei*, to date, the only known afrosoricidan that has gone extinct in recent millennia (Goodman et al., 2007). Furthermore, biostratigraphic analysis demonstrates the decline of endemic rodents in tandem with increases in the representation of the introduced rodents *Rattus* sp. and *Mus musculus* (Vasey and Burney, unpublished data).

Domestic dogs (*Canis lupus familiaris*), cattle (*Bos indicus*), and the possibly non-native soricomorphid, *Suncus madagascariensis*, are also present among the bones recovered in 2003, amply indicating the post-human settlement context of the more recently deposited sediments in the cave. We note, as did Walker (1967), the presence of burned bones on the surface. However, we are of the opinion that these are fully modern remains, probably left by local fishermen, who occasionally enter the cave to cook a meal. On the other hand, a skull of *Archaeolemur* from

Andrahomana once thought to bear signs of a fatal crushing blow from an axe, or similar tool (Walker, 1967), has recently been radiocarbon dated to the mid-Holocene (3975 ± 53 ^{14}C yr BP; Perez et al., 2005), making it entirely unlikely that humans directly caused the death of this animal. Presumably most of the larger taxa entered the cave by accidentally falling through one of many skylights, which today are frequently camouflaged at the surface by vegetation. Many of the smaller animals were likely deposited by raptors from roost sites in the form of discarded prey remains or regurgitated pellets.

An overview of the primates recovered bears mentioning because this is the most taxonomically rich order represented at Andrahomana and because the most significant find of the 2003 excavations draws from this order: the remains of *Hadropithecus stenognathus*. The faunal list includes eleven species of primates, consisting of six extinct species, and five extant species (*Lemur catta*, *Propithecus verreauxi*, *Microcebus* sp., *Cheirogaleus medius*, and *Avahi laniger*), one of which (*Avahi laniger*) no longer lives on this side of the Anosyenne Mountains divide as discussed above. Only two specimens of *Cheirogaleus* are present in the recent collection despite the reported coexistence in the general region of Tolagnaro today of *C. medius*, *C. crossleyi*, and *C. major* (Hapke et al., 2005). Presently, *Lemur catta* regularly frequents the cave, and *Propithecus verreauxi* and *Microcebus* sp. can be observed in nearby forests. The abundant *Microcebus* subfossils in the cave deposits appear to belong to a single species, most likely *M. griseorufus*, another denizen of dry forest.

Of the extinct primate species, four (*Hadropithecus stenognathus*, *Archaeolemur majori*, *Megaladapis edwardsi*, and *Pachylemur insignis*) are well represented in subfossil deposits from Andrahomana. Two (*Megaladapis madagascariensis* and *Archaeolemur* sp., cf. *edwardsi*) are poorly represented. *Megaladapis madagascariensis* is represented by a single specimen (distal radius) in the Sikora collection in the Vienna Naturhistorisches Museum (VNM 1934.V.56). Most of the *Archaeolemur* from Andrahomana fit comfortably within the size range of *A. majori*, but there are a few specimens in both the BMNH and VNM collections (representing both postcranial and cranial fragments) that are well outside this range of variation, and appear to represent *A. edwardsi* (Godfrey et al., 1999; LRG, unpubl. observations).

Numerous elements of a single subadult *Hadropithecus stenognathus* were recovered from location I (Godfrey et al., 2006a). In addition to isolated teeth and cranial fragments, these elements include the first associated fore- and hind-limb bones, and a number of previously unknown elements: the first scaphoid, hamate, metacarpals, scapular fragment, whole sacrum, vertebrae (including the first several caudal vertebrae), and ribs (Godfrey et al., 2006a; Lemelin et al., 2006, 2008). Alan Walker pointed out the possibility that the cranial fragments belonged to a skull that Sikora had found in 1899 at Andrahomana and that Lorenz von Liburnau (1902) described. Tim Ryan has now used CT scanning of the newly found orbits and Sikora's cranium in Vienna to confirm this association (Ryan et al., 2008).

These discoveries have led to a reassessment of prior hind-limb attributions for *Hadropithecus*, and a re-evaluation of its locomotor behavior. The newly discovered skeletal elements confirm the hind-limb allocations for *Hadropithecus* described by Godfrey et al. (1997) and refute earlier attributions by Lamberton (1938). They prove that *Hadropithecus*, like *Archaeolemur*, had a long tail, relatively short limbs, and a robust body build. Of particular interest are the new carpals and metacarpals that provide evidence for pronograde quadrupedalism and terrestriality (Godfrey et al., 2006a; Lemelin et al., 2006, 2008). An isolated upper molar of *Hadropithecus* from AHA-I was sectioned by Gary Schwartz, and from this specimen, data on enamel thickness, enamel prism characteristics, and the chronology of dental development in *Hadropithecus* were derived (Godfrey et al. 2005, 2006a,b). Research on the dental microstructure of that molar has demonstrated that molar crown formation time was prolonged in *Hadropithecus* and is more like that of extant hominoids (gorillas, chimpanzees, orangutans) than extant lemurs or even other extinct giant lemurs, whether larger or smaller in body size. The cuspal enamel of *H. stenognathus* is not as thick or heavily decussated as in *Archaeolemur*; these differences, along with differences in their stable isotope signatures, underscore variation in trophic adaptations within the Archaeolemuridae (Godfrey et al., 2005; Godfrey et al., 2008).

Terrestrial gastropods are well-represented in the Andrahomana fossil record. Some of the types present as fossils are still living in the area, including large species in the genera *Helicophanta*, *Tropidophora* and *Clavator*. Within the Pleistocene eolianites, shells of a *Clavator* species were fairly common. The general impression from the Holocene stratigraphy is that the prehuman snail fauna has generally survived to the present in the area, but detailed analysis, including identification to species, should be undertaken. The Andrahomana vicinity is rich in both fossil and living snails. Emberton (1997) has identified 80 extant land snail species in extreme southeastern Madagascar.

Discussion

Biogeography and Paleoecology

Located on the southeastern coast of Madagascar, Andrahomana is just west of the Anosyenne Mountains, and thus in dry habitat. Today, the high plateau of central Madagascar behaves as a formidable barrier separating the wet forests of the east and the dry forests of the west, and there are striking differences between the respective faunas as well as floras of these regions. The boundary between wet and dry biota is very sharp in places; the eastern and

Table 2. List of subfossil taxa recovered from deposits at Andrahomana by Burney *et al.* (this publication) and by previous collectors.

Class	Order	Family	Burney *et al.*	Previous Collectors
Aves	Aepyornithiformes	Aepyornithidae		*Aepyornis* sp.[a, b, c]
			Mullerornis	
	Anseriformes	Anatidae		*Centrornis* sp.[a]
	Procellariiformes	Procellariidae	*Puffinus* sp.	
	Falconiformes	Falconidae	*Falco newtoni*	
	Galliformes	Numidae	*Numida meleagris*	
	Gruiformes	Turnicidae	*Turnix nigricollis*	
		Rallidae	*Gallinula chloropus*	
	Columbiformes	Columbidae	*Streptopelia picturata*	
	Psittaciformes	Psittacidae	*Coracopsis vasa*	
	Cuculiformes	Cuculidae	*Coua cursor*	
			Coua cristata	
	Strigiformes	Tytonidae	*Tyto alba*	
		Strigidae	*Otus rutilis*	
	Apodiformes	Apodidae	*Apus* sp.	
	Coraciiformes	Upupidae	*Upupa marginata*	
	Passeriformes	Alaudidae	*Mirafra hova*	
		Sylviidae	*Nesillas* cf. *lantzii*	
			Thamnornis chloropetoides	
		Monarchidae	cf. *Tersiphone mutata*	
		Zosteropidae	*Zosterops maderaspatana*	
		Vangidae	*Vanga curvirostris*	
			Leptopterus viridis	
			Cyanolanius madagascarinus	
		Corvidae	*Corvus albus*	
		Ploceidae	*Ploceus sakalava*	
			Foudia madagascariensis	
Mammalia	Afrosoricida	Tenrecidae	*Geogale aurita*	"*Cryptogale australis*"[c]
			Microgale brevicaudata	
			Microgale longicaudata	
			Microgale nasoloi	
			Microgale pusilla	
			Microgale macpheei	
				"*Paramicrogale decaryi*"[c] (*Microgale principula*)
			Echinops telfairi	
			Setifer setosus	
			Tenrec ecaudatus	"*Centetes ecaudatus*"[b, c]
	Soricomorpha	Soricidae	*Suncus madagascariensis*	
	Chiroptera	Pteropodidae		"*Pteropus edwardsi*"[a, b] (*Pteropus rufus*)
			Eidolon dupreanum	
			Rousettus madagascariensis	"*Pelophilous madagascariensis*"[c]
		Hipposideridae	*Hipposideros commersoni*	
			Triaenops furculus	
		Vespertilionidae	*Miniopterus gleni*	
		Molossidae	*Mormopterus jugularis*	
			Mops leucostigma	

Table 2. Continued.

Class	Order	Family	Burney *et al.*	Previous Collectors
	Primates	Cheirogaleidae	*Microcebus* sp.	"*Cheirogaleus myoxinus*"[c]
			Cheirogaleus medius	"*Cheirogaleus samati*"[a]
		Lemuridae	*Lemur catta*	*Lemur catta*[c, d]
			Pachylemur insignis	"*Lemur insignis*"[a, b, c]
		Indriidae	*Propithecus verreauxi*	*Propithecus verreauxi*[a, b, c, d]
				Avahi laniger[d]
		Archaeole-muridae	*Archaeolemur majori*	*Archaeolemur majori*[a, c, d]
				Archaeolemur edwardsi[d]
			Hadropithecus stenognathus	*Hadropithecus stenognathus*[d]
		Megaladapidae	*Megaladapis edwardsi*	*Megaladapis edwardsi*[a, b, c, d, e]
				Megaladapis madagascariensis[d]
	Carnivora	Viverridae		"*Viverra fosa*" (var. nov. *alluaudi*, large size)[a, c]
		Eupleridae		*Cryptoprocta ferox* (var. nov. *spelea*, large size)[b, c]
		Canidae	*Canis lupus familiaris*	*Canis familiaris*
	Artiodactyla	Bovidae	*Bos indicus*	"*Bos madagascariensis*"[a, b, c]
		Hippopotamidae	*Hippopotamus lemerlei*	*Hippopotamus lemerlei*[a, d]
	Rodentia	Nesomyidae	*Eliurus myoxinus*	
			Eliurus sp. (larger species)	
			Hypogeomys australis	*Hypogeomys* nov. sp.[c]
			Macrotarsomys bastardi	
			Macrotarsomys petteri	*Nesomys rufus*[d]
		Muridae	*Mus musculus*	*Mus musculus*[b]
			Rattus sp.	"*Mus decumanus*"[a, b, c]
Reptilia	Testudines	Pelomedusidae	*Pelomedusa subrufa*	
		Testudinidae	*Dipsochelys* sp.	"*Geochelone* (*Testudo*) *grandidieri*"[a, b]
			Geochelone radiata	"*Geochelone* (*Testudo*) *radiata*"[b]
	Squamata	Chamaeleonidae	*Furcifer* cf. *verrucosus*	
		Gekkonidae	*Paroedura* sp.	
		Gerrhosauridae	*Zonosaurus* cf. *trilineatus*	
	Serpentes	Boidae	*Acrantophis* sp.	
		Colubridae	*Leioheterodon* sp.	
	Crocodylia	Crocodylidae	*Crocodylus niloticus*	
				Crocodilus robustus[a, b, c]
Amphibia	Anura	Mantellidae	*Laliostoma labrosa*	
		Ranidae	*Ptychadena mascareniensis*	
		Microhylidae	*Scaphiophryne* sp.	

Note: Further information concerning previous collections can be found in Appendix 1. The Alluaud, Gaubert and Grandidier Collections were all published in Grandidier (1902). Earlier nomenclature (i.e., synonyms) of various taxa from previous collections is retained in the previous collections column, listed in quotes and parentheses.
[a] Alluaud Collection
[b] Gaubert Collection
[c] Grandidier Collection
[d] Sikora Collection
[e] Walker Collection

western slopes of Andohahela in southeastern Madagascar provide a good example (Goodman, 2000). Yet in other places, the high plateau serves as a region of considerable exchange (see for example, Goodman et al., 2007). The sharp ecotonal boundaries that exist on the eastern and western slopes of mountains such as Andohahela may be recent effects of rapid orogeny (see de Wit, 2003). It is also clear that, in the past, the geographic boundaries of typically wet- and dry-adapted species were quite fluid; fingers of eastern forest once spread across the island.

Isolated forests with eastern elements occur in the west, e.g., the region of Zombitse-Sakaraha, east of Morondava, and the mist oasis of the Analavelona Massif, near Toliara (Du Puy et al., 1994; Langrand and Goodman, 1997; Carleton et al., 2001, Ganzhorn, 2006), and typical dry-loving species occur in some forests of the East (reviewed in Ganzhorn, 2006). A number of lemur species and other fauna are today, or were in the recent past, spread across the east-west divide. For example, it is now known that *Hapalemur simus*, restricted today to humid forests in the southeast (Irwin et al., 2005), once lived in the extreme north (Ankarana and Mt. des Français), central Madagascar (Ampasambazimba), the northwest (Anjohibe), and the extreme west (Bemaraha) (Godfrey et al., 2004). Paleoecological data confirm that the southwest was recently moister than it is today (Burney, 1993), and the Holocene distributions of rodents and birds prove the existence of a corridor south of $\sim 20^{\circ}$ latitude through which animals adapted to moist environments were able to spread westward (Goodman and Rakotondravony, 1996; Goodman and Rakotozafy, 1997).

There are several possible explanations for the observed mixture of wet- and dry-adapted fauna at Andrahomana. One is that these taxa were not actually synchronous but are a mixed assemblage of species that lived in the region at different times; their presence at Andrahomana would then reflect temporal fluctuation in the climate and vegetation of the area. Another is that the tolerance of certain species to variation in habitat was greater in the past than it is today. A third possibility is that the habitats themselves were richer, supporting a larger number of sympatric species with different resource requirements. Direct and indirect anthropogenic factors (hunting, deforestation, introduction of exotic species) may have contributed to changes and diminutions in the geographic ranges of endemic species. Regardless of whether past transitions between wet and dry biomes were gradual or abrupt in southern Madagascar (either temporally or spatially), the mixture of wet- and dry-adapted species at Andrahomana certainly reflects the position of the cave within the zone of transition.

CAVE GENESIS AND CHRONOLOGY

Although the eolianite units at Andrahomana are almost certainly too old for radiocarbon dating and even less conventional methods such as whole rock amino-acid racemization (see Hearty et al., 2000), some rough estimates can be made for Andrahomana's chronology of formation. For example, the cave has been formed by solution since the third eolianite unit was deposited (the topmost Aepyornian). That surely means that the cave was formed since the last interglacial depositional event, a minimum of approximately 130 kyr BP (isotope stage 5e).

Speleothems >1 m in diameter are found inside, and these were almost certainly deposited prior to cave collapse (the air is too dry in the cave today to permit significant dripstone formation). Similar formations in another cave in Madagascar required more than 40 kyr to reach a similar size (Burney et al. 1997). Combining these observations, the following scenario is plausible, but not proven by the data presented: 1) the limestone was laid down over the last quarter million years or more; 2) the cave was excavated by ground-water dissolution over the last ca. 100,000 years; 3) after perhaps 40,000 years of speleothem growth, the ceiling of the cave began to collapse, drying out the inside of the cave and permitting rapid sedimentation from terrestrial sources; 4) during the Holocene, sea level reached the bottom of the lowermost cave entrance; 5) extreme marine events, since mid-Holocene times, occasionally breached the interior of the cave, contributing to structural collapse and depositing marine sands and other material inside up to the highest parts of the floor, >8 m above present sea level.

If these linked scenarios are correct, mid-to-late Pleistocene fossils may be incorporated into the eolianite, the uppermost sediments are a mixture of Holocene terrestrial and marine materials, and deep down, below any excavation levels reached so far, and perhaps in fissure fills higher up, there could be mid-to-late Pleistocene cave breccias, perhaps containing bones and shells from times poorly sampled in fossil sites in Madagascar. Thus Andrahomana has some potential for filling the later portion of the large Cenozoic blind spot that has characterized paleontology in Madagascar (see Table 1 in Krause et al., 2006). For resolving the interesting questions regarding the timing of human arrival and the fate of the extinct subfossil fauna, however, the cave is not ideal. Because of the apparent disturbance, removal, and reworking of Holocene sediments, only limited stratigraphic resolution has been obtained in the excavated sediments.

It is abundantly clear from the detailed history of site exploration and development in Appendix 1 that, despite its extremely remote location, the site has attracted a great deal of attention from paleontologists. Ironically, however, none of these accomplished collectors provided any stratigraphic detail or information concerning the age or provenance of the many fossils collected. This is unfortunate, as much of the accessible deposits were removed or disturbed before the initiation of the present study. Confirming associations and finding previously undescribed elements of *Hadropithecus stenognathus* would alone justify continued efforts. The discovery of associated forelimb and hind-limb bones has indeed informed and improved reconstructions of the behavior of *Hadropithecus* (see reviews by Godfrey et al., 1997, 2006a). Far from completing the study of this interesting cave and exhausting its potential, our recent work at Andrahomana, which has yielded a site map, new insights on the stratigraphy and geochronology of the site, evidence for mega-tsunamis or other extreme marine events, and the collation of historical records for the site, merely underscores the need for more research. Two high priorities for future research would be larger-scale excavation and methodical searching for Pleistocene age breccias and fissure fills.

Until recently, the great isolation of the site has provided some protection from vandalism and looting of the natural treasures of the site. The ornate speleothems, abundant fossil bones and shells, and mineral deposits of the cave area are potentially vulnerable to the growing illegal trade in these materials (Krause et al., 2006). Local authorities, quite naturally, are anxious to see access to the site improved in anticipation of ecotourism revenues. Several local tour operators now offer visits to the site and more are planned according to local authorities. It is important, however, that any future development plans for the area include provision of some form of protection for the site.

Acknowledgments

This research was supported by NSF BCS-0129185 (to DAB, LRG, and WLJ), BCS-0237388 (to LRG), and a College of Liberal Arts and Sciences Research Stipend from Portland State University (to NV) and conducted under collaborative agreements with the Département de Paléontologie et d'Anthropologie Biologique, Université d'Antananarivo, and the Académie Malgache. Paul S. Martin and Alan C. Walker encouraged us to investigate the site and provided unpublished notes on their 1966 expedition. Steve Goodman, Chris Raxworthy, and Alexander Wolf assisted in identifying specimens, and Michael Carleton and Steve Goodman provided helpful reviews of the manuscript.

References

Alluaud, C., 1900, Correspondance (Letter addressed to Mr. Guillaume Grandidier in Fort Dauphin, August 30, 1900): Bulletin du Muséum National d'Histoire Naturelle Paris, v. 6, p. 327–330.

Battistini, R., 1964, Étude géomorphologique de l'extrême sud de Madagascar: Laboratoire de Géographie, Antananarivo; Éditions Cujas, Paris.

Besairie, H., 1972, Géologie de Madagascar I. Les terrains sédimentaires: Annales Géologiques de Madagascar, v. 35, p. 1–463.

Brook, G.A., Burney, D.A., and Cowart, J.B., 1990, Desert paleoenvironmental data from cave speleothems with examples from the Chihuahuan, Somali-Chalbi, and Kalahari deserts: Palaeogeography, Palaeoclimatology, Palaeoecology, v. 76, p. 311–329.

Burney, D.A., 1993, Late Holocene environmental change in arid southwestern Madagascar: Quaternary Research, v. 40, p. 98–106.

Burney, D.A., Brook, G.A., and Cowart, J.B., 1994, A Holocene pollen record for the Kalahari Desert of Botswana from a U-series dated speleothem: The Holocene, v. 4, no. 3, p. 225–232.

Burney, D.A., James, H.F., Grady, F.V., Rafamantanantsoa, J.-G., Ramilisonina, Wright, H.T., and Cowart, J.B., 1997, Environmental change, extinction, and human activity: evidence from caves in NW Madagascar: Journal of Biogeography, v. 24, p. 755–767.

Burney, D.A., James, H.F., Burney, L.P., Olson, S.L., Kikuchi, W., Wagner, W.L., Burney, M., McCloskey, D., Kikuchi, D., Grady, F.V., Gage, R., and Nishek, R., 2001, Fossil evidence for a diverse biota from Kaua'i and its transformation since human arrival: Ecological Monographs, v. 71, no. 4, p. 615–641.

Burney, D.A., Burney, L.P., Godfrey, L.R., Jungers, W.L., Goodman, S.M., Wright, H.T., and Jull, A.J.T., 2004, A chronology for late prehistoric Madagascar: Journal of Human Evolution, v. 47, p. 25–63.

Carleton, M.D., and Goodman, S.M., 2003, *Macrotarsomys*, Big-footed mice, *in* Goodman, S.M., and Benstead, J.P., eds., The natural history of Madagascar, Chicago and London, University of Chicago Press, p. 1386–1388.

Carleton, M.D., Goodman, S.M., and Rakotondravony, D., 2001, A new species of tufted-tailed rat, genus *Eliurus* (Muridae: Nesomyinae), from western Madagascar, with notes on the distribution of *E. myoxinus*, *in* Proceedings of the Biological Society of Washington, v. 114, p. 977–987.

Decary, R., 1927, for the year 1926, Une mission scientifique dans le sud-est de Madagascar: Bulletin de l'Académie Malgache, v. 9 (nouvelle série), p. 79–86.

Decary, R., 1928, for the year 1927, Contribution à la botanique et la géologie de la région Fort-Dauphin — Andrahomana: Bulletin de l'Académie Malgache, v. 10 (nouvelle série), p. 13–18.

Decary, R., and André Kiener, 1971, Inventaire schématique des cavités de Madagascar: Annales de Spéléologie, v. 26, p. 31–46.

de Wit, M.J., 2003, Madagascar: Heads it's a continent, tails it's an island: Annual Review of Earth and Planetary Sciences, v. 31, p. 213–248.

Dorr, L.J., 1997, Plant collectors in Madagascar and the Comoro Islands, Royal Botanic Gardens, Kew.

Du Puy, B., Abraham, J.P., and Cooke, A.J., 1994, Les plantes, *in* Goodman, S.M., and Langrand, O., eds., Inventaire biologique Forêt de Zombitse. Recherches pour le développement, Série Sciences biologiques, No. Spécial, Antananarivo, Centre d'Information et de Documentation Scientifique et Technique, p. 15–29.

Eger, J.L., and Mitchell, L., 2003, Chiroptera, Bats, *in* Goodman, S.M., and Benstead, J.P., eds., The natural history of Madagascar, Chicago and London, University of Chicago Press, p. 1287–1302.

Emberton, K.C., 1997, Diversities and distributions of 80 land snail species in southeastern-most Madagascan rainforests, with a report that lowlands are richer than highlands in endemic and rare species: Biodiversity and Conservation, v. 6, p. 1137–1154.

Ganzhorn, J.U., 2006, Lemur biogeography, *in* Lehman, S.M., and Fleagle, J.G., eds., Primate biogeography, progress and prospects, New York, Springer, p. 229–254.

Geay, F., 1908, Rapport d'explorations aux régions Nord-Est, Sud-Sud-Ouest, Sud, et Sud-Sud-Est de Madagascar, 1904–1907: Privately printed by the author, 74 Avenue des Gobelins, Paris.

Godfrey, L.R., 1977, Structure and function in *Archaeolemur* and *Hadropithecus* (subfossil Malagasy lemurs): The postcranial evidence [Ph.D. thesis], Cambridge, Harvard University.

Godfrey, L.R., and Jungers, W.L., 2002, Quaternary fossil lemurs, *in* Hartwig, W.C., ed., The primate fossil record, New York, Cambridge University Press, p. 97–121.

Godfrey, L.R., Jungers, W.L., Wunderlich, R.E., and Richmond, B.G., 1997, Reappraisal of the postcranium of *Hadropithecus* (Primates, Indroidea): American Journal of Physical Anthropology, v. 103, p. 529–556.

Godfrey, L.R., Jungers, W.L., Simons, E.L., Chatrath, P.S., and Rakotosamimanana, B., 1999, Past and present distributions of lemurs in Madagascar, *in* Rakotosamimanana, B., Rasamimanana, H., Ganzhorn, J.U., and Goodman, S.M., eds., New Directions in Lemur Studies, New York, Kluwer Academic / Plenum Publishers, p. 19–53.

Godfrey, L.R., Simons, E.L., Jungers, W.L., DeBlieux, D.D., and Chatrath, P.S., 2004, New discovery of subfossil *Hapalemur simus*, the greater bamboo lemur, in western Madagascar: Lemur News, v. 9, p. 9–11.

Godfrey, L.R., Semprebon, G.M., Schwartz, G.T., Burney, D.A., Jungers, W.L., Flanagan, E.K., Cuozzo, F.P., and King, S.J., 2005, New insights into old lemurs: the trophic adaptations of the Archaeolemuridae: International Journal of Primatology, v. 26, p. 825–854.

Godfrey, L.R., Jungers, W.L., Burney, D.A., Vasey, N., Ramilisonina, Wheeler, W., Lemelin, P., Shapiro, L.J., Schwartz, G.T., King, S.J., Ramarolahy, M.F., Raharivony, L.L., and Randria, G.F.N., 2006a, New discoveries of skeletal elements of *Hadropithecus stenognathus* from Andrahomana Cave, southeastern Madagascar: Journal of Human Evolution, v. 51, p. 395–410.

Godfrey, L.R., Schwartz, G.T., Samonds, K.E., Jungers, W.L., and Catlett, K.K., 2006b, The secrets of lemur teeth: Evolutionary Anthropology, v. 15, p. 142–154.

Godfrey, L.R., Jungers, W.L., Schwartz, G.T., and Irwin, M.T., 2008, Ghosts and orphans: Madagascar's vanishing ecosystems, *in* Fleagle, J.G., and Gilbert, C.C., eds., Elwyn Simons, A Search for Origins, New York, Springer, p. 361–395.

Goodman, S.M., 2000, Description of the Reserve Naturelle Integrale d'Andohahela, Madagascar, and the 1995 biological inventory of the reserve: Fieldiana Zoology, new series, v. 94, p. 1–7.

Goodman, S.M., 2003, Checklist to the extant land mammals of Madagascar, *in* Goodman, S.M., and Benstead, J.P., eds., The natural

history of Madagascar, Chicago and London, University of Chicago Press, p. 1187–1190.
Goodman, S.M., and Rakotondravony, D., 1996, The Holocene distribution of *Hypogeomys* (Rodentia: Muridae: Nesomyinae) on Madagascar, *in* Lourenço, W.R., ed., Biogéographie de Madagascar, Paris, ORSTOM éditions, p. 283–293.
Goodman, S.M., and Rakotozafy, L.M.A., 1997, Subfossil birds from coastal sites in western and southwestern Madagascar: A paleoenvironmental reconstruction, *in* Goodman, S.M., and Patterson, B.D., eds., Natural change and human impact in Madagascar, Washington D.C., Smithsonian Institution Press, p. 257–279.
Goodman, S.M., and Soaramalala, V., 2005, A new species of *Macrotarsomys* (Rodentia: Muridae: Nesomyinae) from southwestern Madagascar, *in* Proceedings of the Biological Society of Washington, v. 118, p. 450–464.
Goodman, S.M., Vasey, N., and Burney, D.A., 2006, The subfossil occurrence and paleoecological implications of *Macrotarsomys petteri* (Rodentia: Nesomyidae) in extreme southeastern Madagascar: Comptes Rendus Palevol, v. 5, p. 953–962.
Goodman, S.M., Raselimanana, A.P., and Wilmé, L. (eds), 2007, Inventaires de la faune et de la flore du couloir forestier d'Anjozorobe-Angavo. Recherches pour le Developpement, Série Sciences Biologique no. 24. Centre d'Information et de Documentation Scientifique et Technique, Antananarivo, Madagascar.
Goodman, S.M., Vasey, N., and Burney, D.A., 2007, Description of a new species of subfossil shrew-tenrec (Afrosoricida: Tenrecidae: *Microgale*) from cave deposits in southeastern Madagascar, *in* Proceedings of the Biological Society of Washington, v. 320, p. 367–376.
Grandidier, A., 1885, Histoire de la géographie, Paris, Imprimerie Nationale.
Grandidier, G., 1902, Observations sur les lémuriens disparus de Madagascar: Collections Alluaud, Gaubert, Grandidier: Bulletin du Muséum d'Histoire Naturelle, v. 8, p. 497–505, 587–592.
Grandidier, G., 1903, Description de l'*Hypogeomys australis*, une nouvelle espèce de rongeur subfossile de Madagascar: Bulletin du Muséum d'Histoire Naturelle, Paris, v. 9, p. 13–15, with figures.
Grandidier, G., 1928, Description de deux nouveaux mammifères insectivores de Madagascar: Bulletin du Muséum National d'Histoire Naturelle, Paris, v. 34, p. 63–70.
Hapke, A., Fietz, J., Nash, S.D., Rakotondravony, D., Rakotosamimanana, B., Ramanamanjato, J.-B., Randria, G.F.N., and Zischler, H., 2005, Biogeography of dwarf lemurs, Genetic evidence for unexpected patterns in southeastern Madagascar: International Journal of Primatology, v. 26, p. 873–901.
Hearty, P.J., Kaufman, D.S., Olson, S.L., and James, H.F., 2000, Stratigraphy and whole-rock amino acid geochronology of key Holocene and last interglacial carbonate deposits in the Hawaiian Islands: Pacific Science, v. 54, p. 423–442.
Heim de Balsac, H., 1972, Insectivores, *in* Battistini, R., and Richard-Vindard, G., eds., Biogeography and ecology of Madagascar, The Hague, Dr. W. Junk, p. 629–660.
Irwin, M.T., Johnson, S.E., and Wright, P.C., 2005, The state of lemur conservation in south-eastern Madagascar: population and habitat assessments for diurnal and cathemeral lemurs using surveys, satellite imagery and GIS: Oryx, v. 39, p. 204–218.
Jenkins, P.D., 2003, *Microgale*, Shrew tenrecs, *in* Goodman, S.M., and Benstead, J.P., eds., The natural history of Madagascar, Chicago and London, University of Chicago Press, p. 1273–1278.
Jungers, W.L., 1976, Osteological form and function: The appendicular skeleton of *Megaladapis*, a subfossil prosimian from Madagascar (Primates, Lemuroidea), [Ph.D. thesis], Ann Arbor, University of Michigan.
Krause, D.W., O'Connor, P.M., Rasoamiaramanana, A.H., Buckley, G.A., Burney, D.A., Carrano, M.T., Chatrath, P.S., Flynn, J.J., Forster, C.A., Godfrey, L.R., Jungers, W.L., Rogers, R.R., Samonds, K.E., Simons, E.L., and Wyss, A.R., 2006, The importance of keeping the island's vertebrate fauna in the public domain: Madagascar Conservation & Development, v. 1, p. 43–47.
Lamberton, C., 1938, for the year 1937. Contribution à la connaissance de la faune subfossile de Madagascar, Note III, Les Hadropithèques: Bulletin de l'Académie Malgache (nouvelle série), v. 20, p. 127–170.
Langrand, O., and Goodman, S.M., 1997, Brève description biologique de la region des forêts de Vohibasia et d'Isoky-Vohimena, *in* Langrand, O., and Goodman, S.M., eds., Inventaire biologique Forêt de Vohibasia et d'Isoky-Vohimena, Recherches pour le développement, Série Sciences biologiques, No. 12, Antananarivo, Centre d'Information et de Documentation Scientifiique et Technique, p. 11–28.
Lemelin, P., Hamrick, M.W., Godfrey, L.R., Jungers, W.L., and Burney, D.A., 2006, New hand bones of *Hadropithecus stenognathus*: Implications for the paleobiology of the Archaeolemuridae: American Journal of Physical Anthropology, v. Suppl. 42, p. 120.
Lemelin, P., Hamrick, M.W., Richmond, B.G., Godfrey, L.R., Jungers, W.L., and Burney, D.A., 2008, New hand bones of *Hadropithecus stenognathus*: Implications for the paleobiology of the Archaeolemuridae: Journal of Human Evolution, v. 54, p. 405–413.
Lorenz von Liburnau, L., 1899, Herr Custos Dr. Ludwig v. Lorenz berichtet über einen fossilen Anthropoiden von Madagascar: Anzeiger der Kaiserlichen Akademie der Wissenschaften in Wien, v. 36, p. 255–257.
Lorenz von Liburnau, L., 1901, Über einige Reste ausgestorbener Primaten von Madagaskar: Denkschrift der Kaiserlichen Akademie der Wissenschaften in Wien, v. 70, p. 1–15.
Lorenz von Liburnau, L., 1902, Über *Hadropithecus stenognathus* Lz. Nebst bemerkungen zu einigen anderen austestorbenen Primaten von Madagascar: Denkschrift der Kaiserlichen Akademie der Wissenschaften in Wien, v. 72, p. 243–254.
Lorenz von Liburnau, L.R., 1905, *Megaladapis edwardsi* G. Grandidier: Denkschrift der Kaiserlichen Akademie der Wissenschaften in Wien, v. 77, p. 451–490.
MacPhee, R.D.E., 1987, The shrew tenrecs of Madagascar: systematic revision and Holocene distribution of *Microgale* (Tenrecidae, Insectivora), New York: American Museum of Natural History (American Museum Novitates, No. 2889).
Major, C.I.F., 1899, On subfossil mammals from Madagascar, *in* Proceedings of the Zoological Society of London, v. 64, p. 988–989.
Masse, W., Bryant, E., Gusiakov, V., Abbott, D., Rambolamana, G., Raza, H., Courty, M., Breger, D., Gerard-Little, P., and Burckle, L., 2006, Holocene Indian Ocean cosmic impacts: The mega-tsunami chevron evidence from Madagascar [abs.]: Eos (Transaction of the American Geophysical Union), v. 87, p. 43B–1244.
Perez, V.R., Godfrey, L.R., Nowak-Kemp, M., Burney, D.A., Ratsimbazafy, J., and Vasey, N., 2005, Evidence of early butchery of giant lemurs in Madagascar: Journal of Human Evolution, v. 49, p. 722–742.
Ryan, J.M., 2003, *Nesomys*, Red forest rat, *voalavo mena*, *in* Goodman, S.M., and Benstead, J.P., eds., The Natural History of Madagascar, Chicago and London, University of Chicago Press, p. 1388–1389.
Ryan, T.M., Burney, D.A., Godfrey, L.R., Göhlich, U., Jungers, W.L., Vasey, N., Ramilisonina, Walker, A., and Weber, G., 2008, A reconstruction of the Vienna skull of *Hadropithecus stenognathus*: American Journal of Physical Anthropology, v. suppl. 46, p. 184.
Sikora, F., 1897, Sept ans à Madagascar: Bulletin de géographie d'Aix-Marseille, v. 21, p. 163–174, 277–285.
Simons, E.L., Burney, D.A., Chatrath, P.S., Godfrey, L.R., Jungers, W.L., and Rakotosamimanana, B., 1995, AMS ^{14}C dates for extinct lemurs from caves in the Ankarana Massif, northern Madagascar: Quaternary Research, v. 43, p. 249–254.
Stuiver, M., Reimer, P.J., Bard, E., Beck, J.W., Burr, G.S., Hughen, K.A., Kromer, B., McCormac, F.G., Plicht, J.v.d., and Spurk, M., 1998, INTCAL98 ^{14}C, Radiocarbon v. 40, p. 1041–1083.
Tattersall, I., 1973, Cranial anatomy of the Archaeolemurinae (Lemuroidea, Primates): Anthropological Papers of the American Museum of Natural History, v. 52, p. 1–110.
Tattersall, I., 1982, The primates of Madagascar, New York, Columbia University Press.
Thalmann, U., 2003, *Avahi*, Woolly lemurs, *Avahy*, *Fotsy-fe*, *Ampongy*, *Tsarafangitra*, *Dadintsifaky*, *in* Goodman, S.M., and Benstead, J.P., eds., The Natural History of Madagascar, Chicago and London, University of Chicago Press, p. 1340–1342.
Thevenin, A., 1907, Note sur des fossiles rapportés de Madagascar par M. Geay: Bulletin du Muséum d'Histoire Naturelle, v. 13, p. 85–88.
Walker, A.C., 1967, Locomotor adaptation in recent and fossil Madagascar lemurs, [Ph.D. thesis], London, University of London.
Walker, A., 2002, Looking for lemurs on the Great Red Island, *in* Bowen, T., ed., Backcountry Pilot: Flying Adventures of Ike Russell, Tucson, University of Arizona Press, p. 99–104.
Zapfe, H., 1971, Catalogus Fossilium Austriae, Ein systematisches Verzeichnis aller auf österreichischem Gebiet festgestellten Fossilien, Heft. XV: Index Palaeontologicorum Austriae, Vienna, Springer-Verlag.

Appendix 1: History of the exploration of Andrahomana

1840	A map of the southern coast of Madagascar published by Leguével de Lacombe (later reproduced in A. Grandidier, 1885) shows a village at the Bay of Andrahomana labeled "Andrahoum."
1855	Marguin (cited by Grandidier, 1885) publishes a map of the site of the caverns ("Cap Andavaka" – in Malagasy, the "place of the caverns") and a detailed map of the "Baie d'Andrahomana." Neither of Marguin's maps is reproduced in Grandidier (1885).
1885	Alfred Grandidier (1885) briefly describes the existence of caverns on the southern coast of Madagascar in his "Histoire de la géographie." In 1892 this book was revised, reprinted and issued as the first volume of his monumental "Histoire Physique, Naturelle et Politique de Madagascar." Sometimes credited with having discovered the caves (e.g., see Decary, 1927), Alfred Grandidier actually learned of them from the Malagasy and through the experience of other westerners who had traveled to Madagascar in some cases well before Grandidier's first trip there (in 1865). Grandidier (1885) states that Cap Andavaka was known to 16th century European explorers of Madagascar.
1899	Austrian pipe-carver and naturalist, Franz (or François) Sikora, and a team of some twenty Malagasy workers, excavate Andrahomana Cave for a period of 18 days. Specimens of extinct lemurs and associated fauna collected during this expedition were sent to the Naturhistorisches Museum in Vienna and to the British Museum of Natural History in London. Sikora apparently left no written records documenting the exact location of his dig within the cave, nor did he make a log of stratigraphic associations. His most detailed treatment of his explorations, "Sept Ans à Madagascar," was published two years prior to his expedition to Andrahomana (Sikora, 1897). However, in terms of the sheer volume of specimens belonging to subfossil lemurs, Sikora's osteological collection from Andrahomana remains unsurpassed by those of subsequent explorers. Among Sikora's discoveries were the first complete skull and hemimandible, plus associated postcranial bones, of *Archaeolemur majori* (sent to the Natural History Museum, London) as well as a nearly complete skull and other skeletal elements of *Hadropithecus stenognathus* (sent to the Vienna Naturhistorisches Museum). Sikora's expedition to Andrahomana was briefly documented by Alluaud (1900). The specimens that Sikora collected there were studied initially by C.I. Forsyth Major (1899) and by Lorenz von Liburnau (1899, 1901, 1902, 1905), and later by Walker (1967), Tattersall (1973, 1982), Jungers (1976), and Godfrey (1977). Sikora also collected over 40 specimens of an extinct species of *Hypogeomys* (see below), now at the British Museum (Natural History).
1900	French entomologist Charles Alluaud conducts the first of a series of expeditions to Andrahomana and other localities in southern Madagascar. Only his first expedition (August 21–August 27, 1900) is well documented in the literature (Alluaud 1900, a letter dated August 30, 1900 and addressed to Guillaume Grandidier). On this expedition, Alluaud was accompanied by a French soldier, Lieutenant Gaubert. The two traveled together from the Poste de Manambaro to Ranopiso, and then to the rat-infested, recently constructed, Poste d'Andrahomana, located on a hill over the small peninsula bordering the Baie d'Andrahomana. Alluaud's (1900) letter to Grandidier describes the difficulty the two experienced in gaining access to the cave as well as various other frustrations. He complains that the cave had been completely excavated (*tout fouillé*) by his predecessor, Franz Sikora. It is noteworthy, however, that Alluaud and Gaubert spent only three days (August 23–25) actually excavating in or near the cave, and they had hired Malagasy helpers on only two of them. The team found relatively few subfossil specimens (although there were some giant tortoise and extinct lemur bones in the lot). Part of Alluaud's contribution was the construction of a path for easier access to the cave, and a botanical survey. The bounty of this first expedition was sent to the Muséum National d'Histoire Naturelle in Paris in 1900.
1901–02	On separate occasions, Charles Alluaud, Lieutenant Gaubert and Guillaume Grandidier (the son of Alfred) visit or revisit Andrahomana, to collect more specimens of extinct lemurs. These expeditions were apparently more successful than Alluaud and Gaubert's first one, but they are poorly described in the literature. Separate Alluaud, Gaubert, and G. Grandidier collections were sent to Paris in the spring of 1902 and were described by G. Grandidier (1902). No *Hadropithecus stenognathus* was listed as having been collected by any of these explorers. However, some *Hadropithecus* bones that may have come from Andrahomana are in the collections of the Paris museum (Godfrey et al., 2006a). Prize specimens of these missions were the types (MNHN MAD 1646 and MNHN MAD 1647) of a new species of extinct rodent, *Hypogeomys australis*, found by Alluaud and initially described by Grandidier (1903) (Goodman and Rakotondravony, 1996).
1902	Franz Sikora dies at the age of 39, fewer than three years after he had led his pioneering expedition to Andrahomana (Zapfe, 1971).

Appendix 1. Continued.

1906	French pharmacist and naturalist Martin François Geay collects bones of lemurs, rodents, and bats at the caverns of Andrahomana. Geay had studied natural history in France under the tutelage of Alphonse Milne-Edwards. He spent several years in Madagascar (1904–1907) collecting plants, wood, fossils, mollusks, fish, birds, reptiles, and rocks for the Paris natural history museum (Thevenin, 1907; Dorr, 1997). During that time, he sent 70 crates containing about 14,000 specimens to Paris. In his privately published book, Geay (1908, p. 99–100) briefly describes his trip to Andrahomana, stating only that he collected lemur, rodent, and bat bones there, and describing the terrestrial deposits into which the cave was cut. Geay also offers the following explanation for the name of the bay, Andrahomana (literally, ''an'' = at or where, ''rano'' = water, ''homana'' = eaten: ''where the water is devoured''). At the end of Andrahomana Bay is a meandering brook that winds around tall, gloomy, and entirely denuded rocks bordering the ocean. The water of the brook disappears into (i.e., is eaten or consumed by) the sands of the beach.
1906?	Gaston-Jules Decorse (a French military doctor who collected plants, insects and fossils for the natural history museum in Paris) explores the region of Cap Andavaka (Decary, 1927, for the year 1926). Decorse was very interested in terrestrial mollusks and he collected specimens in the calcareous dunes near Andrahomana. Thevenin (1907) describes several explorers, including Grandidier and Decorse, collecting *Aepyornis* eggshell in the region.
1926	French military officer and naturalist Raymond Decary leads a scientific exploratory expedition to southern Madagascar (including Andrahomana) for the Museum National d'Histoire Naturelle (Paris). This mission began in June, 1926. Decary (1927) found little here in the way of giant subfossils, but he did find numerous bones of micromammals and other small vertebrates. He also published a survey of the plants and geology of the region (Decary, 1928).
1927	Decary sends some of the specimens that he collected at Andrahomana to Grandidier for study. Over the following 12 years, both Grandidier and Decary dispatch specimens from Andrahomana to the Museum of Comparative Zoology, Harvard University. These include some *Lemur catta*, *Microcebus* sp. (probably *M. griseorufus*), and some insectivores (now recognized as *Microgale principula* and *Geogale aurita*).
1928	Guillaume Grandidier (1928) names several new species of insectivores on the basis of specimens from Andrahomana Cave. He gave the name *Paramicrogale decaryi* to specimens with a relatively short and wide skull, and *Cryptogale australis* to others with a long and narrow skull. *Paramicrogale decaryi* was later synonymized with *Microgale* by Heim de Balsac (1972) and then with *M. principula* by MacPhee (1987). *Cryptogale australis* was later synonymized with *Geogale aurita* by Heim de Balsac (1972).
1964	René Battistini (1964) publishes his dissertation monograph on the geomorphology of southern Madagascar, with notes on the geology of Andrahomana.
1966	Bush pilot Ike Russell and his wife Jean accompany Alan Walker and Paul Martin on a flight from mainland Africa to Antananarivo (Walker, 2002; Paul Martin unpublished notes), and then to a number of subfossil sites, including Andrahomana. To reach Andrahomana, Russell landed his small aircraft on the dry bed of Lake Erombo, several miles from the cave. From there, Walker and Martin hiked to the cave while the Russells remained with their plane. Once in the cave, Walker and Martin found a piece of the scapula and a finger bone of *Megaladapis edwardsi*, as well as pieces of a smashed carapace and plastron of a giant tortoise that had fallen into the cave from above. They could only visit the cave for a short period before having to return first by foot to Erombo and then by plane to Fort Dauphin.
1971	Raymond Decary and André Kiener (1971) publish an inventory of caves of Madagascar.
1983	Ross MacPhee, Elwyn Simons, Prithijit Chatrath, Neil Wells, and Martine Vuillaume-Randriamanantena visit the cave August 18 for a few hours in connection with a Duke University Primate Center expedition to southern Madagascar. Although impressed with the beauty of the area, the group found only ''very recent bones of *Microcebus*, *Propithecus*, *Rattus*, birds, and turtles. A few hand/foot bones of large size were discovered…they could be those of a giant lemur'' (R. MacPhee, pers. comm., 2007).
2000	David Burney, Malagasy students, and local guides make a reconnaissance of the cave August 24–27, conducting a small controlled excavation at AHA-B and making surface collections and sediment borings.
2003	July 16 to August 8, Burney makes expedition to Andrahomana accompanied by the coauthors of this paper and local guides. Group undertakes mapping, and excavates sites AHA-F and AHA-I.
2006	Laurie Godfrey and colleagues revise postcranial attributions for *Hadropithecus stenognathus* on the basis of associated skeletal materials found at AHA-I in 2003 (Godfrey et al., 2006a). Collaborations with Steve Goodman lead to naming a subfossil species of shrew-tenrec (*Microgale macpheei*; Goodman, Vasey, and Burney, 2007) and publishing the first known fossil occurrence of the recently described nesomyid rodent *Macrotarsomys petteri* (Goodman et al., 2006).

P. E. Van Beynen, L. Soto, and J. Polk – Variable calcite deposition rates as proxy for paleo-precipitation determination as derived from speleothems in Central Florida, U.S.A. *Journal of Cave and Karst Studies,* v. 70, no. 1, p. 25–34.

VARIABLE CALCITE DEPOSITION RATES AS PROXY FOR PALEO-PRECIPITATION DETERMINATION AS DERIVED FROM SPELEOTHEMS IN CENTRAL FLORIDA, U.S.A.

PHILIP E. VAN BEYNEN*[,1], LIMARIS SOTO[2], AND JASON POLK[1]

Abstract: Deposition rates derived from speleothems have been shown to be a useful paleoclimatic proxy. Past studies have shown that the most common climatic parameter measured by variable deposition rates is precipitation, where increased precipitation leads to increased calcite deposition. This was the premise of our study, where three Floridian stalagmites' deposition rates were measured and compared to paleohydrologic indicators taken from the sample or from other regional records. Deposition rates were measured by determining the volume of calcite precipitated between TIMS U-series dates ($mm^3\ yr^{-1}$), thereby accounting for morphological changes on the stalagmite over its depositional history. Most prior research relied on a simple linear interpolation between known ages to calculate rate ($mm\ yr^{-1}$). Results show three distinct periods of increased deposition for our stalagmites centered on 2.0, 1.25 and 0.5 ka BP. A comparison with Mg/Ca and Sr/Ca ratios and calcite deposition tentatively shows elevated elemental ratios during the three aforementioned periods. Elevated trace element ratios have been shown to be correlated with increased residence time of percolation waters in the overlying bedrock above caves and consequently decreased rainfall. To corroborate this finding, paleo-precipitation records from Little Salt Spring, Florida and Lake Miragoane, Haiti, were examined for coeval arid periods with our stalagmites. Both records do possess similar dry periods and provide added support that the region experienced periods of abrupt aridity over the last two millennia. The combined effect of a change in the mean position of the Intertropical Convergence Zone and the easterly winds associated with the North Atlantic High appear to be the major causes for these times of aridity.

INTRODUCTION

The deposition rates of speleothems can provide information about paleoclimatic variations, including precipitation, temperature, and soil activity, above a cave (Kaufmann and Dreybrodt, 2004; White, 2004). The rate of speleothem deposition is determined by soil carbon dioxide concentration, drip rate, and temperature, all of which are climate related and can affect the rate and shape of deposition (Dreybrodt, 1999). Hiatuses in a speleothem can indicate periods of climate change that include glacial periods, droughts, and changes in the hydrologic pattern of water flow. Faster deposition rates can be indicative of a warmer, wetter climate in the area, whereas slower deposition rates can result from cooler, drier conditions above the cave (Hennig et al., 1983; Musgrove et al., 2001; van Beynen et al., 2004).

The deposition rate of speleothems is a function of supersaturation (P_{CO_2}) of percolation waters and drip rate (rainfall amount) (Baker et al., 1998). The deposition rate of stalagmites can then be used as a paleo-environmental proxy for surface precipitation (Baker et al., 1993; Genty and Quinif, 1996; Holmgren et al., 1999; Qin et al., 1999). The determination of speleothem deposition rates has evolved to a high level of accuracy due to radiogenic dating methods, such as U-series TIMS mass spectrometry (Li et al., 1989; Dorale et al., 1992; Gascoyne, 1992; Musgrove et al., 2001). Through the use of accurate U/Th dates combined with speleothem lengths, deposition rates can be calculated with high precision, also providing evidence of hiatuses and deposition rate variability (Dreybrodt, 1999).

The purpose of this study is to develop and improve the understanding of the paleoclimate of Florida, with emphasis on whether speleothems can record hydrologic responses to changing atmospheric circulation patterns that affect the Florida Peninsula. The approach taken in this study was to measure shifts in speleothem deposition rate and determine the paleoclimatic significance of those shifts. Hence, we tested the following hypothesis: Increased deposition rates derived from speleothems are indicative of wetter conditions above the cave.

To test such a hypothesis requires an accurate chronology of these changes in calcite precipitation rate. Uranium-series disequilibria dating is the method used here to achieve this goal. Many studies have demonstrated that the speleothems provide reliable chronologies using the U-

* Corresponding author.
[1] Department of Environmental Science and Policy, University of South Florida, 4202 E Fowler Ave, NES 107, Tampa, FL 33620, vanbeyne@cas.usf.edu
[2] Department of Geology, University of South Florida, 4202 E Fowler Ave, Tampa, FL 33620

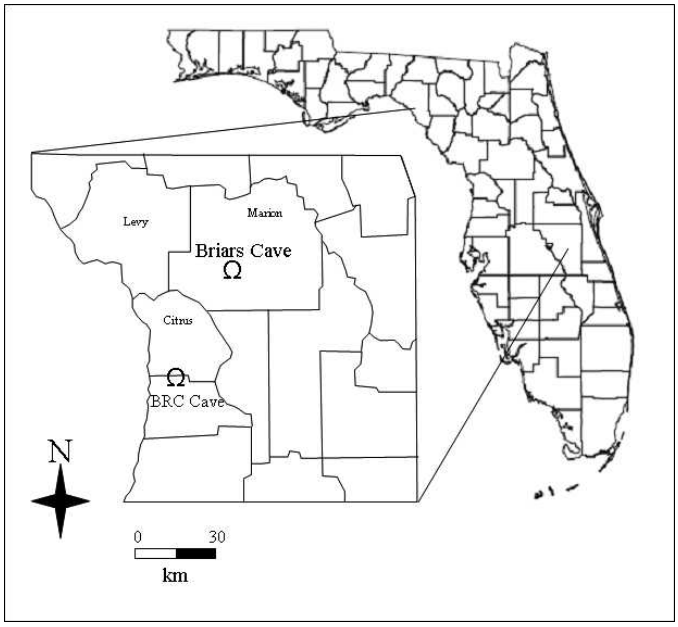

Figure 1. Location of study sites, Briars Cave and Brown Rat Cave, in relation to one another.

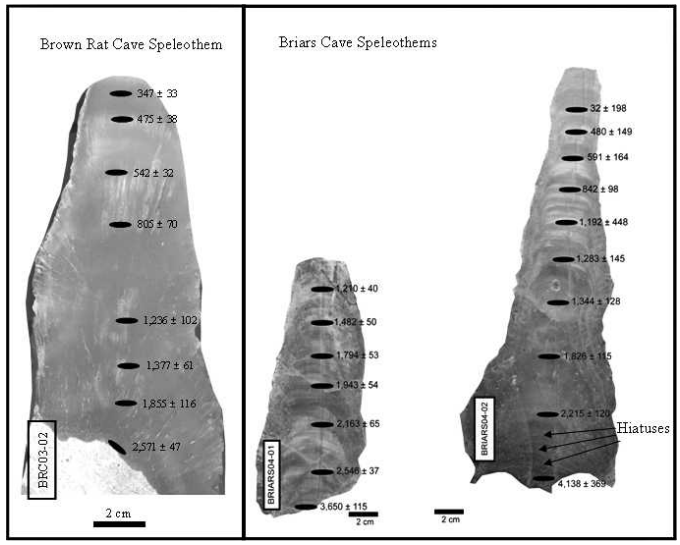

Figure 2. Photographs of the three speleothems used in this study.

series method (Harmon et al., 1978; Dorale et al., 1992; Gascoyne, 1992; Frumkin and Stein, 2004; Lachneit et al., 2004; Polyak et al., 2004). To fully address the hypothesis, the volume of calcite precipitated between these dates for multiple stalagmites will determine the variable deposition rate for each speleothem.

STUDY AREA

The study area consists of two caves, Brown Rat Cave (BRC), in Hernando County, and Briars Cave in Marion County, both in Florida (Fig. 1). They are located in the Brooksville Ridge section of the Ocala Arch that contains sinkholes, dry karst valleys, and interfluvial hills (Reeder and Brinkmann, 1998). The geology in the region is dominated by a series of carbonates that include the Eocene Ocala (location of both caves) and Oligocene Suwannee Limestones, which are unconformably overlain by the Hawthorn Group characterized by carbonates interspersed with siliclastics and phosphorite redeposition forming admixtures with dolomite, quartz sand, and Mg-rich clays (Scott, 1997). Approximately two meters of Pleistocene-aged quartz sands overlie these units in most parts of the region, although they drain rapidly.

With a length of ~1 km, BRC in Brooksville Ridge is one of the longest dry caves in Florida, and has a single, man-made entrance. Consequently, relative humidity levels in the cave would have been at ~100% until the entrance was created. The cave developed within the Ocala Limestone, and the vegetation above the cave is characterized as hardwood hammocks populated by oak, hickory and maples (Armstrong et al., 2003). The average temperature of the Brooksville Ridge area is 21.3 °C, and the average total precipitation is 1356 mm per year (Southeast Regional Climate Center). The stalagmite BRC03-02 was collected from this cave, which does not flood during hurricanes (as in Hurricanes Jeanne and Frances of 2004) or thunderstorms.

Briars Cave is located on the southern outskirts of Ocala. The cave underlies a low hill between two sinkholes. Briars Cave trends NE-SW and consists of a dry upper level and a partially flooded lower passage (Florea et al., 2003). The cave is approximately 1 km long, making it one of the longest caves in the state of Florida, with only one small tight entrance. The vegetation in the vicinity of the cave is characterized by hardwood species, including oak. The average temperature of Marion County is 22 °C, and the average annual precipitation is 1330 mm (Southeast Regional Climate Center). Two stalagmite samples, BRIARS04-01 and BRIARS04-02, were collected from the same area of the cave. A Hendy test (Hendy, 1971), undertaken for the latter of the two speleothems to determine whether the isotopes were deposited in equilibrium with the ambient waters, showed relative humidity levels in the cave would have remained close to ~100%.

METHODS

SAMPLE COLLECTION

Upon collection, the three stalagmites were cut vertically along their depositional axes, and polished to clarify the positioning of the lamina. Calcite samples of 250 mg were collected for U-series dating from all speleothems using a dental-bit equipped Dremel® tool. Samples were drilled at approximately 20–30 mm intervals along the growth axis of the stalagmite (Fig. 2). Exactly equal

increments could not be attained in instances where the potential sampling area possessed a small void, or a dramatic color change or possible dirty calcite. We tried to sample from clear, homogenous calcite, which could not be achieved at a predetermined distance from the stalagmite base.

U-series Dating

Successful dating of speleothems by U/Th methods depends on satisfying three criteria: 1) the specimen must contain a measurable amount of uranium (>0.02 ppm) and thorium; 2) the specimen must contain negligible initial ^{230}Th. This can be measured through the presence of the isotope ^{232}Th because it will be present in any thorium-bearing minerals that may occur in the insoluble detritus, but is not part of the decay chain; and 3) the specimen must not have undergone dissolution and re-crystallization that would alter the initial U/Th isotopic composition (Latham and Schwarcz, 1992; White, 2004).

The samples were analyzed at the Radiogenic Laboratory at the University of New Mexico. U and Th are measured on a Micromass Sector 54 thermal ionization mass spectrometer with a high-abundance sensitivity filter (Lachniet et al., 2004). All isotopes of interest were measured on an ion-counting Daly multiplier with abundance sensitivity in the range of 20 ppb at one mass unit in the mass range of U and Th, requiring very little background correction, even for samples with large ^{232}Th content. U isotopic standards, such as NBL-112, were measured along with samples. Typical analytical uncertainties are in the range of 0.2% for U isotope composition, similar or somewhat lower precision for Th, depending on the age and size of the sample measured. A detailed account of the technique can be found in Polyak and Asmerom (2001).

Deposition Rates

When calculating deposition rates, it is important to consider that the speleothem morphology is not a constant linear relation (Franke, 1965; Curl, 1973; Gams, 1981; Baldini, 2001). Because the shape of the stalagmite can vary significantly over its depositional history, we calculated the deposition rates as a volume and not simply linear distance of calcite deposition between known ages. This approach of measuring speleothem deposition rate is similar one taken by Baldini (2001). Half of the stalagmite was photocopied to have a one-dimensional picture of the sample. Deposition lines were draw onto the copy to mark the different visible layers between the speleothem. Because the stalagmites were already dated, each known date was marked on the photocopy. With the dates and the exact location of them on the speleothem, a quantitative approach was applied. We used the formula of the frustum of a cone

$$V = \frac{1}{3}\pi h(r^2 + rR + R^2) \quad (1)$$

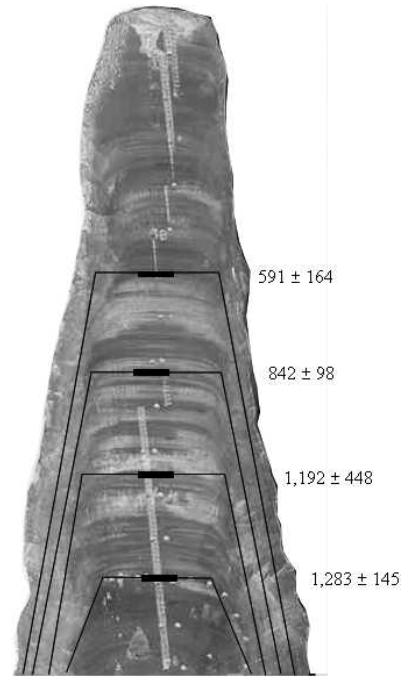

Figure 3. Diagram showing how the frustum of a cone is fitted to the growth layers for part the upper portion of BRIARS04-02.

to calculate the volume (mm^3) of calcite deposited between dated horizons. Figure 3 shows how the cross-section of the frustum of a cone is fitted to a portion of BRIARS04-02 between known dates. On occasion, to replicate the deposition between two dates, several different sized frustums had to be used. To calculate the deposition rate (calcite deposition), the volume of calcite was divided by the time of deposition (mm^3 yr^{-1}).

Results

U-series Dating

The entire suite of TIMS U-series dates for all three speleothems used in this study is presented in Table 1. All ages are reported as years before present. The speleothems meet all three criteria mentioned above. The uranium and thorium levels are sufficient for dating. All Th/U ages are in correct stratigraphic order (Fig. 4). This result suggests that all the speleothems remained closed systems (i.e., no dissolution or recrystallization) for their entire depositional histories; hence, no uranium migration occurred within any speleothem. The ^{230}Th/^{232}Th ratios (Table 1) are indicative of very little detrital Th being present in any of the samples. Clean calcite ^{230}Th/^{232}Th ratios are generally greater than 50, and the values for BRC and BC samples are well above that threshold value, some values approaching 1,136.

Depositional trends for each speleothem show a linear relationship for the majority of the growth period (Fig. 4). Only during the first 30 mm did each speleothem deviate

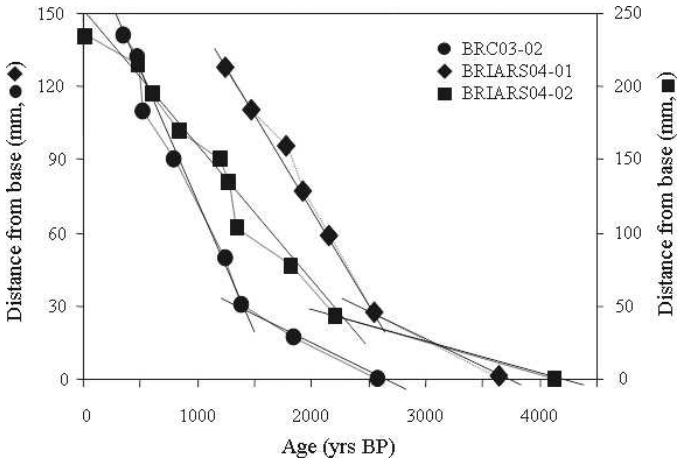

Figure 4. Age vs. depth plot for the Floridian speleothems. Solid lines show the linear trend for each speleothem.

from this linearity. Such deviation represents a slower deposition rate, which may be caused by the available calcite being spread over a larger area. For the carrot type stalagmites used in this study, such an initial slower deposition rate is common.

DEPOSITION RATES

The deposition rates calculated using the U-series dates are presented in Table 2. Eight dates in stratigraphic order were used to develop deposition rates for sample BRC03-02 (Fig. 5a). This stalagmite grew from around 2.6 to 0.35 ka BP. The average deposition rate (calcite deposition) for this sample was 375 $mm^3\ yr^{-1}$. In the early stage of accumulation, the deposition rate was 63 $mm^3\ yr^{-1}$, a very low calcite accumulation for the speleothem. A significant change occurred from 1.8 to 1.3 ka BP when the rate increased with a deposition rate of 337 $mm^3\ yr^{-1}$. A continued increase in deposition rate occurred from 1.3 to 1.2 ka BP, when calcite accumulated at 326 $mm^3\ yr^{-1}$ (Fig. 5a). At around 0.5 ka BP, the deposition rate increased considerably, being close to 1164 $mm^3\ yr^{-1}$, the highest rate measured in any speleothem in this study.

Speleothems collected from Briars Cave were also analyzed for deposition rates. For BRIARS04-01 seven dates in stratigraphic order establish that the speleothem grew from 3.6 to 1.2 ka BP (Table 2). The average rate of deposition for the speleothem was 224 $mm^3\ yr^{-1}$ (Fig. 5a). The lowest rate was from ~3.6 to 2.5 ka BP, attaining a value of 40 $mm^3\ yr^{-1}$. The stalagmite deposition from 2.1 to 1.9 ka BP increased considerably, averaging ~385 $mm^3\ yr^{-1}$, the highest rate for this speleothem, although it was followed by another rapid period of calcite deposition from 1.9 to 1.8 ka BP, with a rate of 366 $mm^3\ yr^{-1}$. A decrease in deposition rate occurred after 1.8 to 1.2 ka BP where the values diminished to nearly half of the previous ones.

Stalagmite BRIARS04-02 has ten dates in stratigraphic order showing that it has grown continuously from 4.5 ka BP until the present (Table 2). However, the youngest date of 32 years ±198 has such a high error compared to the actual date (Fig. 5a) that it will not be included in any further analysis. The average rate of deposition for this sample was 542 $mm^3\ yr^{-1}$, the highest of all the speleothems. A slow deposition rate of 51 $mm^3\ yr^{-1}$ was recorded at the base of the stalagmite from 4.1 to 2.2 ka BP. However, with only two dates delineating this 2,000 year period, it is not possible to identify any periods of more rapid calcite deposition that may have occurred during speleothem growth. BRIARS04-02 contains a few possible hiatuses during this period, which would account for the low deposition rates. Three distinct horizons are present within this zone that are not found in any other intervals for this or the other speleothems. Only with more frequent dating could the timing of these potential hiatuses be resolved. At approximately 2.2 to 1.8 ka BP, a significant increase in deposition rate was recorded; this is consistent with an increased deposition rate recorded at the same time for BRIARS04-01. The rate was the highest from 1.35 to 1.3 ka BP, attaining a value of 972 $mm^3\ yr^{-1}$. Another major change was recorded from 0.6 to 0.5 ka BP, with a deposition rate of 915 $mm^3\ yr^{-1}$: this increase in deposition rate was also recorded in the speleothem BRC03-02.

As aforementioned, most speleothem studies examining deposition rates calculate the rate in mm yr^{-1}, as in the number of mm calcite deposited between each date. To show how this technique may give an unrealistic impression of how quickly a speleothem was deposited, Figure 5b allows a comparison between the volumetric ($mm^3\ yr^{-1}$) and linear (mm yr^{-1}) methods. It is readily apparent that the linear method tends to exaggerate deposition rate as seen in BRC03-02 at ~0.5 ka BP and for BRIARS04-02 at ~1.3 ka BP. The volumetric technique accentuates episodes of augmented deposition but also periods that are not apparent in the linear method. For example, BRC03-02 has a noticeable increase at ~1.3 ka BP that cannot be seen in Figure 5a.

DISCUSSION

Our initial hypothesis stated that increased deposition rates were indicative of wetter conditions above the cave. This hypothesis is derived from previous paleoclimate studies using speleothems that showed the rate of deposition is controlled by the amount of precipitation falling above the cave, such that an increase in precipitation leads to more speleothem growth (Hennig et al., 1983; Lauritzen and Lundberg, 1999). However, not all studies support this conclusion, with some showing that drier conditions can lead or have led to an increase in deposition rate (Denniston et al., 1999; Fairchild et al., 2000). While our hypothesis proposes the first scenario, we tested it by correlating the deposition rates outlined above with trace

Table 1. U-series dates for Floridian speleothems. All ages assuming a $^{230}Th/^{232}Th$ initial ratio of 10 ± 2 ppm.

Sample	Distance from base (mm)	U (ppm) Error × 10^{-3}	Th (ppm) ×10^{-3} Error × 10^{-5}	$^{230}Th/^{232}Th$	$^{234}U/^{238}U$ Error × 10^{-3}	$^{230}Th/^{238}U$ Error × 10^{-3}	Uncorrected Age (yr B.P.)	Corrected Age (yr B.P.)
Briars04-01	130	1.031 ± 0.6	8.4 ± 0.1	233.8 ± 3.9	1.008 ± 0.5	0.012 ± 0.1	1,263 ± 38	1,210 ± 40
	110	1.249 ± 1.0	2.5 ± 0.2	1136.1 ± 102.2	1.010 ± 0.5	0.014 ± 0.1	1,495 ± 50	1,482 ± 50
	95	1.201 ± 0.7	5.5 ± 0.2	601.5 ± 21.4	1.012 ± 0.3	0.017 ± 0.1	1,824 ± 53	1,794 ± 53
	77	1.353 ± 1.0	9.1 ± 0.2	446.1 ± 8.3	1.013 ± 0.4	0.018 ± 0.1	1,987 ± 49	1,943 ± 54
	58	1.030 ± 0.6	3.4 ± 0.2	989.2 ± 45.1	1.012 ± 0.3	0.020 ± 0.1	2,185 ± 65	2,163 ± 65
	27	0.953 ± 0.7	6.0 ± 0.2	622.3 ± 18.3	1.017 ± 0.7	0.024 ± 0.1	2,587 ± 36	2,546 ± 37
	0	1.193 ± 0.6	43.9 ± 0.5	158.7 ± 2.0	1.018 ± 0.2	0.036 ± 0.1	3,891 ± 105	3,650 ± 115
Briars04-02	235	0.474 ± 0.2	15.3 ± 0.3	11.5 ± 0.2	1.004 ± 0.4	0.002 ± 0.2	246 ± 167	32 ± 198
	215	0.399 ± 0.2	16.1 ± 0.2	27.9 ± 0.3	1.004 ± 0.4	0.007 ± 0.1	748 ± 65	480 ± 149
	195	0.399 ± 0.2	13.6 ± 0.2	36.1 ± 0.6	1.008 ± 0.5	0.008 ± 0.1	817 ± 120	591 ± 164
	170	0.381 ± 0.2	9.5 ± 0.1	60.3 ± 0.9	1.002 ± 0.4	0.009 ± 0.1	1,009 ± 51	842 ± 98
	150	0.403 ± 0.2	10.2 ± 0.2	81.2 ± 1.9	1.015 ± 0.4	0.013 ± 0.4	1,359 ± 441	1,192 ± 448
	135	0.418 ± 0.3	9.9 ± 0.2	90.6 ± 1.7	1.002 ± 0.6	0.013 ± 0.1	1,441 ± 122	1,283 ± 145
	103	0.349 ± 0.2	10.6 ± 0.2	75.9 ± 1.1	1.004 ± 0.4	0.014 ± 0.1	1,546 ± 78	1,344 ± 128
	78	0.285 ± 0.2	4.2 ± 0.2	193.4 ± 7.1	1.002 ± 0.6	0.017 ± 0.1	1,925 ± 104	1,826 ± 115
	43	0.346 ± 0.2	6.8 ± 0.2	178.6 ± 5.1	1.004 ± 0.4	0.021 ± 0.1	2,345 ± 100	2,215 ± 120
	0	0.607 ± 0.3	36.1 ± 0.3	112.6 ± 1.1	1.006 ± 0.4	0.041 ± 0.3	4,553 ± 313	4,138 ± 369
BRC03-02	141	0.897 ± 0.3	2.9 ± 0.2	184.4 ± 34.1	1.068 ± 0.3	0.004 ± 0.1	367 ± 32	347 ± 33
	132	0.972 ± 0.4	3.9 ± 0.3	202.4 ± 17.0	1.075 ± 0.3	0.005 ± 0.1	500 ± 36	475 ± 38
	110	1.102 ± 0.5	4.6 ± 0.3	211.8 ± 12.5	1.069 ± 0.6	0.005 ± 0.1	550 ± 29	524 ± 32
	90	1.111 ± 0.5	8.3 ± 0.3	182.9 ± 54.0	1.071 ± 0.6	0.008 ± 0.1	851 ± 66	805 ± 70
	50	0.928 ± 0.2	17.0 ± 0.3	118.1 ± 2.1	1.073 ± 0.7	0.013 ± 0.1	1,350 ± 85	1,236 ± 102
	31	0.825 ± 0.1	6.3 ± 0.2	299.6 ± 9.6	1.076 ± 0.4	0.014 ± 0.1	1,424 ± 56	1,377 ± 61
	17	0.839 ± 0.6	20.7 ± 0.3	130.2 ± 1.9	1.075 ± 0.4	0.020 ± 0.1	2,007 ± 88	1,855 ± 116
	0	1.033 ± 0.5	5.1 ± 0.1	849.9 ± 19.0	1.080 ± 0.3	0.026 ± 0.1	2,601 ± 45	2,571 ± 47

Table 2. Deposition rates for Floridian speleothems. * Date of 32 years ±198 has been deleted from the dataset due to unacceptable error relative to age.

Time Intervals (years)	Time of Deposition (years)	Volume of Calcite (mm^3)	Calcite Deposition (mm^3/yr)
BRC03-02 (2571-1855)	716	44829	63
BRC03-02 (1855-1377)	478	160898	337
BRC03-02 (1377-1236)	141	45900	326
BRC03-02 (1236-805)	431	67057	156
BRC03-02 (805-524)	281	65220	232
BRC03-02 (524-475)	49	57022	1164
BRC03-02 (475-347)	128	65313	510
BRC03-02 (347-0)	347	73788	213
BRIARS04-01 (3650-2546)	1104	43649	40
BRIARS04-01 (2546-2163)	383	76308	199
BRIARS04-01 (2163-1929)	220	84738	385
BRIARS04-01 (1929-1794)	149	54585	366
BRIARS04-01 (1794-1482)	312	54333	174
BRIARS04-01 (1482-1210)	272	49388	182
BRIARS04-02 (4138-2215)	1923	98059	51
BRIARS04-02 (2215-1826)	389	309237	795
BRIARS04-02 (1826-1344)	482	106266	220
BRIARS04-02 (1344-1283)	61	59322	972
BRIARS04-02 (1283-1192)	91	79194	870
BRIARS04-02 (1192-842)	350	93840	268
BRIARS04-02 (842-591)	251	115830	461
BRIARS04-02 (591-480)	111	101601	915
BRIARS04-02 (480-0)*	480	52969	110

elements extracted from one of the speleothems and with other paleo-precipitation proxy data from the region.

The first approach is to try to reject the hypothesis by comparing trace elements with deposition rates for the same speleothem. Fairchild et al. (2000) demonstrated a link between Mg/Ca and Sr/Ca ratios in the dripwaters in two caves and the residence time of water in the bedrock above the cave. Longer residence times will lead to enhanced dolomite dissolution of the bedrock, thereby augmenting Mg and Sr levels. The Hawthorn Group, which lies above Briars Cave, has Mg rich clays and Sr bearing siliciclastics and dolomite interspersed within the carbonates (Scott, 1997). Decreased rainfall above the cave promotes longer residence times of percolating waters. Taking these findings and applying them to our study, Mg/Ca and Sr/Ca ratios and deposition rates were compared for BRIARS04-02 (Fig. 6) as this is currently the only speleothem examined in this study with a trace element record. While we do not have the same high resolution of the trace elements for the deposition rates, it is apparent that periods of increased calcite deposition coincide with higher Mg/Ca and Sr/Ca ratios, especially during periods centered on 2.0 and 1.25 ka BP. This result then suggests that the deposition rate is negatively related to rainfall, causing us to reject our initial hypothesis.

The reason for an increase in deposition rate during drier periods is probably due to the increase in the calcite saturation state of the seepage waters. A slower flow of water through the bedrock would allow more time for dissolution of the bedrock. Within the cave, a decrease in drip rate would lead to a thinner film of water on the speleothem and more degassing. Both situations would increase the deposition rate for the speleothem. This agrees with Fairchild et al. (2000), who found that increased calcite precipitation in the cave occurred during the winter when the recharge to the cave was reduced due to the frozen ground. Baldini (2001) provides a different explanation whereby a decrease in the drip rate during drier periods allows more CO_2 degassing on the stalactite above the stalagmite, thereby increasing deposition rates on the stalactite and decreasing deposition on the paired stalagmite. Determining which of these explanations applies to the central Floridian stalagmites requires comparison of deposition rate with regional paleo-precipitation records.

Little Salt Spring (LSS) is located within 100 km of our study sites and Alvarez Zarikian et al. (2005) interpreted variations in the stable oxygen isotope ratio ($\delta^{18}O$ values) of *Cytheridella ilosvayi* (an ostracod species) as measures of changing precipitation. More negative $\delta^{18}O$ values corresponded to drier periods and conversely, more positive values indicated wetter conditions. Figure 7 shows a comparison between their $\delta^{18}O$ record and our deposition rates from BRIARS04-02. It is readily apparent that during more negative phases in the $\delta^{18}O$ (dry periods), deposition

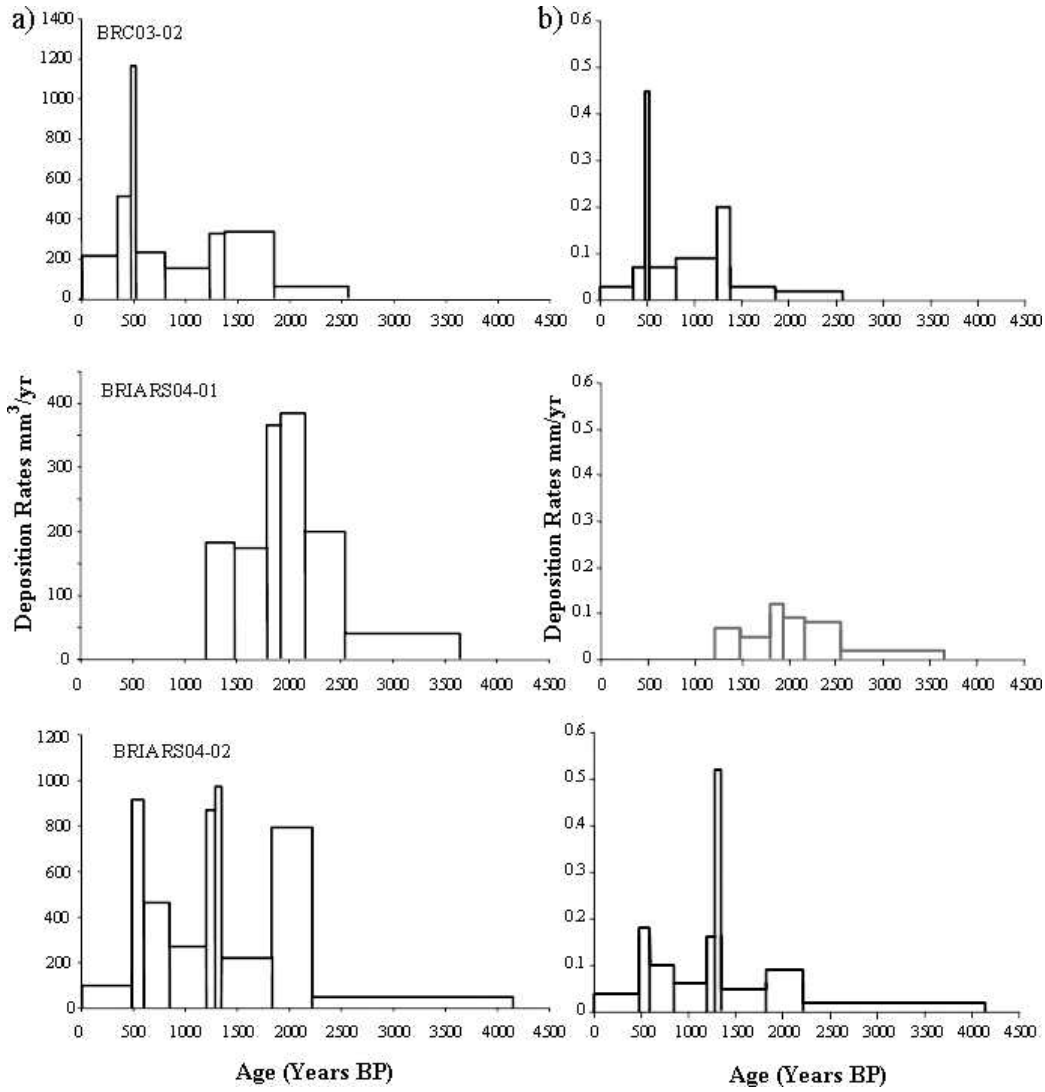

Figure 5. a) Variable deposition rates ($mm^3\ yr^{-1}$) for each stalagmite. Note the different timescales on the y-axes. b) Extension rates ($mm\ yr^{-1}$) for each speleothem using the traditional linear method.

rates for BRIARS04-02 increased and during more positive $\delta^{18}O$ intervals, calcite precipitation decreased. LSS attained maximum aridity for the late Holocene between 2.6–2.0 ka BP (Alvarez Zarikian et al., 2005), corresponding with the first major dry period in the BRIARS04-02 speleothem record. In all, the three phases of aridity in LSS during the last 3.0 ka coincide with increased calcite deposition. This provides more evidence for refuting our initial hypothesis and suggests that for this particular study, decreased precipitation leads to an increase in speleothem deposition rate. It should be noted that our resolution of dating from 2.5 to 4.2 ka BP precludes any detailed comparison of trends, although the other low deposition rates do appear to coincide with more positive $\delta^{18}O$ values in LSS.

Another regional comparison of paleo-precipitation can be made with Lake Miragoane, Haiti (Hodell et al., 1991). $\delta^{18}O$ values from ostracodes found in the sediments reflect changes in precipitation/evaporation (P/E) ratios. More negative $\delta^{18}O$ values show a P/E increase indicating higher lake levels. Figure 5 shows that Lake Miragoane recorded the same arid period centered on 2.0 ka as the speleothem and LSS records. The wet periods before 2.0 ka and later at ~1.0 ka as measured in the other records are also found in Haiti. From these two paleo-records, it appears that the Fairchild et al. (2000) explanation holds for our Floridian speleothems. However, we cannot irrefutably discount a potential contribution of the Baldini (2001) degassing mechanism.

Paleoclimatic Interpretation

With the number of dates we have for each speleothem, the best resolution attained is ~100 years. Consequently we cannot discuss decadal-scale climate influence, only

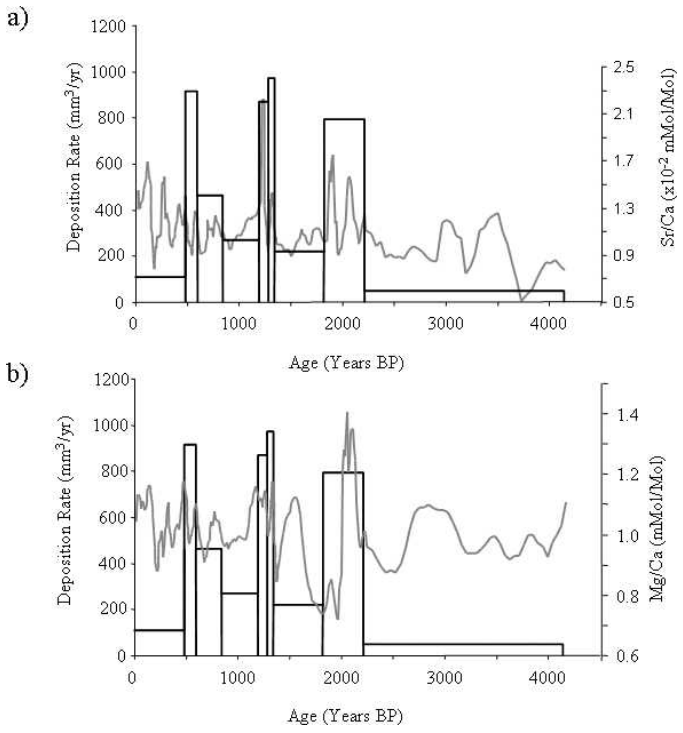

Figure 6. Comparison between the trace elements and deposition rates for BRIARS04-02. a) Five point running mean applied to the Sr/Ca ratios, b) Five point running mean applied to the Mg/Ca ratios.

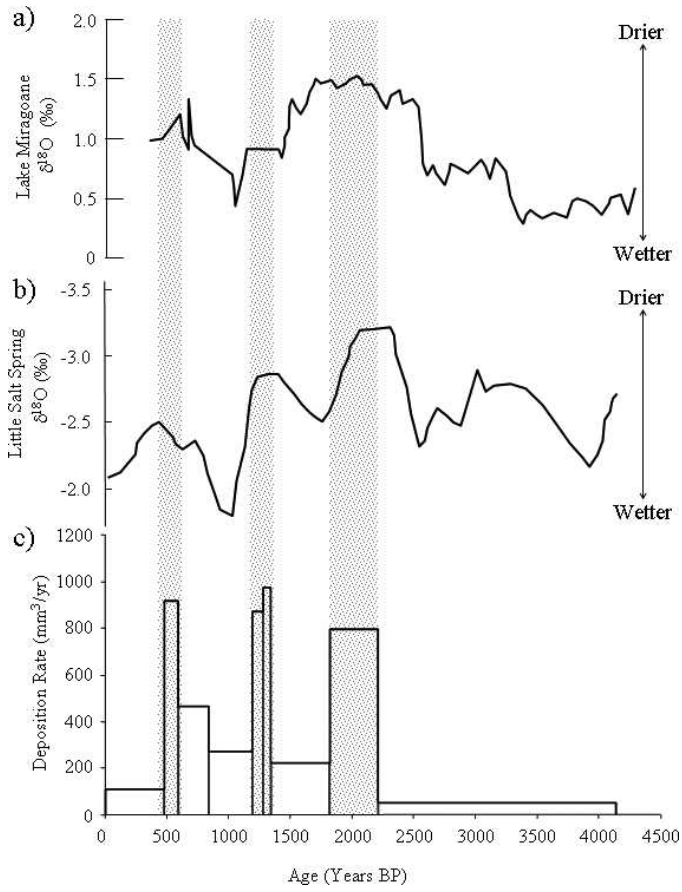

Figure 7. Regional paleoprecipitation comparison for a) $\delta^{18}O$ value Lake Miragoane record, Haiti (5 point running mean); b) $\delta^{18}O$ value record from Little Salt Spring, Florida; c) Deposition rates from BRIARS04-02. Shaded areas denote periods of aridity. Note that $\delta^{18}O$ values are plotted on an inverted axis.

those in the centennial timeframe. This excludes the Atlantic Multidecadal Oscillation (AMO - Enfield et al., 2001). During the cold phase of the AMO, Central Florida experiences drier conditions, with a period of 60–80 years. However, this is of shorter duration than can be resolved by our records. Another factor that produces drought in the region is the western extension of the North Atlantic High (NAH), which directs subsiding air into Florida leading to reduced rainfall. However, at other times the NAH is positioned further to the east, and can also direct warm moist Caribbean air into the peninsula, increasing rainfall.

It has been suggested that increased transport of Caribbean surface waters and moisture into the Gulf of Mexico associated with the northward migration of the average position of the ITCZ would influence precipitation in the region (Hodell et al., 1991; Poore et al., 2003). The more northerly position of the ITCZ would enhance easterly winds bringing precipitation to Haiti (Hodell et al., 1991) and the Gulf of Mexico (Poore et al., 2003). Consequently, a southward shift in the ITCZ mean position would produce periods of aridity. These shifts were proposed to have occurred over a millennial time-scale. The similarities of the deposition rates from the Floridian speleothems and the LSS - Haiti paleoprecipitation interpretations (Fig. 7) appear to record this regional atmospheric-ocean influence suggested by Poore et al. (2003). The easterly winds discussed by these authors are generated by the NAH and consequently provide some insight into how this high pressure system has affected Florida's climate during the late Holocene.

CONCLUSIONS

By calculating the volume of calcite deposited between U-series dates, and dividing this by the years between those dates, a more realistic estimate of changing deposition rates can be achieved, as opposed to the method of merely measuring the millimeters of calcite deposited each year along the growth axis between known ages. This latter method does not recognize changes in the shape of the speleothem over time.

The results from our study suggest that for the speleothems examined, deposition rate is controlled by rainfall above the cave, but not in the accepted manner as suggested by Hennig et al. (1983), Gascoyne (1992) or Lauritzen and Lundberg (1999). They suggested wetter

periods led to greater calcite precipitation. Our study appears to contradict that finding; periods of aridity increase the rate of speleothem growth. Such a result supports the research done by Fairchild et al. (2000). They found Mg/Ca and Sr/Ca ratios in cave calcite are negatively related to rainfall and our increased deposition rates correspond with periods of higher Mg/Ca and Sr/Ca ratios. A paleo-precipitation record from the region (Alvarez Zarikian et al., 2005) agrees with our periods of aridity in Central Florida. These periods of aridity are mostly caused by a southward shift in the mean position of the ITCZ and a weakening of the NAH easterly winds that direct warm water and moist air into the Northern Gulf of Mexico.

Future work will involve a calibration study of Briars Cave, measuring the Mg/Ca and Sr/Ca ratios in cave dripwaters and relating it to rainfall data above the cave to test if our explanation of the trace elements corresponds to that of Fairchild et al. (2000). Secondly, as more funds become available, we hope to improve the resolution of our deposition rate reconstruction with more U/Th dates.

Acknowledgements

We thank Amy Frappier, Peter Harries and Peter Rowe for their thoughtful review of the manuscript. Ethan Goddard analyzed the trace elements and Victor Polyak and Yemane Asmerom helped in the production of the TIMS dates. This article was partial funded by University of South Florida New Researcher Grant.

References

Alvarez Zarikian, C.A., Swart, P.K., Gifford, J.A., and Blackwelder, P.L., 2005, Holocene paleohydrology of Little Salt Spring, Florida, based on ostracod assemblages and stable isotopes: Palaeogeography, Palaeoecology, Palaeoclimatology, v. 225, p. 134–156.

Armstrong, B., Chan, D., Collazos, A., and Mallams, J.L., 2003, Doline and aquifer characteristics within Hernado, Pasco, and Northern Hillsborough Counties: Karst Studies of West Central Florida. Southwest Florida Water Management District, Brooksville, p. 39–51.

Baker, A., Genty, D., Dreybrodt, W., Barnes, W.L., Mockler, N.J., and Grapes, J., 1998, Testing theoretically predicted stalagmite deposition rate with recent annually laminated samples: Implications for past stalagmite deposition: Geochimica et Cosmochimica Acta, v. 62, p. 393–404.

Baker, A., Smart, P.L., and Ford, D.C., 1993, Northwest European palaeoclimate as indicated by growth frequency variations of secondary calcite deposits: Palaeogeography, Palaeoclimatology, Palaeoecology, v. 100, no. 3, p. 291–301.

Baldini, J.U.L., 2001, Morphologic and dimensional linkage between recently deposited speleothems and drip water from Browns Folly Mine, Wiltshire, England: Journal of Cave and Karst Studies, v. 63, no. 3, p. 83–90.

Curl, R.L., 1973, Minimum diameter stalagmites: Bulletin of the National Speleological Society, v. 36, p. 1–9.

Dorale, J.A., González, L.A., Reagan, M.K., Pickett, D.A., Murrell, M.T., and Baker, R.G., 1992, A high-resolution record of Holocene climate change in speleothem calcite from Coldwater Cave, northeast Iowa: Science, v. 258, p. 1626–1630.

Denniston, R.F., González, L.A., Asmerom, Y., Baker, R.G., Reagan, M.K., and Bettis, E.A., 1999, Evidence for increased cool season moisture during the middle Holocene: Geology, v. 27, no. 9, p. 815–818.

Dreybrodt, W., 1999, Chemical kinetics, speleothem growth and climate: Boreas, v. 28, no. 3, p. 347–356.

Enfield, D.B., Mestas-Nuñez, A.M., and Trimble, P.J., 2001, The Atlantic multidecadal oscillation and its relation to rainfall and river flows in the continental U.S: Geophysical Research Letters, v. 28, p. 277–280.

Fairchild, I.J., Borsato, A., Tooth, A.F., Frisia, S., Hawkesworth, C.J., Huang, Y., McDermott, F., and Spiro, B., 2000, Controls on trace element (Sr-Mg) compositions of carbonate cave waters: implications for speleothem climatic records: Chemical Geology, v. 166, p. 255–269.

Florea, L., Hashimoto, T., Kelley, K., Miller, D., and Mrykalo, R., 2003, Karst Geomorphology and Relation to the Phreatic Surface, Briars Cave, Marion County, Florida: Karst Studies of West Central Florida. Southwest Florida Water Management District, Brooksville, p. 9–19.

Franke, H.W., 1965, The theory behind stalagmite shapes: Studies in Speleology, v. 1, p. 86–95.

Frumkin, A., and Stein, M., 2004, The Sahara — East Mediterranean dust and climate connection revealed by strontium and uranium isotopes in a Jerusalem speleothem: Earth and Planetary Science Letters, v. 217, p. 451–464.

Gams, I., 1981, Contributions to morphometrics of stalagmites, *in* Beck, B.F., ed., Proceedings of the International Congress of Speleology, v. 1, p. 276–278.

Gascoyne, M., 1992, Paleoclimatic determination from cave calcite deposits: Quaternary Science Reviews, v. 11, p. 609–632.

Genty, D., and Quinif, Y., 1996, Annually laminated sequences in the internal structure of some Belgian stalagmites; importance for paleoclimatology: Journal of Sedimentary Research, v. 66, no. 1, p. 275–288.

Harmon, R.S., Schwarcz, H.P., and Ford, D.C., 1978, Stable isotope geochemistry of speleothems and cave waters from Flint Ridge-Mammoth Cave System, Kentucky: Implications for terrestrial climate change during the period 230,000 to 100,000 years B.P.: Journal of Geology, v. 86, p. 373–384.

Hendy, C.H., 1971, The isotopic geochemistry of speleothems I. The calculation of the effects of different modes of formation on the isotopic composition of speleothems and their applicability as paleoclimate indicators: Geochimica et Cosmochimica Acta, v. 35, p. 801–824.

Hennig, G.J., Gruen, R., and Brunnacker, K., 1983, Speleothems, travertines, and paleoclimates: Quaternary Research, v. 20, no. 1, p. 1–29.

Hodell, D.A., Curtis, J.H., Jones, G.A., Higuera-Gundy, A., Brenner, M., Binford, M.W., and Dorsey, K.T., 1991, Reconstruction of Caribbean climate change over past 10,500 years: Nature, v. 352, p. 790–793.

Holmgren, K., Karlen, W., Lauritzen, S.E., Lee-Thorp, J.A., Partridge, T.C., Piketh, S., Repinski, P., Stevenson, C., Svanered, O., and Tyson, P.D., 1999, A 3000-year high-resolution stalagmite-based record of palaeoclimate for northeastern South Africa: The Holocene, v. 9, no. 3, p. 295–309.

Kaufmann, G., and Dreybrodt, W., 2004, Stalagmite deposition and paleo-climate: an inverse approach: Earth and Planetary Science Letters, v. 224, p. 529–545.

Lachniet, M.S., Burns, S.J., Piperno, D.R., Asmerom, Y., Polyak, V.J., Moy, C.M., and Christenson, K., 2004, A 1500-year El Niño/Southern oscillation and rainfall history for the Isthmus of Panama from speleothem calcite: Journal of Geophysical Research, v. 109, D20117 p.

Latham, A.G., and Schwarcz, H.P., 1992, Carbonate and sulphate precipitates, *in* Ivanovich, M., and Harmon, R.S., eds., Uranium-series disequilibrium; applications to Earth, marine, and environmental sciences: Oxford, Clarendon Press, p. 423–459.

Lauritzen, S.E., and Lundberg, J., 1999, Speleothems and climate: a special issue of the Holocene: Holocene, v. 9, p. 643–647.

Li, W.-X., Lundberg, J., Dickin, A.P., Ford, D.C., Schwarcz, H.P., McNutt, R., and Williams, D., 1989, High-precision mass-spectrometric uranium-series dating of cave deposits and implications for palaeoclimatic studies: Nature, v. 339, p. 524–536.

Musgrove, M.L., Banner, J.L., Mack, L.E., Combs, D., James, H., and Edwards, R.L., 2001, Geochronology of late Pleistocene to Holocene speleothems from central Texas: Implications for regional paleoclimate: GSA Bulletin, v. 113, no. 12, p. 1532–1543.

Polyak, V.J., Rasmussen, J.B., and Asmerom, Y., 2004, Prolonged drought period in the southwestern United States through the Younger Dryas: Geology, v. 32, no. 1, p. 5–8.

Polyak, V.J., and Asmerom, Y., 2001, Late Holocene climate and cultural changes in the southwestern United States: Science, v. 165, p. 971–981.

Poore, R.Z., Dowsett, H.J., Verardo, S., and Quinn, T.M., 2003, Millennial- to century-scale variability in Gulf of Mexico Holocene climate records: Paleoceanography, v. 18, no. 2, 1048, doi: 10.1029/2002PA000868.

QinXiaoguang, TanMing, LiuTungsheng, WangXianfeng, LiTieying, and LuJinpo, 1999, Spectral analysis of a 1000-year stalagmite lamina thickness record from Shihua Cavern, Beijing, China, and its climatic significance: The Holocene, v. 9, p. 689–694.

Reeder, P., and Brinkmann, R., 1998, Paleoenvironmental reconstruction on an Oligocene aged island remnant in Florida, USA: Cave and Karst Science, v. 25, no. 1, p. 7–13.

Scott, T.M., 1997, Miocene to Holocene history of Florida, *in* Randazzo, A.F., and Jones, D.S., eds., The Geology of Florida, The University of Florida Press, Gainesville, p. 57–68.

South East Regional Climate Center, http://cirrus.dnr.state.sc.us/cgi-bin/sercc/cliMAIN.pl?fl1046

Van Beynen, P.E., Henry, P.S., and Derek, C.F., 2004, Holocene climatic variation recorded in a speleothem from McFail's Cave, New York: Journal of Cave and Karst Studies, v. 66, no. 1, p. 20–27.

White, W., 2004, Paleoclimate records from speleothem in limestone caves, *in* Sasowsky, I.D., and Mylroie, J., eds., Studies of Cave Sediments - Physical and Chemical Records of Paleoclimate, Kluwer Academic/Plenum Publishers, New York, p. 135–175.

K. W. Stafford, L. Rosales-Lagarde, and P. J. Boston – Castile evaporite karst potential map of the Gypsum Plain, Eddy County, New Mexico and Culberson County, Texas: A GIS methodological comparison. *Journal of Cave and Karst Studies,* v. 70, no. 1, p. 35–46.

CASTILE EVAPORITE KARST POTENTIAL MAP OF THE GYPSUM PLAIN, EDDY COUNTY, NEW MEXICO AND CULBERSON COUNTY, TEXAS: A GIS METHODOLOGICAL COMPARISON

KEVIN W. STAFFORD[1,2], LAURA ROSALES-LAGARDE[1,2], AND PENELOPE J. BOSTON[1,2]

Abstract: Castile Formation gypsum crops out over ~1,800 km^2 in the western Delaware Basin where it forms the majority of the Gypsum Plain. Karst development is well recognized in the Gypsum Plain (i.e., filled and open sinkholes with associated caves); however, the spatial occurrence has been poorly known. In order to evaluate the extent and distribution of karst development within the Castile portion of the Gypsum Plain, combined field and Geographic Information System (GIS) studies were conducted, which enable a first approximation of regional speleogenesis and delineate karst-related natural resources for management. Field studies included physical mapping of 50, 1-km^2 sites, including identification of karst features (sinkholes, caves, and springs) and geomorphic mapping. GIS-based studies involved analyses of karst features based on public data, including Digital Elevation Model (DEM), Digital Raster Graphic, (DRG) and Digital Orthophoto Quad (DOQ) formats. GIS analyses consistently underestimate the actual extent and density of karst development, based on karst features identified during field studies. However, DOQ analyses coupled with field studies appears to produce accurate models of karst development. As a result, a karst potential map of the Castile outcrop region was developed which reveals that karst development within the Castile Formation is highly clustered. Approximately 40% of the region effectively exhibits no karst development (<1 feature/km^2). Two small regions (<3 km^2 each) display intense karst development (>40 features/km^2) located within the northern extent of the Gypsum Plain, while many regions of significant karst development (>15 features/km^2) are distributed more widely. The clustered distribution of karst development suggests that speleogenesis within the Castile Formation is dominated by hypogenic, transverse processes.

INTRODUCTION

The gypsum facies of the Castile Formation crops out over an area of ~1800 km^2 in Eddy County, New Mexico and Culberson County, Texas on the western edge of the Delaware Basin (Fig. 1). The region has traditionally been referred to as the Gypsum Plain (Hill, 1996), which covers an area of ~2800 km^2 and is composed of outcrops of the Castile and Rustler Formations (Fig. 2). The region is located in the semi-arid southwest on the northern edge of the Chihuahuan Desert, where annual precipitation averages 26.7 cm with the greatest rainfall occurring as monsoonal storms in late summer (July – September) (Sares, 1984). Annual temperature averages 17.3 °C with an average annual minimum and maximum of 9.2 °C and 25.2 °C, respectively.

Throughout Castile outcrops, surficial karren occurs extensively in regions of exposed bedrock, including well-developed rillenkarren, spitzkarren, kamenitzas and tumuli. Sinkhole development is widespread, including both closed and open sinkholes ranging from near-circular features to laterally extensive, incised arroyo-like features. Cave development ranges widely, from small epigenic recharge features to large, complex polygenetic features (Stafford, 2006). The region hosts the second longest documented gypsum cave in North America, Parks Ranch Cave, Eddy County, N.M., with a surveyed length of 6596 m (Stafford, 2006). In addition, many other significant gypsum caves have been documented by the Texas Speleological Survey (TSS) (e.g., Reddell and Fieseler, 1977) and GYPsum KArst Project (GYPKAP) (Eaton, 1987; Belski, 1992; Lee, 1996). However, no systematic investigation has been conducted within the region with respect to karst development. Prior to this study, 246 karst features, primarily caves, were documented within the Castile outcrop region. The BLM (Bureau of Land Management) documented 45 of the total reported karst features (Jon Jasper, 2006, pers. com.); while the TSS

[1] Dept of Earth and Environmental Science, New Mexico Institute of Mining and Technology, Socorro, NM 87801, USA. kwstafford@juno.com, lagarde@nmt.edu and pboston@nmt.edu
[2] National Cave and Karst Research Institute, Carlsbad, NM, 88220, USA

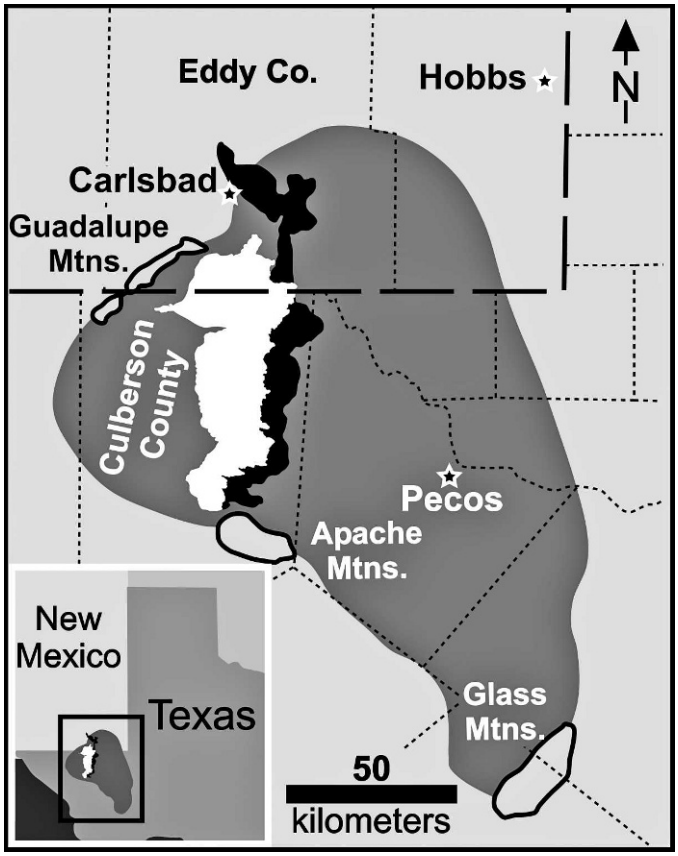

Figure 1. Location map showing location of Gypsum Plain including outcrop areas of the Castile Formation (solid white) and the Rustler Formation (solid black) within the Delaware Basin (dark gray), Eddy County, NM and Culberson County, Texas. Location of the Delaware Basin in relation to Texas and New Mexico is illustrated in bottom left corner, with the enlarged region outlined by the small black rectangle (adapted from Kelley, 1971, Dietrich et al., 1995 and Hill, 1996).

documented 201 of the total reported karst features (Jim Kennedy, 2006, pers. com.).

The rapid solution kinetics and high solubility of gypsum promotes extensive karst development. Gypsum solubility (2.53 g L^{-1}) is approximately three orders of magnitude greater than limestone (1.5 mg L^{-1}) in pure water and two orders of magnitude less than halite (360 g L^{-1}) (Klimchouk, 1996). The high solubility and near-linear solution kinetics of evaporites encourage intense surface dissolution that often forms large sinkholes, incised arroyos and caves that are laterally limited with rapid decreases in passage aperture away from inflows through epigenic speleogenesis (Klimchouk, 2000a). Additionally, the high solubilities of evaporites favor the development of hypogenic transverse speleogenesis driven by mixed convection (forced and free) (Klimchouk, 2000b). Forced convection is established by regional hydraulic gradients in confined settings, while free convection is generated where steep density gradients establish as fresh-waters are continuously supplied to the dissolution fronts (the upper levels) through the simultaneous sinking of saturated fluids by density differences (Anderson and Kirkland, 1980). Therefore epigenic and hypogenic karstic features likely both exist in the study area, often superimposed on each other.

The work we report here focuses on delineating the extent and distribution of karst development within the outcrop region of the Castile Formation, in order to predict regions of intense versus minimal karst development, which can be used for karst resource management as well as a first approximation for understanding regional speleogenesis. A dual approach involving field and Geographic Information System (GIS) analyses were utilized in order to define karst variability within the study area, including field mapping of 50, 1-km^2 regions and GIS analyses, using ESRI ArcGIS 9.2 software, of public data (i.e., Digital Elevation Model [DEM]; Digital Raster Graphic [DRG]; and Digital Orthophoto Quad [DOQ]) for the entire region. The combined results were used to develop a karst potential map of the Castile Formation outcrop region, while simultaneously evaluating different GIS-based techniques for karst analyses.

GEOLOGIC SETTING

The Castile Formation was deposited during the late Permian (early Ochoan), subsequent to deposition of the Guadalupian Capitan Reef, which is well-known for the caves it hosts in the Guadalupe Mountains (e.g., Hose and Pisarowicz, 2000). Castile evaporites represent deep-water deposits within a stratified, brine-filled basin (i.e., Delaware Basin) (Kendall and Harwood, 1989), bounded below by clastics of the Bell Canyon Formation, on the margins by Capitan Reef carbonates, and above by additional evaporitic rocks of the Salado and Rustler Formations (Fig. 2) (Kelley, 1971). Castile evaporites crop out along their western dissolution front in the Gypsum Plain (Fig. 1), dip to the east where they reach a maximum thickness of 480 m in the subsurface (Hill, 1996), and are characterized as massive to laminated sulfates (gypsum/anhydrite) interbedded with halite (Dietrich et al., 1995). Increased thickness in the east has been attributed to dissolution of intrastratal halite to the west and increased deposition to the east in the Ochoa Trough during the Permian (Anderson et al., 1972).

The Castile Formation, including outcrops in the Gypsum Plain, has experienced minimal tectonic deformation although located on the eastern edge of major tectonic events. Triassic and Laramide tectonism produced regional tilting to the northeast, broad flexures and fracturing with minimal offset within southeastern New Mexico and west Texas. The far western edge of the Delaware Basin has been down-dropped along the far eastern margin of Basin

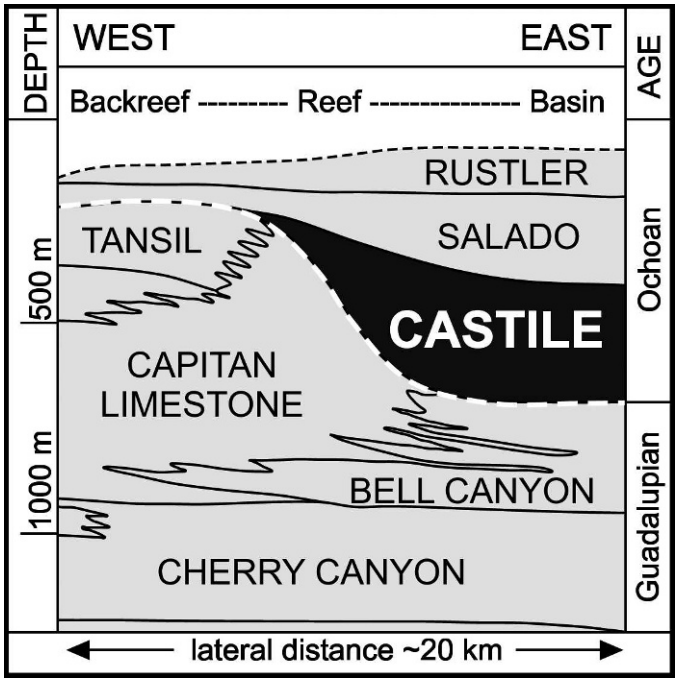

Figure 2. Diagrammatic representation of late Permian (Guadalupian and Ochoan) deposits associated with the Guadalupe Mountains (left) and Delaware Basin (right). Note that the Castile Formation fills in the basin and marks the beginning of the Ochoan (dashed white line) (adapted from Hill, 1996).

and Range block faulting; however, within the remaining Delaware Basin, the effects are limited to near-vertical joints (Horak, 1985). As a result of tectonism, Castile evaporites currently dip 3 to 5 degrees to the northeast with abundant conjugate joint sets oriented at ~ N75°E and ~N15°W. Associated with joint sets along the western dissolution front, solution subsidence valleys have developed from subsurface dissolution of halite beds (Hentz and Henry, 1989).

In addition to tectonic deformation, some sulfate rocks have been exposed to significant diagenesis. Original laminated (varved) gypsum often exhibits massive and nodular fabrics that are likely the result of plastic deformation associated with anhydrite/gypsum mineral conversion (Machel and Burton, 1991). Calcitized evaporites are common (often referred to as castiles or calcitized masses), generally forming clusters or linear trends of biogenic limestone associated with bacterial sulfate reduction (Kirkland and Evans, 1976). Selenite is locally abundant, forming linear features and fracture fillings (likely associated with mineral conversion), as well as lenticular masses (probably associated with calcitization processes). Diagenetic fabric alteration within Castile evaporites probably has exerted significant influence on establishing preferential flow paths for karst development within the Gypsum Plain.

Field Studies

Field mapping was conducted at 50, 1-km^2 sites within the Castile outcrop area (Fig. 3A). Field sites were randomly selected using ESRI ArcGIS 9.2 software in order to obtain an accurate representation of karst development within the Castile outcrop region and minimize any human biases that might be introduced into site selection. Ten field mapping sites were shifted up to two kilometers away from GIS-defined locations, in order to avoid anthropogenic features (i.e., roads, houses, quarries), while two sites were shifted up to four kilometers to avoid regions where land access was not available.

Each field site was defined as a one kilometer square region. Transect surveys were conducted on 100-meter line spacing, such that ten, one kilometer long transects were traversed in each of the 50 field sites. Smaller line-spacing (40 m) for transect surveys was compared with 100-meter line spacing through independent surveys by two of the authors at five field sites, which identified less than 10% additional karst features (i.e., sinkholes and caves). Because of the results of sub-sampling and the location of the study region within the semi-arid southwest, where vegetation is sparse and does not commonly obscure karst features, 100-meter spaced traverse surveys were found to be sufficient to document more than 90% of surficial karst features. During field mapping, identified feature locations were recorded with a hand-held GPS (Global Positioning System) and individual features were characterized based on size (length, width, depth), geomorphic expression (closed sink, open sink [i.e., cave], spring) and geologic occurrence (laminated, massive and nodular gypsum; gypsite; calcitized evaporite).

Field mapping identified 389 individual karst features, including 236 open sinkholes with free drains (i.e., caves or smaller solutional conduits that connect directly to sinkholes), 147 filled sinkholes, four caves with no associated sinkhole, and two springs. However, of the 236 open sinkholes, only 39 contained caves that were large enough to be humanly enterable. Of the 50 field sites, 12 contained no karst features and 14 sites contained more than 10 features (Fig. 4). Only two sites contained more than 30 features, one with 31 and one with 48.

Features were found in a wide range of gypsum fabrics (Fig. 5). Caves are largely developed in laminated (~43% of features) (Fig. 5A) and massive fabrics (~26% of features) (Fig. 5B); however, numerous small surficial caves form in gypsite (~28% of features) (Fig. 5D). Caves were occasionally found in selenite (<2% of features) (Fig. 5C) and calcitized masses (<2% of features) (Fig. 5E). Filled sinkholes were generally found in gypsite or alluvium; however, this likely only represents surficial mantling over deeper features in most cases.

Sinkhole area and volume ranged widely within the surveyed sites. The average open sinkhole area was 1.99×10^3 m^2 (0.3 to 4.12×10^4 m^2) with an average volume of

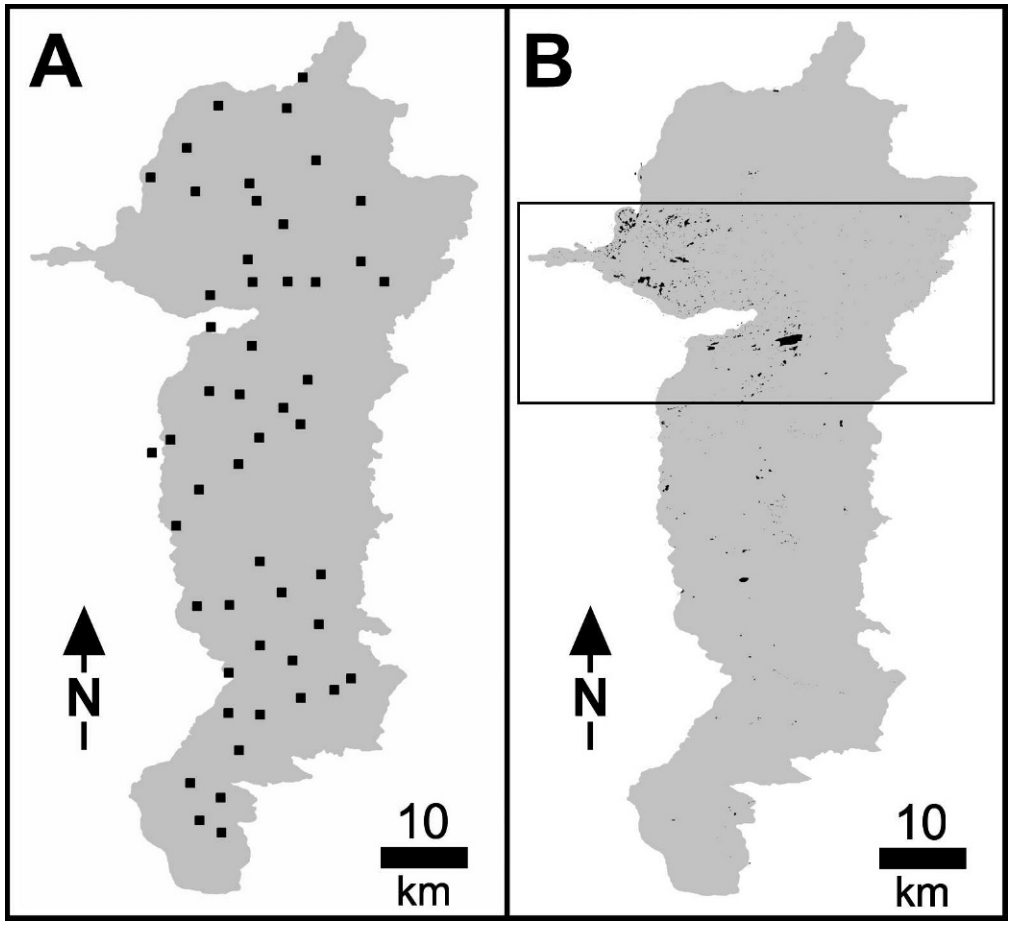

Figure 3. A) Castile outcrop region (gray) showing location of the 50 randomly selected 1 km^2 sites where field mapping was conducted; B) Castile outcrop region (gray) showing sinks (closed depressions) determined by DEM analysis (boxed area includes ~75% of the closed depressions identified through DEM analysis).

1.73×10^3 m^3 (8.0×10^{-2} to 4.71×10^4 m^3). The average area of closed sinkholes was 1.01×10^3 m^2 (3.0×10^{-2} to 2.36×10^4 m^2) with an average volume 3.70×10^2 m^3 (5.0×10^{-3} to 6.54×10^3 m^3). Sinkhole area was calculated by treating features as simple ellipses based on the maximum width and length measured in the field, while sinkhole volume was calculated by treating features as conical ellipses based on elliptical area and sinkhole depth. Therefore, approximated sinkhole areas and volumes probably overestimate true values.

GIS ANALYSES

In the last decade GIS has been recognized as a powerful tool for geographic analyses and has become a useful tool for cave and karst studies (e.g., Szukalski et al., 2002). Public data is available in multiple formats through government agencies, such as United States Geological Survey (USGS), New Mexico Bureau of Geology and Mineral Resources (NMBGMR), and Texas Natural Resource Inventory Service (TNRIS), which enables GIS analyses of large karst regions at zero cost.

GIS analyses of karst terrains have been used in various studies to delineate karst development. Florea et al. (2002) combined known point locations for karst features with digitized sinkholes from DRGs to develop karst potential maps in Kentucky, while Denizman (2003) conducted similar studies in Florida. Taylor et al. (2005) demonstrated the use of DEMs for delineating sinkholes in Kentucky. Hung et al. (2002) used an integrated approach involving analyses of multispectral imagery, aerial photography, and DEMs to evaluate relationships between lineaments and cave development.

Because most previous karst studies using GIS have focused on one or two techniques, multiple public data formats (DEM, DRG and DOQ) were compared and evaluated in this study, not only to characterize the extent of karst development but to also test the intercomparability of different methodologies. Physical mapping of karst features in the field, described in the previous section, was further compared with GIS techniques to fully evaluate the accuracy of GIS-based approaches. While field mapping identified the true occurrence of karst features within specific regions, the GIS analyses only represent approx-

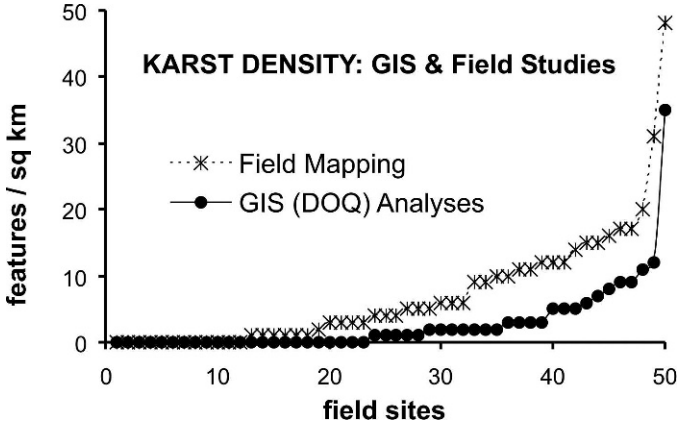

Figure 4. Comparative plot showing karst features identified during field mapping compared with features identified through DOQ analyses for the 50, 1 km^2 field sites. Field mapping and DOQ analyses are only shown because most DEM and DRG analyses showed no features in the regions where field mapping was conducted. Note that DOQ analysis identified ~35% of features that were located during field mapping.

imations based on the geomorphic expression of karst features (Fig. 6, 7).

Digital elevation models (DEM) were analyzed to define closed depressions (i.e., sinks) within the Castile outcrop region. Closed depressions were identified by creating a new DEM with filled sinks through GIS processing, which was compared with the original DEM to determine the difference between datasets (Fig. 3B, 6B) (Taylor et al., 2005). The resulting data included 554 individual sinkholes with an average area of 2.57×10^4 m^2 (6.0×10^2 to 8.70×10^5 m^2); however, approximately 80% of the identified features occurred within a 26 km (16 mile) wide strip immediately south of the New Mexico–Texas state line. Less than 5% of the features occurred north of the strip of abundant closed depressions, while the remainder was distributed south of the strip (Fig. 6B). Although all public data used for DEM analyses had 10-meter postings, the resulting sinkhole map suggests that there is significant variability in the source material used to create these DEMs. The region of sinkhole abundance appears to represent well the actual closed depressions within the study area, while regions outside this area appear to significantly underestimate feature abundance.

Digital raster graphics (DRG) of 1:24,000 USGS topographic maps were analyzed for the study area and all closed depressions were digitized as indicators of individual karst features (Fig. 6C, 7B); however, it is likely that multiple karst features exist within some large, closed depressions. From DRGs, 552 individual closed depressions were identified (Fig. 7B), with an average area of 1.54×10^4 m^2 (53 m^2 to 1.74×10^6 m^2), based on GIS spatial analyses. Because topographic maps of this region are based on 20 foot (6.1 m) contour intervals, numerous small sinkholes, including most of the features documented during field mapping, are not represented. However, most of the karst features documented by the BLM and TSS are represented as sinkholes on DRGs because topographic maps have traditionally been used for locating and identifying karst features.

Digital orthophoto quads (DOQ) within the study region have a resolution of one meter. DOQ analyses were conducted by visually picking probable karst features (Fig. 6D) at a resolution of 1:4,000. Features were identified based on geomorphic expression through comparison with known cave and karst features, either documented by the BLM in New Mexico and the TSS in Texas or features documented during field mapping. Based on comparison with known features, 3,237 individual features were identified within the Castile outcrop region (Fig. 7C).

Spatial analyses of feature densities were performed in order to delineate karst development within the study area. Three sets of data were processed separately to evaluate karst density, including: 1) known caves documented by the TSS and BLM (Fig. 7D); 2) DRG defined sinks (Fig. 7E); and 3) features identified through DOQ analyses (Fig. 7F). Density analyses of features identified from DEM data was not conducted because of the apparent high degree of variability in quality of these public data sets. All density analyses indicate intense karst development within the northwestern portion of the study area and a general decrease in feature abundance towards the east.

Discussion

Studies conducted to determine the extent and distribution of karst development vary widely (Veni, 2002), but GIS-based studies have enabled significant advances in geographic analyses within the last decade. Analyses of known karst distributions and features identified through GIS within the Castile outcrop region all show similar trends for areas of significant karst development. However, the degree of resolution of various public data used in GIS analyses produces substantial differences in evaluation of karst development throughout the entire region (Fig. 8), suggesting that field studies should always be coupled with any GIS-based studies. Sinkholes identified through DEM analyses were not used to develop karst density maps because of the apparent variability within the original data used to develop the DEMs. However, the DEM variability illustrates an important point, in that public data must be interpreted with caution.

Analysis of previously documented cave and karst features within the Castile outcrop region indicate small clusters of caves, focused in the northwestern region of the study area, largely along the dissolutional margin of the Castile Formation; however, only minor regions of karst development are observed scattered throughout the rest of

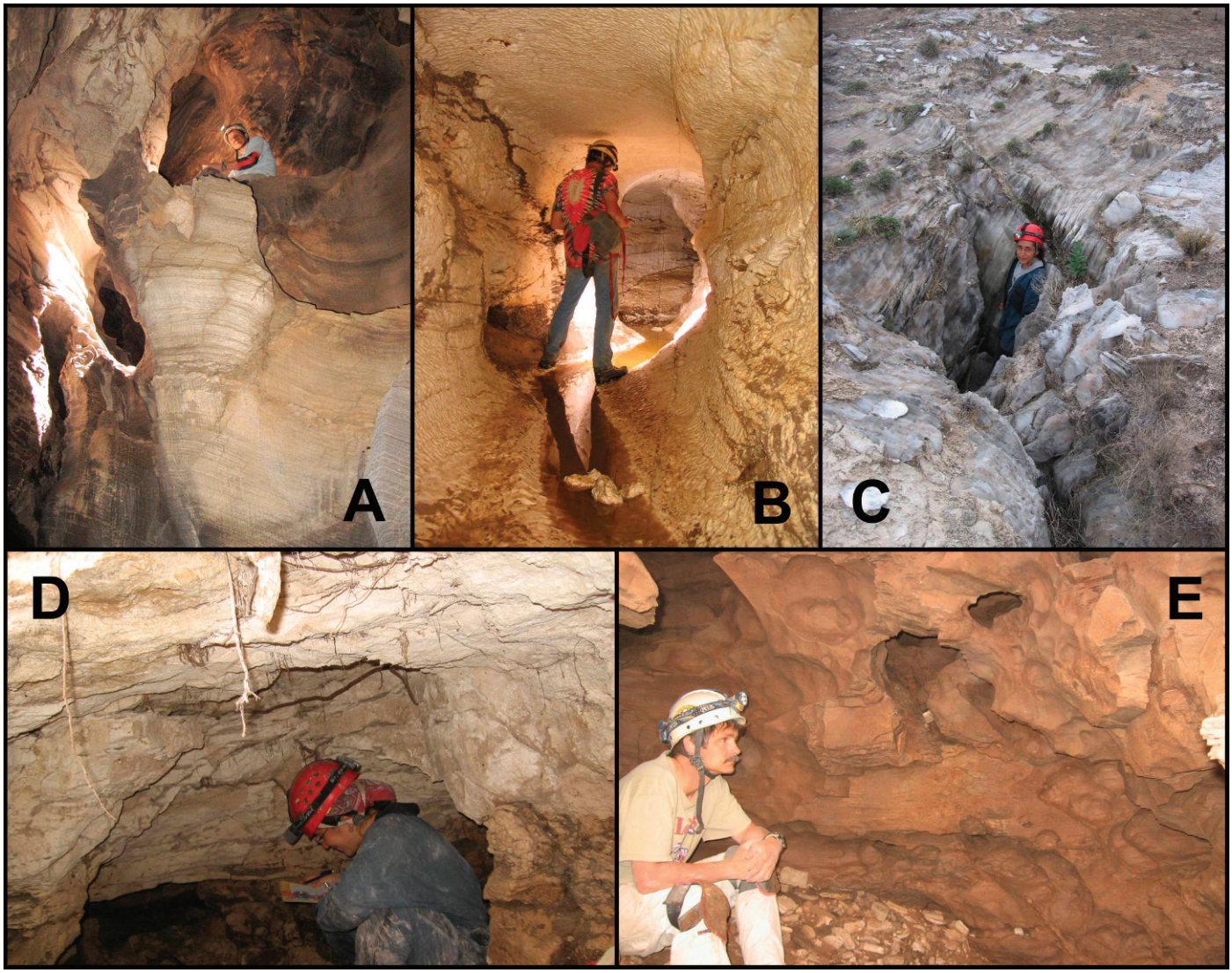

Figure 5. Cave development in the Castile Formation occurs within a wide range of lithologic fabrics. A) Plummet Cave: laminated gypsum; B) Parks Ranch Cave: massive gypsum; C) Black Widow Hole: selenite; D) Pokey Cave: gypsite, and e) Dead Bunny Hole: biogenic limestone (calcitized evaporite).

the study area (Fig. 7D). Based on previously documented features, approximately 95% of the study area effectively exhibits no karst development (<1 feature/km^2). Studies based on documented karst features inherently create biased results that may not accurately depict the complete distribution of karst development. Biases are introduced by variable access to portions of a karst region, such as regions where landowner access is not available or regions that are remote with poor road access.

Analysis of closed depressions depicted on DRGs (Fig. 7E) shows similar patterns of karst development as documented karst distributions (Fig. 7D), but do not show any regions with densities greater than 10 features/km^2. DRG analyses shows greater distributions of karst features than documented cave analyses, expanding the predicted boundaries of karst development; however, the majority of the study area (~90%) still appears to have minimal karst development (<1 feature/km^2). As with analyses of documented caves, DRGs appear to underestimate the actual extent of karst development because the contour interval of DRGs prevents distinguishable representation of small closed depressions and narrow, incised karst arroyos.

Analysis of karst features identified on DOQs indicates a significantly greater degree of karst development density and distribution (Fig. 7F) as opposed to other GIS-based analyses. Regions of minimal karst development were reduced to approximately 50% and several regions with karst feature densities greater than 15 features/km^2 were identified. Intense karst development still appears concentrated within the northwestern portion of the study area; however, regions of extensive karst development are

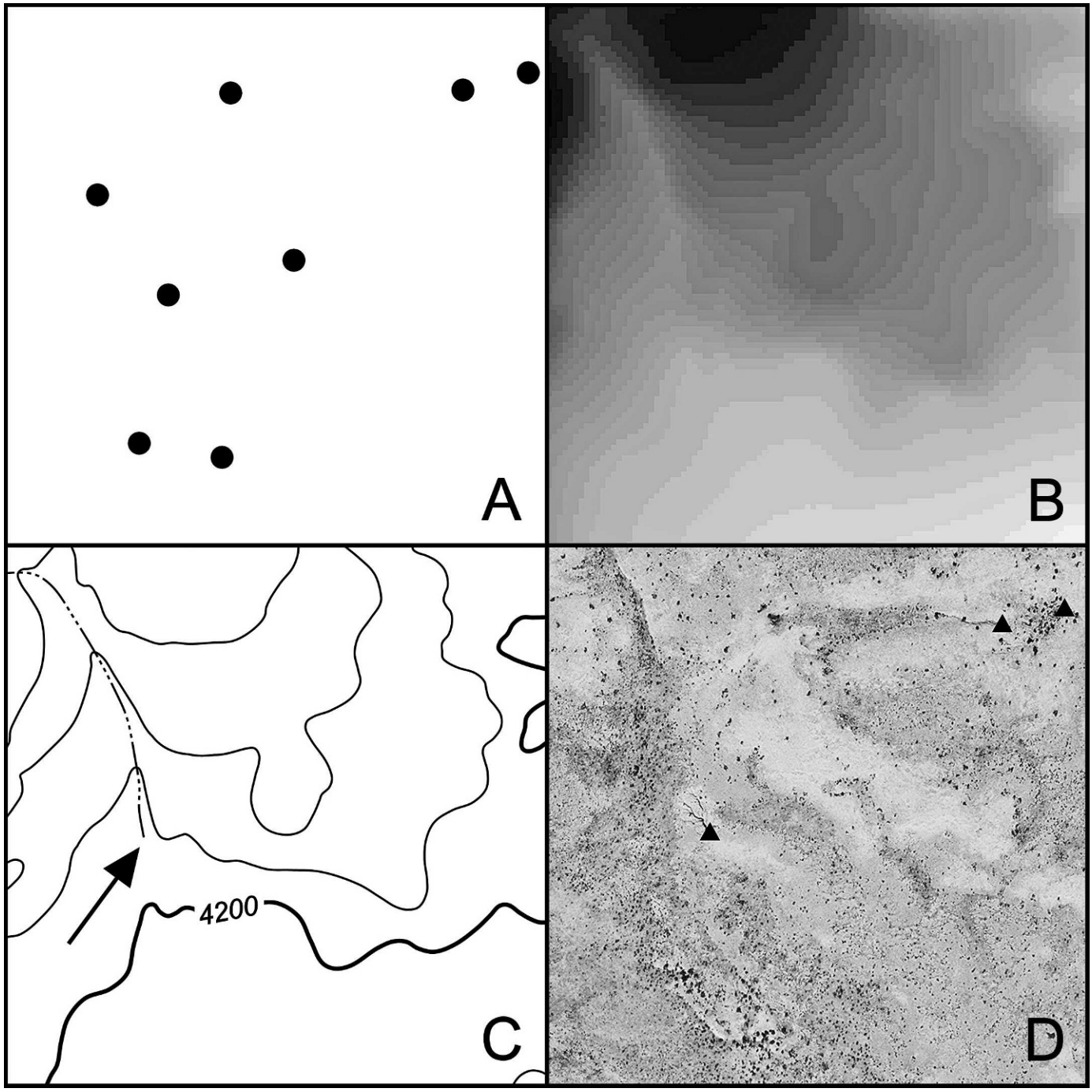

Figure 6. Variability in karst identification through various methodologies within a representative 1 km^2 field site (each square region measures 1 km by 1 km). A) filled black circles represent eight karst features documented through physical mapping of field site; B) original DEM of field site from which no karst features (closed depressions) were identified during GIS analysis (note darker shading in upper left is the highest elevations); C) DRG of field site showing no closed depressions, but a blind-terminated, ephemeral stream suggest sink point (arrow); and D) DOQ of field site showing geomorphic variability and the location of three features (black triangles) which could be resolved through DOQ analysis.

identified throughout the entire western half of the Castile outcrop area, as well as several smaller regions closer to the eastern margin of the study area. Although DOQ analysis shows more extensive karst development, it is inherently biased because features were visually picked based on comparison with the geomorphic expression of known features. Comparison of karst features physically documented during field studies with features identified through DOQ analysis, within the boundaries of field sites mapped, indicates that DOQ analysis consistently underestimates

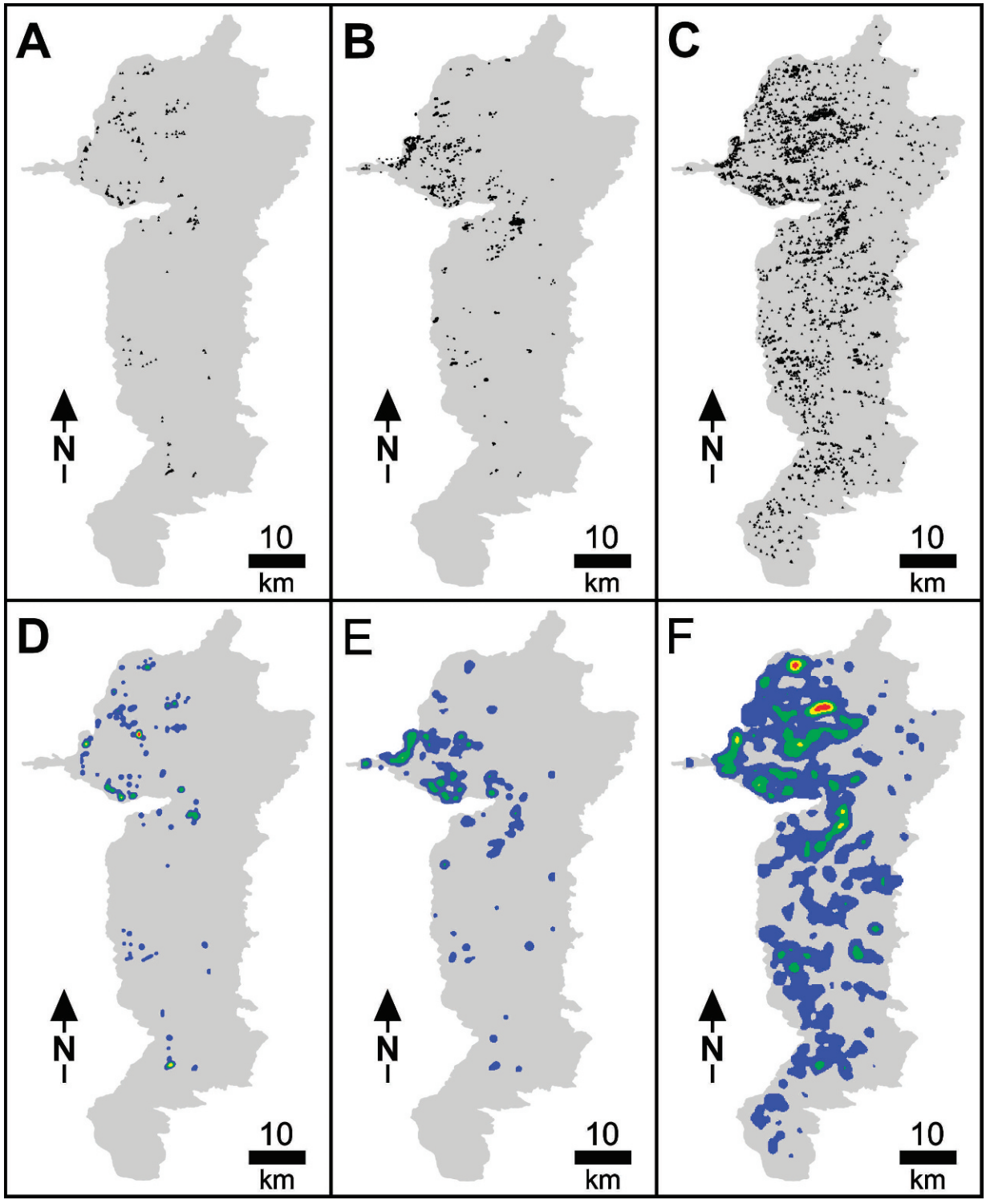

Figure 7. Comparison of data used for density analyses within the Castile outcrop region (grey). A) point data for individual karst features previously documented by the TSS and BLM; B) closed depressions digitized from DRGs; C) point data for individual karst features identified through DOQ analysis; D) karst feature density map based on previously documented karst features in Fig. 6A; E) karst feature density map based on distribution of individual closed depressions digitized from DRGs shown in Fig. 6B; and F) karst density map based on features identified through DOQ analysis shown in Fig. 6C. Color shading in karst density maps represent the number of karst features / km^2, where: gray $\leq$ 1 feature/km^2; blue = 1−5 features/km^2; green = 5−10 features/km^2; yellow = 10−15 features/km^2; and red $\geq$ 15 features/km^2.

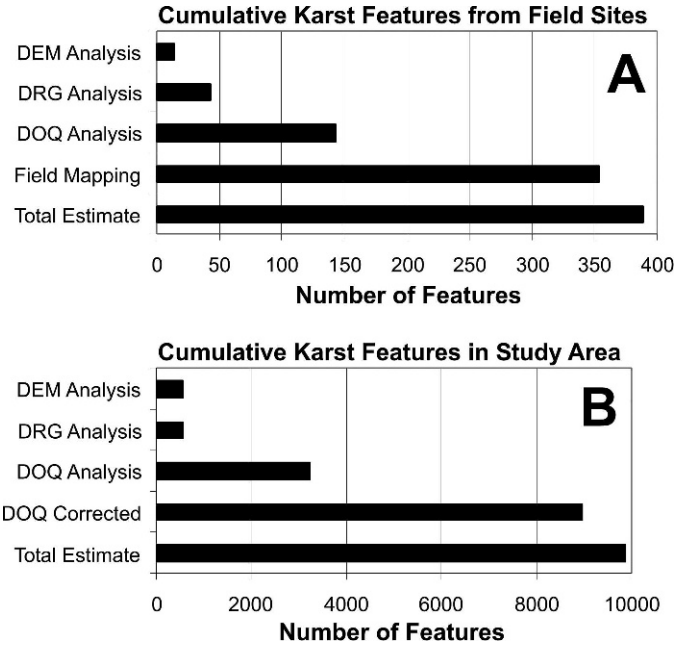

Figure 8. Comparative graphs of the results from various methodologies used to evaluate karst development within the Castile outcrop region. Note that Total Estimate refers to the 10% additional karst features expected based on field tests of smaller transect survey line spacing. A) Cumulative methodology results from the 50, 1-km^2 sites that were physically mapped during field studies. B) Cumulative karst features for the entire Castile outcrop region based on different methodologies, where DOQ Corrected represents the weighting DOQ-defined features by a factor of 2.77 based on the ratio of true features documented during field mapping with those identified through DOQ analysis.

the total number of karst features present (Fig. 4). This underestimation is likely the result of the 1-meter resolution of the DOQ public data.

DOQ analysis appears to best represent karst development within the outcrop region of the Castile Formation; however, all GIS-based analyses appear to under represent the extent of actual karst development as compared to physical karst surveys conducted in the field (Fig. 8). DOQ analyses generally identify 36% of the features documented during field studies (Figs. 4, 6, 7, and 8), while other GIS analyses commonly identify less than 5% of the features documented during field studies. Therefore, DOQ density analysis was weighted by a factor of 2.77 using Spatial Analyst, in order to adjust the densities calculated through GIS as compared to densities documented during field studies. As a result, a karst potential map was developed for the entire outcrop region of the Castile Formation (Fig. 9), which indicates that less than 40% of the outcrop region contains effectively no karst development (<1 feature/km^2), while two small regions (<3 km^2 each) within New Mexico exhibit intense karst development (>40 features/km^2). Comparative tests of line spacing used in transect-based field mapping, suggests that the actual density of karst features may be at least 10% greater (Fig. 8). The karst potential map likely represents karst development relatively accurately within the study area, but a complete physical survey of the entire 1,800 km^2 region would probably show discrepancies.

Conclusions

The development of a karst potential map for the Castile Formation shows that karst development is distinctly clustered within the Gypsum Plain (Fig. 9). Visual interpretation of the clustering distribution of karst features within the Castile outcrop region was confirmed through GIS-based nearest neighbor analyses (Ford and Williams, 1989), which yielded a nearest neighbor index of 0.439. A nearest neighbor index of 1 is classified as random while values greater than 1 approach a regular, evenly spaced pattern while values less than 1 approach greater clustering (Ford and Williams, 1989). A nearest neighbor index of 0.439 indicates significant clustering. Large regions exhibit minimal surficial karst expressions, primarily along the southern and eastern edges of the Castile outcrop area.

The densest regions occur in the northwestern portion of the outcrop area, and commonly contain more than 20 features/km^2 (Fig. 9), with more than 40 features/km^2 locally. The northern of the two densest regions contains the second longest known gypsum cave in North America, Parks Ranch Cave, and is largely included within a BLM critical resource area that does not allow surface occupancy, thus protecting the extensive karst development within this area. However, the second dense karst region should be evaluated through more intense field studies to determine if it should also be protected as a critical resource area.

GIS-based analyses have become an important tool for karst studies. DOQ analysis, coupled with field studies, has been shown to be the most effective method for delineating the actual extent and intensity of karst development within the Castile outcrop area, because of the sparse vegetation associated with the semi-arid southwestern United States. However, this may not be the most effective technique in other regions where vegetation is denser. Although commonly used in many karst regions, DRG analysis within the study area proved to poorly represent the actual extent of karst development within the region because of the low resolution of contour intervals, including significantly underestimating the actual abundance of karst features within the two densest regions. DEM analysis proved to be of little use within the study area, because apparent variability in original data from which the DEMs were constructed does not consistently represent the same resolution.

Although DEM and DRG analyses proved ineffective in the study area, it is likely that these methodologies could

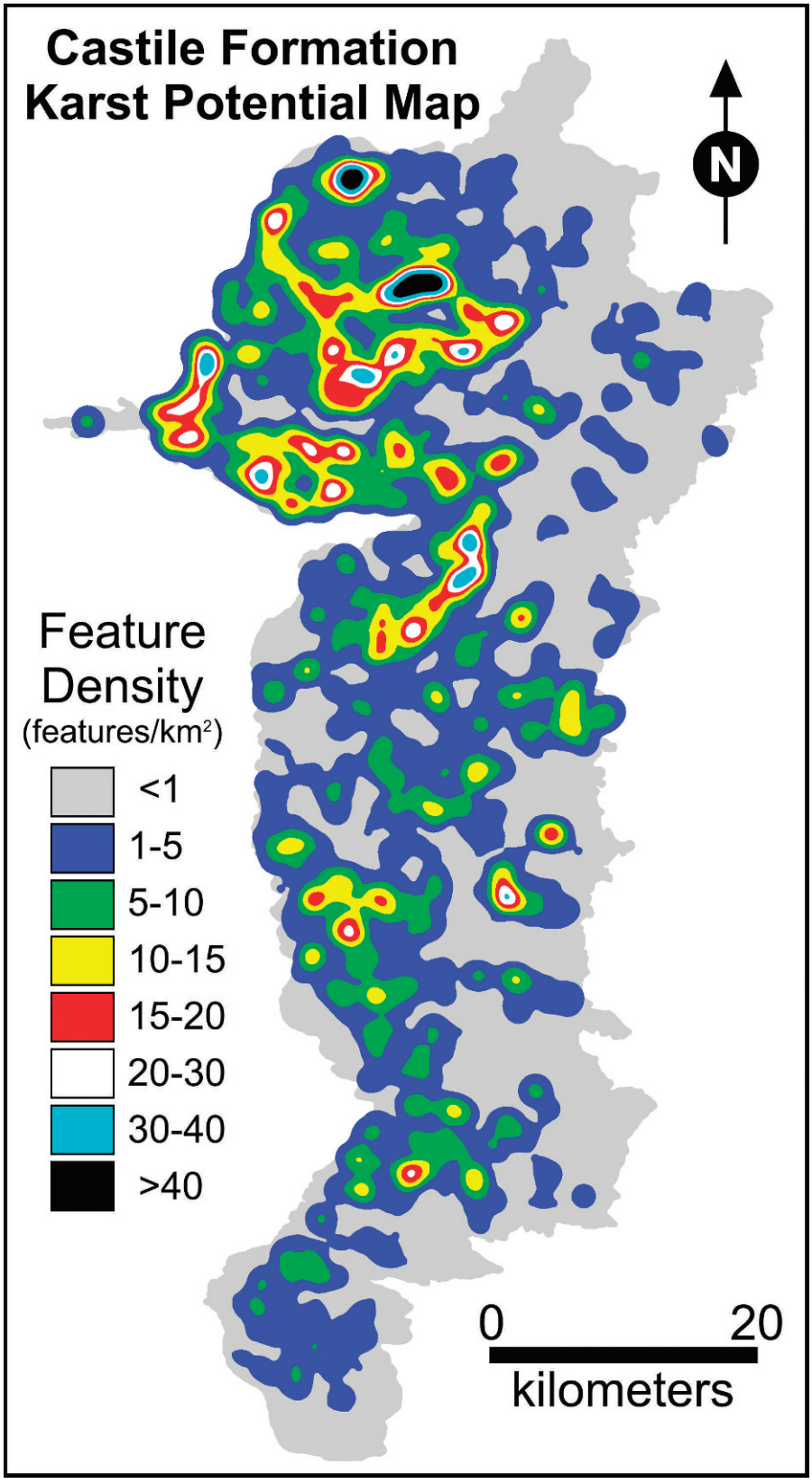

Figure 9. Karst potential map of the Castile Formation outcrop region defined in this study. Note the two dense areas of karst development within the northern portion of the study area with densities greater than 40 features/km^2.

be effective for delineating karst development in other regions where higher resolution DEM or DRG data is available. Ultimately, the scale of karst features within regions being evaluated with GIS methodologies must be compared with the resolution of available GIS data, in order to determine the effectiveness of GIS-based studies. Therefore, caution must be taken when conducting GIS-based karst analyses, which should always be coupled with field studies for verification, not only in densely karsted areas, but also in regions that appear to have minimal karst development.

The distinct clustering pattern of karst provides some insight into the nature of speleogenesis within the region (Figs. 7, 9). Klimchouk (2003) and Frumkin and Fischhendler (2005) suggest that hypogenic karst tends to form in dense clusters separated by regions of minimal karst development because heterogeneities within soluble strata promote transverse speleogenesis in regions where rising fluids become focused along favorable flow paths. In contrast, epigenic karst is generally expressed as more widely distributed features where descending meteoric waters attempt to utilize all available irregularities near the surface and converge with depth. Because convergence occurs with depth in epigenic karst, surficial expressions tend to be less clustered in epigenic dominated karst as opposed to hypogenic karst where convergence occurs near the surface.

Current studies of karst development within the Castile Formation by the authors have found significant morphological evidence within individual caves that supports the interpretation of speleogenesis dominated by hypogene processes. These include the diagnostic suite of hypogenic features (e.g. risers, channels and cupolas) reported by Klimchouk (2007), as well as the widespread occurrence of blanket breccias (Anderson et al., 1978), breccia pipes (Anderson and Kirkland, 1980), evaporite calcitization (Kirkland and Evans, 1976) and native sulfur deposits (Hentz and Henry, 1989) previously reported within the region. Current research is focusing on interpreting the speleogenetic evolution of the Castile Formation, including the diagenetic alteration of calcium sulfate rocks and the development of cavernous porosity. However, this is beyond the scope of this manuscript and will be reported separately in the near-future. While GIS-based analyses provide insight into the speleogenetic processes of the region, detailed field studies of specific features will be required in order to interpret the speleogenetic evolution of the region.

While the karst potential map of the Castile Formation outcrop region alone can only provide limited insight into regional speleogenesis, it can provide an effective tool for land management within Eddy County, New Mexico and Culberson County, Texas. Delineation of karst intense regions can be used in land management planning for road construction and oilfield well and pipeline placements, in order to not only avoid regions of potential geohazards associated with collapse, but also to protect regions of significant ground-water recharge. Whether Castile karst is primarily the result of hypogenic or epigenic speleogenesis, most exposed features currently act as ground-water recharge features, thus the delineation of dense karst regions is crucial for the sustained management of sparse water resources within this portion of the semi-arid southwest. Ultimately, karst potential maps can be used to delineate sensitive regions for karst resource management.

Acknowledgements

The authors are indebted to Jack Blake, Draper Brantley, Stanley Jobe, Lane Sumner and Clay Taylor for their generous access to private ranches in Texas throughout this study. Tim Hunt provided useful information and assistance with University Land in Texas. Jon Jasper and Jim Goodbar provided essential information about known gypsum karst development within New Mexico. Jim Kennedy provided essential information about known gypsum karst development within Texas. The authors are thankful for the useful comments provided by an anonymous reviewer and Amos Frumkin which helped to improve this manuscript. This research was partially funded through grants from the New Mexico Geological Society and the New Mexico Tech Graduate Student Association and support from the National Cave and Karst Research Institute (NCKRI).

References

Anderson, R.Y., Dean, W.E., Kirkland, D.W., and Snider, H.I., 1972, Permian Castile varved evaporite sequence, West Texas and New Mexico: Geological Society of America Bulletin, v. 83, p. 59–85.

Anderson, R.Y., Kietzke, K.K., and Rhodes, D.J., 1978, Development of dissolution breccias, northern Delaware Basin and adjacent areas: New Mexico Bureau of Mines and Mineral Resources Bulletin 159, p. 47–52.

Anderson, R.Y., and Kirkland, D.W., 1980, Dissolution of salt deposits by brine density flow: Geology, v. 8, p. 66–69.

Belski, D., ed., 1992, GYPKAP Report Volume #2: Southwestern Region of the National Speleological Society, Albuquerque, N.M., 57 p.

Denizman, C., 2003, Morphometric and spatial distribution parameters of karstic depressions, lower Suwannee River basin, Florida: Journal of Cave and Karst Studies, v. 65, no. 1, p. 29–35.

Dietrich, J.W., Owen, D.E., Shelby, C.A., and Barnes, V.E., 1995, Geologic atlas of Texas: Van Horn-El Paso Sheet: University of Texas Bureau of Economic Geology, Austin, Texas,

Eaton, J., ed., 1987, GYPKAP 1987 Annual Report: Southwestern Region of the National Speleological Society, Alamogordo, N.M., 35 p.

Florea, L.J., Paylor, R.L., Simpson, L., and Gulley, J., 2002, Karst GIS advances in Kentucky: Journal of Cave and Karst Studies, v. 64, no. 1, p. 58–62.

Ford, D.C., and Williams, P.W., 1989, Karst Geomorphology and Hydrology: London, Unwin Hymam, 601 p.

Frumkin, A., and Fischhendler, I., 2005, Morphometry and distribution of isolated caves as a guide for phreatic and confined paleohydrological conditions: Geomorphology, v. 67, p. 457–471.

Hentz, T.F., and Henry, C.D., 1989, Evaporite-hosted native sulfur in Trans-Pecos Texas: Relation to late-phase Basin and Range deformation: Geology, v. 17, p. 400–403.

Hill, C.A., 1996, Geology of the Delaware Basin, Guadalupe, Apache and Glass Mountains: New Mexico and West Texas: Permian Basin Section: Midland, Texas, SEPM, 480 p.

Horak, R.L., 1985, Trans-Pecos tectonism and its affects on the Permian Basin, *in* Dickerson, P.W., and Muelberger, W.R., eds., Structure and Tectonics of Trans-Pecos Texas: Midland, Texas, West Texas Geological Society, p. 81–87.

Hose, L.D., and Pisarowicz, J.A., eds., 2000, The Caves of the Guadalupe Mountains: Journal of Cave and Karst Studies, v. 62, no. 2, 157 p.

Hung, L.Q., Dinh, N.Q., Batelaan, O., Tam, V.T., and Lagrou, D., 2002, Remote sensing and GIS-based analysis of cave development in the Suoimuoi Catchment (Son La – NW Vietnam): Journal of Cave and Karst Studies, v. 64, no. 1, p. 23–33.

Kelley, V.C., 1971, Geology of the Pecos Country, Southeastern New Mexico: New Mexico Bureau of Mines and Mineral Resources, 78 p.

Kendall, A.C., and Harwood, G.M., 1989, Shallow-water gypsum in the Castile Formation – significance and implications, *in* Harris, P.M., and Grover, G.A., eds., Subsurface and Outcrop Examination of the Capitan Shelf Margin, Northern Delaware Basin: SEPM, Core Workshop No. 13, San Antonio, Texas, p. 451–457.

Kirkland, D.W., and Evans, R., 1976, Origin of limestone buttes, Gypsum Plain, Culberson County, Texas: American Association of Petroleum Geologists Bulletin, v. 60, p. 2005–2018.

Klimchouk, A., 1996, Dissolution and conversion of gypsum and anhydrite: International Journal of Speleology, v. 25, no. 3–4, p. 263–274.

Klimchouk, A., 2000a, Speleogenesis in gypsum, *in* Klimchouk, A., Ford, D.C., Palmer, A.N., and Dreybrodt, W., eds., Speleogenesis: Evolution of Karst Aquifers: Huntsville, National Speleological Society, Inc., p. 261–273.

Klimchouk, A., 2000b, Speleogenesis under deep-seated and confined conditions, *in* Klimchouk, A., Ford, D.C., Palmer, A.N., and Dreybrodt, W., eds., Speleogenesis: Evolution of Karst Aquifers: Huntsville, National Speleological Society, Inc., p. 244–260.

Klimchouk, A., 2003, Conceptualization of speleogenesis in multi-story artesian systems: a model of transverse speleogenesis: Speleogenesis and Evolution of Karst Aquifers, v. 1, no. 2, p. 1–18.

Klimchouk, A., 2007, Hypogene Speleogenesis: Hydrogeological and Morphometric Perspective: Carlsbad, National Cave and Karst Research Institute, Special Paper No. 1, 106 p.

Lee, J., ed., 1996, GYPKAP Report Volume 3: Southwestern Region of the National Speleological Society, 69 p.

Machel, H.G., and Burton, E.A., 1991, Burial-diagenetic sabkha-like gypsum and anhydrite nodules: Journal of Sedimentary Petrology, v. 61, no. 3, p. 394–405.

Reddell, J.R., and Fieseler, R.G., 1977, The Caves of Far West Texas: Austin, Texas Speleological Survey, 103 p.

Sares, S.W., 1984, Hydrologic and geomorphic development of a low relief evaporite karst drainage basin, southeastern New Mexico [M.S. Thesis]: Albuquerque, University of New Mexico, 123 p.

Stafford, K.W., 2006, Gypsum karst of the Chosa Draw area, *in* Land, L., Lueth, V.W., Raatz, W., Boston, P., and Love, D., eds., Caves and Karst of Southeastern New Mexico: Socorro, New Mexico Geological Society Fifty-seventh Annual Field Conference, New Mexico Geological Society, p. 82–83.

Szukalski, B.W., Hose, L.D., and Pisarowicz, J.A., eds., 2002, Cave and karst GIS: Journal of Cave and Karst Studies, v. 64, no. 1, 93 p.

Taylor, C.J., Nelson, H.L., Hileman, G., and Kaiser, W.P., 2005, Hydrogeologic-framework mapping of shallow, conduit-dominated karst — components of a regional GIS-based approach, *in* U.S. Geological Survey Karst Interest Group Proceedings, Rapid City, South Dakota, U.S. Geological Survey Scientific Investigations Report 2005–5160, p. 103–113.

Veni, G., 2002, Revising the karst map of the United States: Journal of Cave and Karst Studies, v. 64, no. 1, p. 45–50.

K. W. Stafford, L. Land, and A. Klimchouk – Hypogenic speleogenesis within Seven Rivers Evaporites: Coffee Cave, Eddy County, New Mexico. *Journal of Cave and Karst Studies,* v. 70, no. 1, p. 47–61.

HYPOGENIC SPELEOGENESIS WITHIN SEVEN RIVERS EVAPORITES: COFFEE CAVE, EDDY COUNTY, NEW MEXICO

KEVIN W. STAFFORD[1,2], LEWIS LAND[2,3], AND ALEXANDER KLIMCHOUK[3,4]

Abstract: Coffee Cave, located in the lower Pecos region of southeastern New Mexico, illustrates processes of hypogenic speleogenesis in the middle Permian Seven Rivers Formation. Coffee Cave is a rectilinear gypsum maze cave with at least four stratigraphically-distinct horizons of development. Morphological features throughout the cave provide unequivocal evidence of hypogenic ascending speleogenesis in a confined aquifer system driven by mixed (forced and free) convection. Morphologic features in individual cave levels include a complete suite that defines original rising flow paths, ranging from inlets for hypogenic fluids (feeders) through transitional forms (rising wall channels) to ceiling half-tube flow features and fluid outlets (cupolas and exposed overlying beds). Passage morphology does not support origins based on epigenic processes and lateral development, although the presence of fine-grained sediments in the cave suggests minimal overprinting by backflooding. Feeder distributions show a lateral shift in ascending fluids, with decreasing dissolutional development in upper levels. It is likely that additional hypogenic karst phenomena are present in the vicinity of Coffee Cave because regional hydrologic conditions are optimum for confined speleogenesis, with artesian discharge still active in the region.

INTRODUCTION

Coffee Cave is located on the east side of the Pecos River valley, approximately 20 km north of Carlsbad, New Mexico at the base of the McMillan Escarpment. The cave is formed in the evaporite facies belt of the Seven Rivers Formation (Fig. 1). Evaporite karst development is extensive throughout the lower Pecos region, not only in the Seven Rivers Formation, but also in other Permian evaporite facies of the Artesia Group (including the Seven Rivers), and the Yeso, San Andres, Castile, Salado and Rustler Formations. Numerous filled sinkholes and caves have been documented within a range that extends several km east and west of the Pecos River, and from Texas to as far north as Santa Rosa in east-central New Mexico. Most solutional openings are relatively small and not humanly enterable, but many features are extensive with complex morphologies, suggestive of multiple phases of speleogenesis. Cave patterns and abundant diagnostic morphologic features at meso-scale within individual caves appear to be the result of hypogenic, largely confined, speleogenesis, while cave sediments and minor entrenchment in some caves suggest a later phase of unconfined development. Although hypogenic features are seen in many caves within the region, this paper will focus on examples from Coffee Cave in relation to the current understanding of regional hydrology and speleogenesis in the Seven Rivers Formation.

Evaporite karst development within the Seven Rivers Formation, as with most evaporite karst phenomena in the United States, has not been thoroughly investigated. Most cave development within the Seven Rivers Formation has only been documented in anecdotal reports (Eaton, 1987; Belski, 1992; Lee, 1996), although evaporite karst has been recognized in association with regional aquifers (Hendrickson and Jones, 1952) and dam leakage along the Pecos River (Cox, 1967). The occurrence of large gypsum sinkholes at Bottomless Lakes State Park near Roswell dramatically illustrates the occurrence of artesian speleogenesis within the Seven Rivers Formation (Quinlan et al., 1987; Land, 2003; 2006). Although poorly documented within the United States, hypogenic evaporite karst has been extensively studied in the Western Ukraine, where large maze caves have developed in confined conditions and were later breached by surface denudation and fluvial entrenchment (e.g., Klimchouk, 1996a; 2000a). Other examples of hypogenic gypsum karst are known from Germany, Russia, Spain and United Kingdom (Klimchouk et al., 1996).

GEOLOGIC SETTING

The Seven Rivers Formation, along with the other four members of the Artesia Group, represents the backreef facies equivalent of the Capitan Reef, which defined the shelf margin of the Delaware Basin during middle Permian (Guadalupian) time (Figs. 2 and 3). The Seven Rivers

[1] Dept of Earth and Environmental Science, New Mexico Institute of Mining and Technology, Socorro, NM 87801, USA (kwstafford@juno.com)
[2] National Cave and Karst Research Institute, Carlsbad, NM, 88220, USA
[3] New Mexico Bureau of Geology and Mineral Resources, Socorro, NM 87801, USA
[4] Ukrainian Institute of Speleology and Karstology, Simferopol, 95007, Ukraine

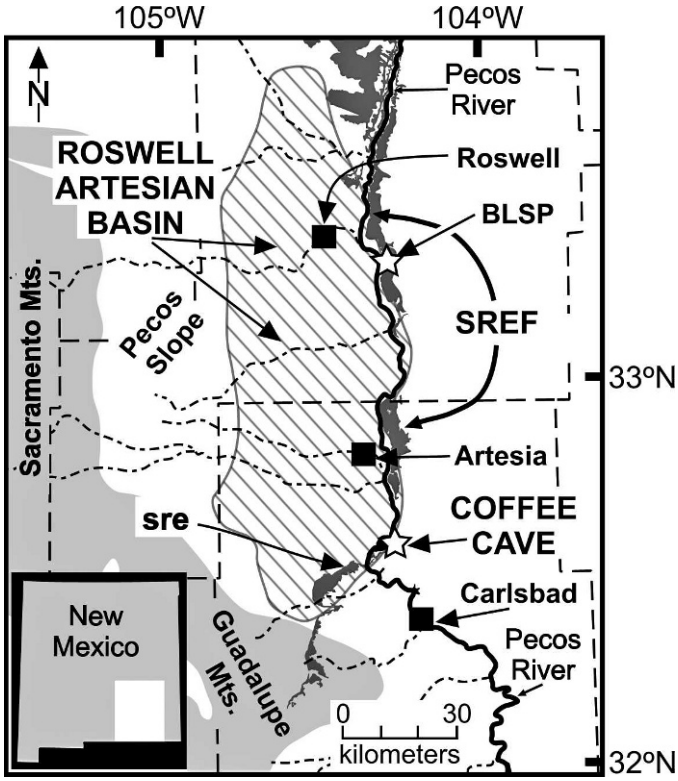

Figure 1. Regional map delineating the Roswell Artesian Basin, outcrop region of the Seven Rivers evaporite facies, and location of Coffee Cave. SREF = Seven Rivers Evaporite Facies. sre = Seven Rivers Embayment. BLSP = Bottomless Lakes State Park (adapted from Kelley, 1971 and Land, 2003).

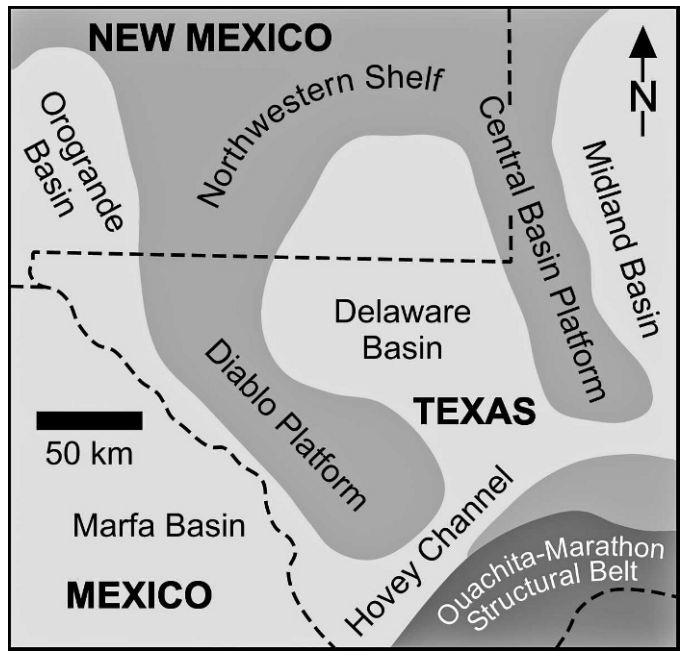

Figure 2. Paleogeographic reconstruction of southeastern New Mexico during the middle Permian, showing the depositional relationship between the Delaware Basin and the Northwestern Shelf where Seven Rivers evaporite facies were deposited (adapted from Scholle et al., 2004).

Formation consists predominantly of dolomite in its near-backreef setting in the Guadalupe Mountains, but becomes increasingly evaporitic further to the north on the Northwestern Shelf (Fig. 2), changing facies into interbedded gypsum and red mudstone (Scholle et al., 2004). Guadalupian rocks were later buried by extensive deposition of late Permian (Ochoan) evaporites that filled the basin and surrounding shelf areas (Fig. 3) (Bachman, 1984). By the end of the Permian, marine sedimentation had effectively ceased (Dickenson, 1981). During the early Triassic, the entire area was uplifted above sea level and the Laramide Orogeny produced regional deformation limited to uplift (1–2 km), tilting to the east and broad anticlinal flexures (Horak, 1985). By the mid-Tertiary, Laramide compression had ceased and shifted to Basin and Range extension (Chapin and Cather, 1994). As a result of tectonism, regional dip of Guadalupian strata in this part of southeastern New Mexico is $\sim$ 1 to 2° to the east and southeast (Fig. 4), with broad flexures and abundant high angle fractures and joints exhibiting minimal offset. Since the late Permian, southeastern New Mexico has been dominated by fluvial erosion, associated sedimentation, and karstic dissolution (Kelley, 1971).

The evaporite facies of the Seven Rivers Formation is up to 150 m thick in the study area, with anhydrite ($CaSO_4$) and bedded salt (NaCl) in the subsurface and gypsum ($CaSO_4 \cdot 2H_2O$) near the surface as a result of sulfate hydration (Kelley, 1971). Dolomite ($CaMg(CO_3)_2$) interbeds are common throughout the evaporite facies, forming laterally-continuous layers that thicken towards the reef and thin away from it. The entire gypsum sequence is capped by dolomite of the Azotea Tongue Member. Seven Rivers sulfates are generally white to grey, nodular to microcrystalline anhydrite/gypsum, forming individual beds ranging from centimeters to meters in thickness (Hill, 1996).

HYDROLOGIC SETTING

Coffee Cave is formed at the base of the McMillan Escarpment, which locally defines the eastern margin of the Pecos River Valley (Fig. 4). The cave is located on the eastern shore of old Lake McMillan, an artificial impoundment that formerly stored water for the Carlsbad Irrigation District (CID). The original McMillan Dam was constructed in 1893, and the reservoir almost immediately began experiencing leakage problems through sinkholes formed in the lake bed. Water flowed through karstic conduits in the underlying Seven Rivers gypsum and returned to the Pecos River by discharge from springs downstream from the lake. Attempts to isolate the worst

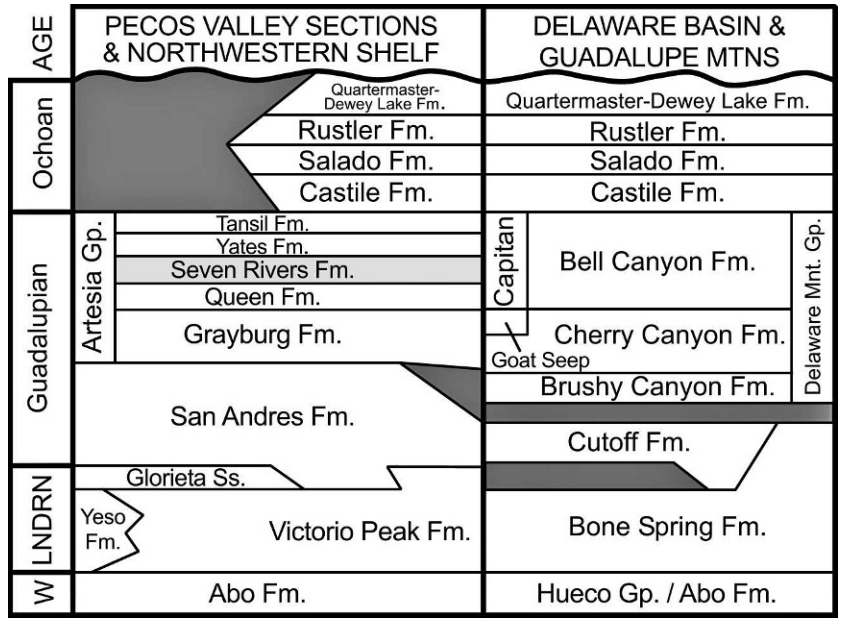

Figure 3. Stratigraphic chart of Permian facies in southeastern New Mexico with comparison of stratigraphic units within the Pecos Valley-Northwestern Shelf and the northern Delaware Basin-Guadalupe Mountains. Coffee Cave is developed in the Seven Rivers Formation (highlighted in gray). W = Wolfcampian; LNDRN = Leonardian (adapted from Zeigler, 2006).

areas of sinkhole formation by construction of a dike along the eastern lake shore were only partially successful (Cox, 1967). McMillan Dam was breached in 1991 and the water allowed to flow into the newly constructed Brantley Reservoir, which is located in the dolomitic facies belt of the Seven Rivers Formation.

The Lake McMillan area lies near the southern end of the Roswell Basin, a karstic artesian aquifer system occupying several hundred square kilometers in the lower Pecos region of southeastern New Mexico (Fig. 1). Ground water in the Roswell Basin is stored in multiple highly porous and transmissive zones within Guadalupian carbonates of the San Andres limestone and the overlying Grayburg and Queen Formations of the Artesia Group (Fig. 4). Secondary porosity is developed in vuggy and cavernous limestones and intraformational solution-collapse breccias, the result of subsurface dissolution of evaporites. Recharge to the aquifer occurs on the Pecos Slope, a broad area east of the Sacramento Mountains where the San Andres limestone crops out. Redbeds and gypsum of the Seven Rivers Formation serve as a leaky upper confining unit for the artesian aquifer (Fig. 4) (Welder, 1983).

Water-bearing zones within the artesian aquifer system rise stratigraphically from north to south, occurring near the middle of the San Andres Formation in the northern Roswell Artesian Basin, and in carbonate rocks of the Grayburg Formation in the southern part of the Basin near Lake McMillan (Fig. 4). The southern boundary of the Artesian Basin is not well-defined, but is usually located, somewhat arbitrarily, along the Seven Rivers Hills southwest of Lake McMillan.

The Seven Rivers confining unit is overlain by a shallow water-table aquifer composed largely of Tertiary and Quaternary alluvial sediment. This material was deposited on the Pecos River floodplain as it migrated eastward due to uplift of the rising Sacramento Mountains to the west. A substantial percentage of recharge to the shallow aquifer is derived from upward flow through leaky confining beds from the underlying artesian aquifer (Welder, 1983). Very locally, in the vicinity of Lake McMillan, the Seven Rivers Formation makes up a large part of the shallow aquifer, probably as solution conduits in the Seven Rivers gypsum.

Since the inception of irrigated agriculture in the lower Pecos Valley in the early 20th Century, most of the discharge from the artesian aquifer has been from irrigation wells. However, substantial natural discharge still occurs along the Pecos River, flowing upward through fractures and solution channels in the overlying Seven Rivers gypsum. This natural discharge has formed a complex of karst springs, sinkhole lakes, and extensive wetlands located along the west side of the Pecos River, east of the city of Roswell (Land, 2005). Along the eastern margin of the Pecos River valley southeast of Roswell, discharge from the artesian aquifer has caused subsurface dissolution of gypsum and upward propagation of collapse chimneys, forming large gypsum cenotes at Bottomless Lakes State Park (Land, 2003; 2006).

In the early 20th Century, many wells in the Artesian Basin flowed to the surface, with yields as high as 21,500 L min^{-1}

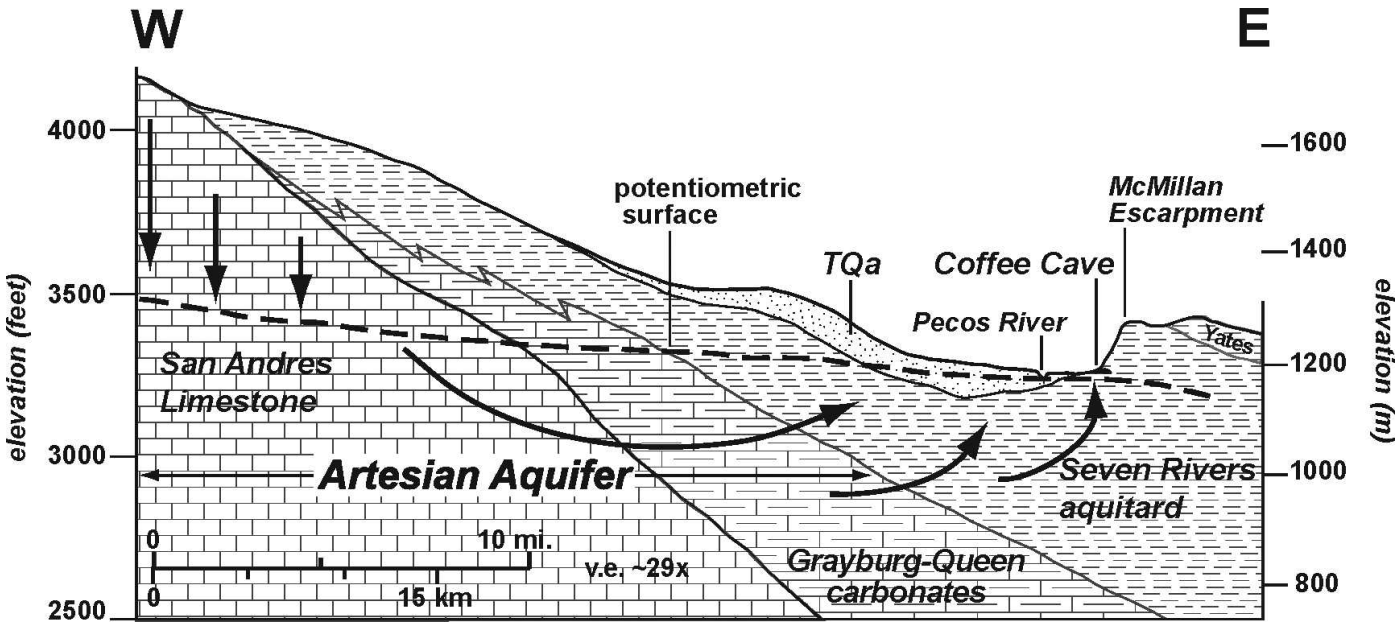

Figure 4. West-East hydrostratigraphic section across southern end of the Roswell Artesian Basin, showing relationship of Coffee Cave to the underlying artesian aquifer. The aquifer is recharged on the Pecos Slope to the west, where the San Andres and Artesia Group carbonates are exposed in outcrop. Ground water flows downgradient toward the Pecos River and upward through Seven Rivers evaporites, which serve as a leaky confining unit for the aquifer. TQa = Tertiary and Quaternary alluvium, mostly floodplain deposits of the ancestral and modern Pecos River and lacustrine sediments in the bed of old Lake McMillan. Note vertical exaggeration is ~29×.

(Welder, 1983). Although decades of intensive pumping have caused substantial declines in hydraulic head, many wells still display strong artesian flow (Land and Newton, 2007). As recently as the 1940s, wells in the vicinity of Lake McMillan flowed to the surface, with water levels reported up to 12 m above ground level (U.S. Geological Survey, 2007). Hydrologic conditions within the southern Artesian Basin thus continue to provide strong potential for hypogenic speleogenesis.

HYPOGENIC SPELEOGENESIS

Karst development is generally described in terms of geomorphology or hydrology, where dissolution is either hypogenic or epigenic (hypergenic). Epigenic speleogenesis, which is well-documented in karst literature, involves surficial features that act as entrance points for descending waters that may either recharge local ground water or form integrated cave networks that function as subsurface bypass features for overland flow (e.g., Ford and Williams, 1989; White, 1988). Epigenic karst is well studied because it naturally forms numerous surface manifestations that are easily recognized and humanly accessible. In contrast, hypogenic speleogenesis is often overlooked because it forms without a direct surface connection, usually in confined or semi-confined settings. Hypogenic karst is often only exposed by surface denudation, and is often overprinted by epigenic processes (Palmer, 1991; Klimchouk, 1996a; 2000b). However, hypogenic caves are occasionally intercepted during mining and drilling operations, where features show little or no overprinting (Kempe, 1996; Klimchouk, 2000b; 2003).

Hypogenic speleogenesis has been referred to broadly (e.g., deep-seated, confined, semi-confined, artesian, transverse) and is often attributed to specific fluid properties (e.g., sulfuric acid, hydrothermal), but in terms of hydrogeology, all types of hypogenic karst are similar. Hypogenic karst phenomena have been described in evaporitic and carbonate rocks. In evaporites, both maze caves (e.g., Klimchouk, 1996b; 2000a) and isolated voids (e.g., Kempe, 1996) are well-documented in Europe and have been attributed to confined speleogenesis. In mature carbonates, hypogenic karst has been associated with deep-seated processes involving acidic (e.g., Palmer, 1991; Lowe et al., 2000) and hydrothermal (e.g., Dublyansky, 2000) fluids. However, sulfuric acid and hydrothermal speleogenesis are simply special subsets where fluid chemistry and temperature, respectively, increase the solubility of host rock.

Following the suggestion of Ford (2006), we adopt the hydrogeological, rather than the geochemical, notion of hypogenic speleogenesis: "…the formation of caves by water that recharges the soluble formation from underlying strata, driven by hydrostatic pressure or other sources of energy, independent of recharge from the overlying or immediately adjacent surface." Hypogenic karst can de-

velop in any environment where fluids enter soluble host rock from below, being undersaturated with respect to the host rock or acquiring aggressiveness due to mixing with shallower flow systems (Klimchouk, 2000b; 2003). When the hydrogeologic framework is established for hypogenic transverse speleogenesis, dissolution may develop 3-D patterns with stratiform components, depending on the specific lithologic and structural host rock properties. Pressurized fluids will attempt to migrate upward toward regions of lower pressure, often valleys or other topographic lows (Tóth, 1999), where the exact flow path depends on the permeability of local rock units and cross-formational fractures. Flow may be horizontal through relatively high permeability units, often sands or carbonates, or vertical through originally low permeability media, often soluble units (Klimchouk, 2000b; 2003).

Hypogenic processes may be the result of either forced or free convection of ground water, or a combination of both. Forced convection is driven by differences in hydraulic head within an aquifer system. Free convection is driven by variability within fluid properties, which sets up density differences within the fluid. Lighter fluids rise and denser fluids sink, usually because of differences in salinity or temperature of the convecting fluids (e.g., Kohout, 1967; Kohout et al., 1988). Anderson and Kirkland (1980) physically modeled this process and showed that brine density convection could result in significant dissolution of soluble rocks, where undersaturated and saturated fluids simultaneously rise and sink, respectively, within a confined system. If limited connectivity occurs between source fluids and soluble rock, simultaneous flow can occur through the same pore throat, but in regions of greater connectivity separate flow paths for ascending and descending fluids may develop. Anderson and Kirkland (1980) considered brine density convection as the primary mechanism through which large vertical breccia pipes developed in the Delaware Basin, where fluids originating in a carbonate aquifer and undersaturated with respect to halite (NaCl) rose through overlying halite beds. As rising fluids dissolved halite, they became denser and subsequently sank back to the carbonate aquifer, thus undersaturated waters were continuously rejuvenated at the dissolution front. Kempe (1996) showed that speleogenesis driven by free convection can create large cavities at the base of thick evaporitic formations with low fracture density. Klimchouk (2000a; 2000b) invoked mixed convection for early stages of confined transverse speleogenesis in fractured gypsum beds in the Western Ukraine, with free convection effects becoming increasingly important during subsequent stages, when head distribution within an aquifer system was homogenized due to increased hydraulic connectivity of aquiferous units.

Although maze caves have recently been shown to form in hypogenic confined settings (Klimchouk, 2003), traditional models involve epigenic speleogenesis. The classic

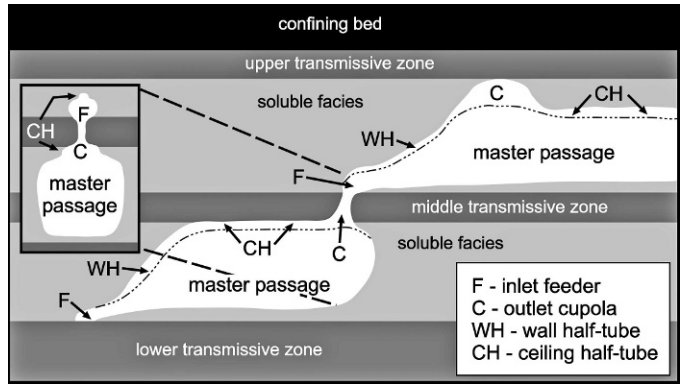

Figure 5. Diagrammatic representation of morphological feature suite indicative of hypogenic speleogenesis. Transmissive zones are dolomite and soluble beds are gypsum in Coffee Cave.

mechanism of epigenic maze cave development was suggested by Palmer (1975; 2000), where water infiltrates from above through porous, insoluble rock. As the fluids descend they are evenly distributed through fractured soluble rock, such that individual passages enlarge at similar rates and converge to form maze patterns. Other epigenic models for maze cave development invoke epigenic fluids that are delivered laterally to fractured rock, primarily in the form of back flooding, with an associated shift from vadose to phreatic dissolution. Whether a maze cave is the result of hypogenic or epigenic speleogenesis, lithologic variability and fracturing dominate maze cave development.

Klimchouk (2000a; 2003) and Frumkin and Fischhendler (2005) have described specific morphological features that are indicative of hypogenic speleogenesis. The morphologic suite consists of feeders, master passages and outlets, which occur within individual levels of hypogenic systems (Fig. 5) (Klimchouk, 2003). Feeders, or risers, are the lowest elevation component within the suite and are characterized as vertical or near-vertical conduits through which undersaturated fluids rise from lower aquifers. Feeders may form as isolated features or feature clusters. Master passages are the commonly explored portions of hypogenic caves, which are often extensive and form the largest passages because of the existence of laterally well-connected and extensive fracture networks encased within certain lithologic horizons. Outlets (i.e., cupolas and domes) occur at the highest elevations within a single level of a hypogenic cave and form the discharge features for transverse flow to higher elevations and lower pressures. Isolated risers and outlets can converge through continued dissolution such that rift-like features may develop that connect levels in a multi-level, hypogenic system. Hypogenic caves form in sluggish flow conditions and show no evidence of fast-flowing fluids, but instead exhibit smooth walls with irregular solution

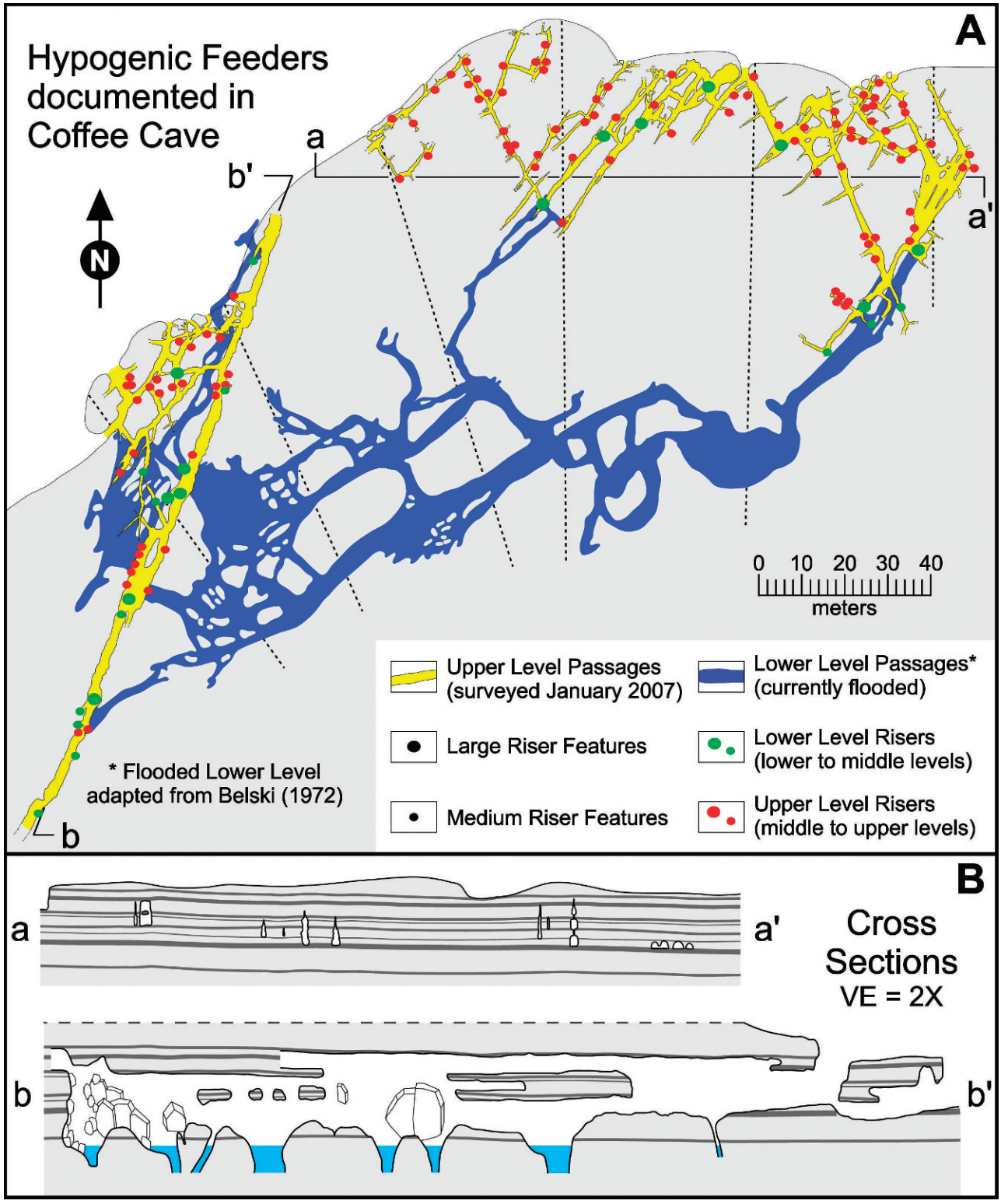

Figure 6. Geomorphic map of Coffee Cave. A) Plan view map of Coffee Cave showing maze passage morphology, hypogenic feeder distribution and delineation between lower flooded cave level and upper dry levels. The boundary between the gray and white regions along the northern edge of Coffee Cave represents the edge of the McMillan Escarpment.; B) Cross sections of Coffee Cave with 2× vertical exaggeration showing relationship of passage levels and dolomite interbeds (solid gray lines). Note that the dashed lines in Figure 6A delineate locations where passage width was measured perpendicular to the McMillan Escarpment for Figure 11.

Figure 7. McMillan escarpment showing large earth fissures (A) and complex entrance network (B).

pockets and residual pendants (Frumkin and Fischhendler, 2005), and various morphologic imprints of rising free convection circulation (Klimchouk, 2000b; 2003).

Coffee Cave

Recently, a resurvey of Coffee Cave was conducted in order to better document the cave's distribution and extent, lithologic variability, and occurrence of morphological features indicative of hypogenic transverse speleogenesis. At present, the lowermost level, which comprises at least half of the known cave, based on the original survey (Belski, 1972), is flooded (Fig. 6A).

Throughout most of the cave, fine-grained sediments and angular collapse blocks commonly cover the floor, obscuring much of the dissolutional floor morphology and displaying a bimodal distribution of allogenic sediment and autogenic breakdown. Passages proximal to the scarp edge have partially collapsed due to scarp retreat, creating large earth fissures on the land surface and a complex entrance network (Fig. 7). The occurrence of abundant surface fissures beyond the known extent of Coffee Cave strongly suggests that numerous maze caves exist along the same erosional scarp, but most are largely blocked by breakdown. Several km to the east of Coffee Cave, clusters of caves occur within the Burton Flats area that exhibit similar morphologic features indicative of hypogenic transverse speleogenesis.

Most passages within the cave are roughly rectangular in cross-section with thin dolomite beds forming the ceiling, floors and intermittent ledges (Fig. 6B, 8). The cave is a three-dimensional maze with most passages oriented northwest and northeast, which probably represents a conjugate fracture set (Fig. 6A). Most passages intercept at sharp angles, while many individual passages terminate in blind alcoves or narrow fractures, often recognized as feeders. Based on previous mapping, the lowermost level appears to be the region of most intense lateral development (Fig. 6A). Successively higher levels of the cave contain progressively smaller passages, creating at least four distinct cave levels, although the two highest levels are generally too small to be humanly accessed. In several regions, individual passages transect all four levels forming major trunk passages, which are intermittently separated into distinct levels (Fig. 6B), while many regions contain upper level passages that transect two or three levels in limited areas. It should be emphasized that the designation of levels within Coffee Cave refers only to distinct cave horizons that are lithologically separated and laterally extensive and which were formed concurrently under a constant, stable hydrologic regime. The term level does not imply hydrologically distinct solutional events or levels related to changes in hydrologic conditions.

Most of the individual cave passages exhibit complex surficial sculpturing within individual gypsum beds and between different lithologies; however, no discernable patterns common to epigenic caves with oriented scallops of similar shape and size were observed. Residual pendants are present throughout the cave. Additional morphological features indicative of rising transverse flow commonly occur on floors, walls and ceilings, including: 1) feeders, 2) rising wall channels, 3) cupolas, and 4) ceiling half-tubes. Generally, complex suites of features occur in a continuous series or in close proximity.

Feeders function as fluid inlet locations, either joining different levels of a cave or terminating blindly in bedrock, generally transmissive dolomite layers. Throughout Coffee Cave, feeders commonly occur as point source (Fig. 9A,B,D), dense clusters (Fig. 9F) or linear fissure-like features (Fig. 9E). Point source feeders are individual

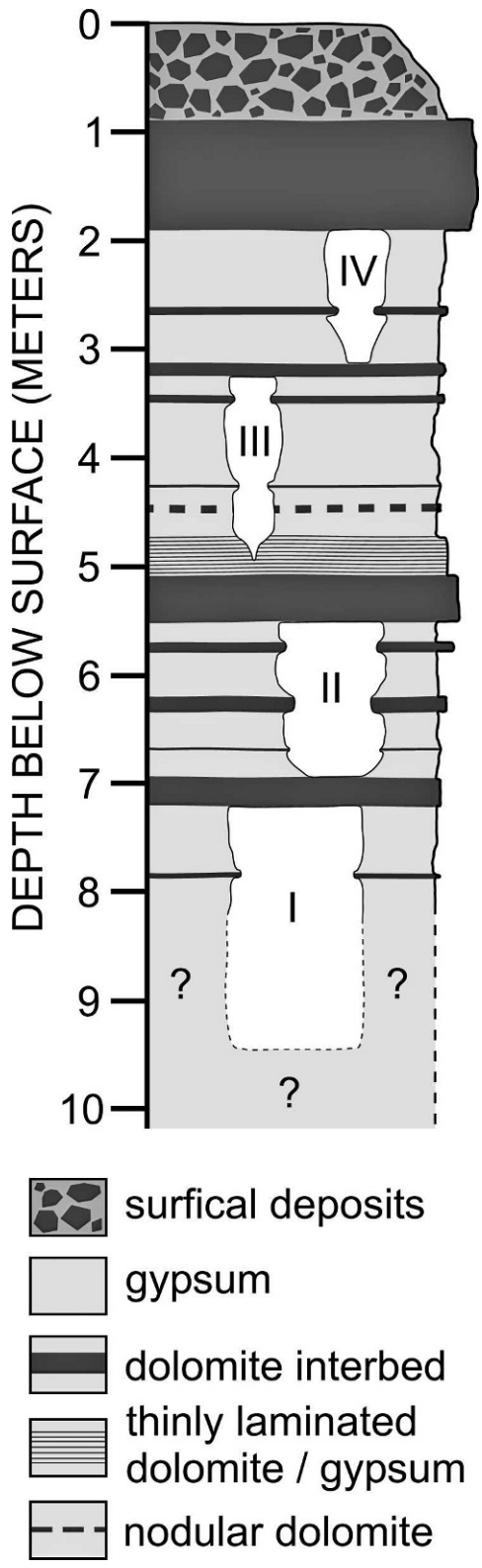

Figure 8. Composite lithologic section through Coffee Cave in relation to the four identified cave levels (designated I – IV on diagram). Levels II, III and IV represent the upper levels that were resurveyed for this study. Level I is currently flooded, hence lithology is unknown (presumably gypsum with dolomite interbeds). Passage cross-sections are average passage representations of distinct levels and do not include connections between levels.

features that generally form along dolomite-gypsum contacts in walls (Fig. 9B) or at the margins of floors (Fig. 9A,C). They are crudely conical features exhibiting an increase in aperture width toward cave passages that generally include minor doming proximal to the open passage (Fig. 9A,B,C). Feeder clusters commonly exist as a dense occurrence of small- to medium-sized feeders within a limited area, but individual feeders within clusters are morphologically similar to point feeders. Linear feeders develop along the axis of passages, forming narrow fissures along fractures, and are often associated with passages that are triangular in cross section and broaden upwards (Fig. 10E). Linear feeders are laterally extensive, as compared to point feeders.

Cupolas are well-documented in the speleogenetic literature as domal ceiling features (Osborne, 2004). However, for the purpose of this paper, they are viewed in a broader sense that encompasses traditional cupolas as well as domes and similar outlet features that may either be closed or open, concave ceiling features. Cupolas are generally elliptical in plan view (Fig. 10A), but may range from near-circular to lenticular. Cupola height ranges from centimeters to meters with inner walls that may vary from gently sloping to near vertical. Closed cupolas, which fall within the traditional descriptions of cupolas and domes, are concave features where the entire inner surface is gypsum bedrock, with the upper surface commonly formed along the contact of transmissive dolomite interbeds (Fig. 10C). In contrast, open cupolas have openings in upper surfaces, either in the center or offset to one side. Cupolas are recognizable in those passages where the ceiling is still within gypsum (Fig. 10A,D). In many passages, the next upper dolomite bed is continuously exposed at the ceiling, but it is apparent that these exposures have formed by merging of closely spaced cupolas (Fig. 10B,C).

Half-tubes (rising wall channels, ceiling channels) are elongate concave structures that occur on ceilings and walls and vary from shallow indentations to deep, incised channels, ranging in width from centimeters to meters with corresponding depths. Generally, half-tubes exhibit smooth rounded interior surfaces and abrupt, well-defined margins with adjacent walls or ceilings (Fig. 9D, 10C). Features on walls are generally vertically oriented, but may shift laterally from bottom to top (Fig. 9D). Ceiling features are usually developed on the underside of dolomite layers and commonly display irregular margins resulting from the coalescing of serial cupolas (Fig. 10B,C). When ceiling half-tubes do not form beneath dolomite beds, they gently slope

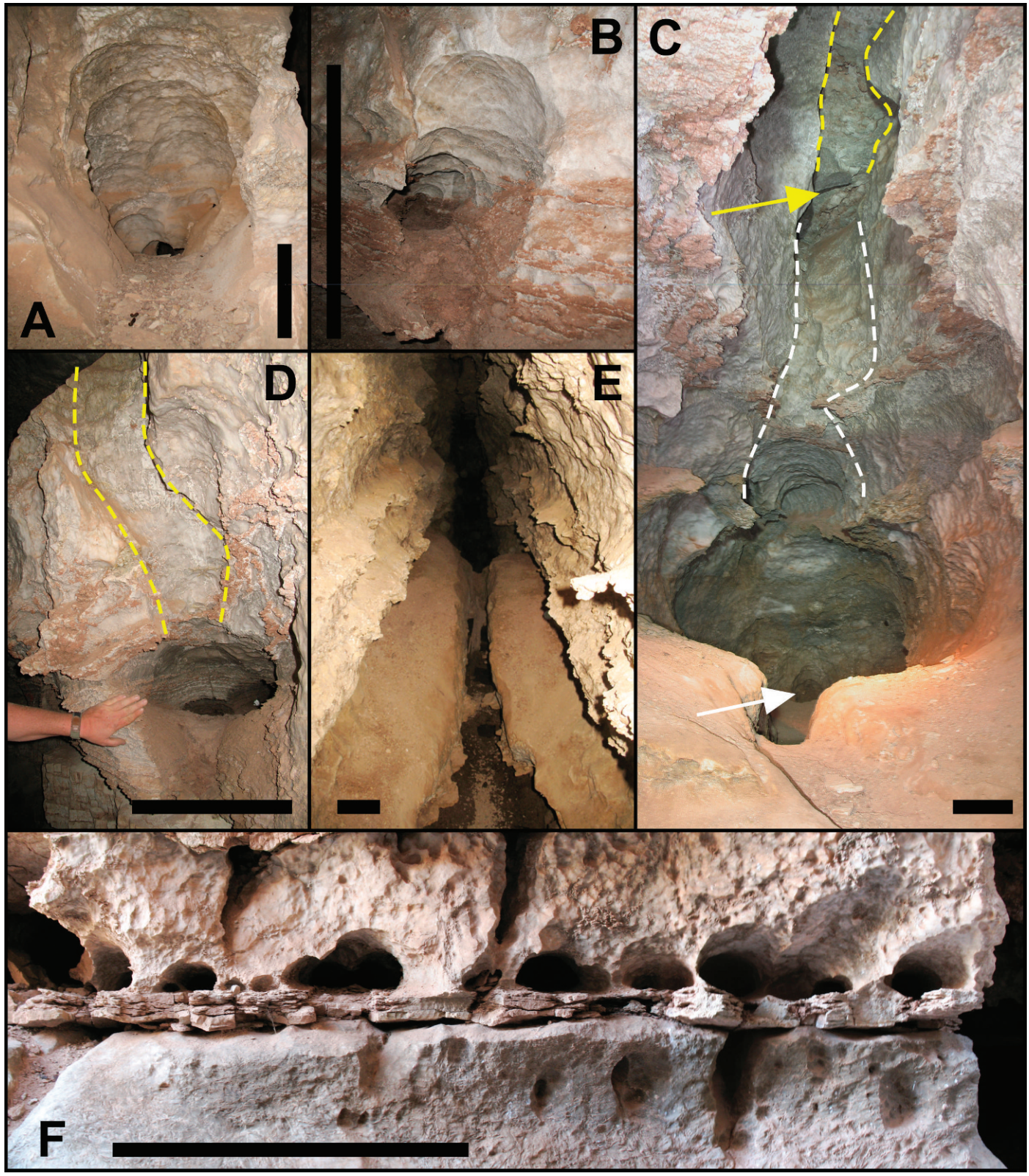

Figure 9. Feeder features in Coffee Cave. Black scale bars in figures are all approximately 0.5 m and camera angle is near-horizontal in all feeder features photos. A) point source feeder showing prominent doming morphology proximal to master passage; B) typical feeder showing development at the top of a dolomitic interbed; C) complete hypogenic morphologic suite showing riser (white arrow), wall channel (dashed white lines), ceiling channel (solid yellow lines) and outlet (yellow arrow); D) well developed wall riser with associated wall channel (dashed yellow lines); E) linear riser developed along axis of master passage; F) dense cluster of small feeders above dolomite interbed with minor vadose overprinting below dolomite interbed.

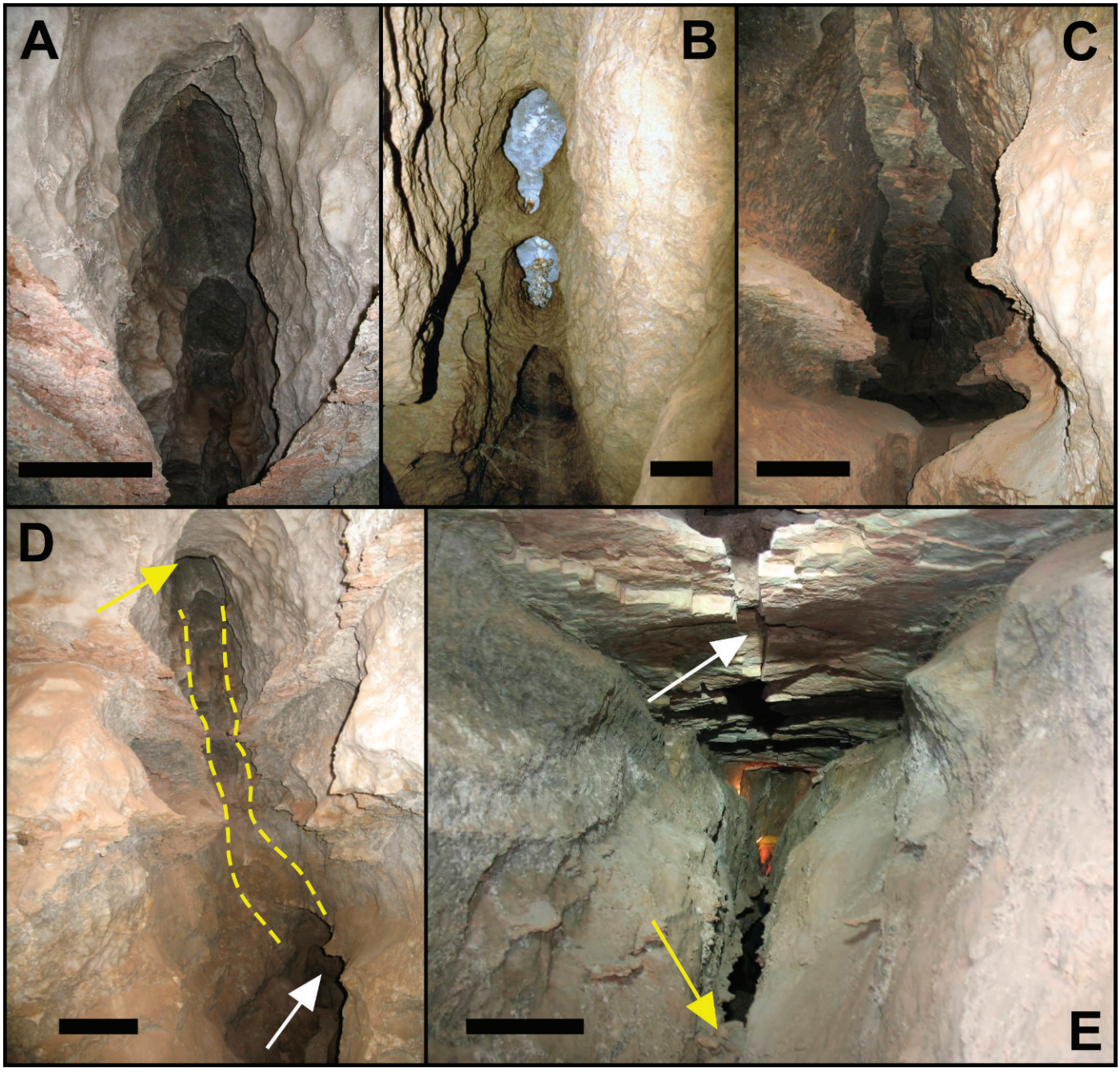

Figure 10. Outlet features in Coffee Cave. Black scale bars in figures are all approximately 0.5 m. A) series of typical ceiling cupolas (camera angle is ~60° up from horizontal, looking towards the ceiling); B) series of cupolas that are in the process of coalescing (camera angle is ~70° up from horizontal, looking toward the ceiling); C) ceiling channel formed by complete coalescing of serial cupolas (camera angle is ~30° up from horizontal, looking towards the ceiling); D) complete hypogenic morphologic suite showing riser (white arrow), wall channel (yellow dashed lines), and ceiling cupola (yellow arrow) (camera angle is roughly horizontal); E) rift-like passage showing linear feeder (yellow arrow), triangular passage and upper dolomite bed that has partially collapsed due to loss of buoyant support (white arrow) (camera angle is roughly horizontal). Figure 10B is from Fuchslabyrinth Cave, Baden-Würtenberg, Germany (developed in vertically heterogeneous beds of Triassic limestone showing lithologic variability between two distinct beds), instead of Coffee Cave, in order to better illustrate the intermediate stage of cupola coalescence.

up to an adjoining half-tube that contacts dolomite. All observed wall half-tubes join with feeders at lower elevations (Fig. 9C,D) and converge with ceiling half-tubes at higher elevations (Fig. 10D). Ceiling half-tubes join with cupolas, which when open, form the lower surface of risers to the next higher cave level; however, when cupolas are closed, they appear as deeper concave structures within a continuous ceiling half-tube (Fig. 10A,B). Both wall and ceiling half-tubes commonly converge from smaller to larger features forming a complex network.

Cupolas, feeders and half-tubes form a composite suite of morphological features throughout Coffee Cave. Therefore, during the resurvey of Coffee Cave, feeders were mapped as a proxy for the distribution of this feature suite (Fig. 6A). Small feeders (less than 10 cm wide) are abundant throughout the cave and could not be represented at the scale of mapping; therefore, mapping was limited to medium (0.1 to 1.0 m diameter) and large (>1.0 m diameter) features. During mapping of feeders, 25 features were identified that connect the lower flooded portion of the cave to the upper levels, including 12 medium and 13 large feeders. In the upper levels of the cave, 107 features were identified, all less than 1 m wide. It is probable that many more feeders exist, but they are either obscured by breakdown and sediments or are located in passages that were too small to be surveyed. Feeders are well distributed, but there appears to be a northward shift in feeder abundance from the lower level to the upper levels.

Observations within Coffee Cave during the first quarter of 2007 indicate that water levels in the cave have risen by at least 2 m in less than 3 months. This rise in water levels may be the result of an increase in hydraulic head in the artesian aquifer, or it may reflect a rise in water levels in the surficial aquifer. Both factors may be in play in the vicinity of the cave, since the water table aquifer is recharged to a large extent by upward leakage from the underlying artesian aquifer. Hydraulic head in the Artesian Basin has been rising since the late 1970s (Land and Newton, 2007), and flooding of the lower levels of Coffee Cave may thus represent, in part, increased artesian flow from the underlying Grayburg Formation (Fig. 4).

Discussion

Coffee Cave is a classic rectilinear maze cave with at least four stratigraphic levels of development and abundant morphologic features suggestive of hypogenic transverse origins with the pronounced role of free convection dissolution. Hydrologically, Coffee Cave is located at the southern end of the Roswell Artesian Basin (Fig. 1), where artesian discharge from wells and springs is well-documented (e.g., Cox, 1967; Welder, 1983). Although water extraction for agricultural use has significantly lowered ground-water levels in the region over the previous century, artesian discharge is still active. Submerged springs in the gypsum cenotes at Bottomless Lakes State Park continue to discharge significant volumes of artesian waters (Land, 2003; 2006), while free-flowing wells in the Coffee Cave area have been reported as recently as the 1940s (U.S. Geological Survey, 2007). In addition to the hydrologic regime in which Coffee Cave is located, interbedded dolomite and gypsum (Fig. 6B, 8), coupled with extensive tectonic fracturing in the Lake McMillan area, make the Seven Rivers Formation ideal for the development of multi-level hypogenic maze caves. However, prior to this study, hypogenic origins for gypsum caves were not reported in this region.

It is instructive to emphasize the difference in the degree of karstification and slope geomorphology between the gypsiferous Seven Rivers outcrops within the Pecos River Valley and outcrops in the Seven Rivers Embayment (Fig. 1) of the Guadalupe Mountains, west of the valley. In the Seven Rivers Embayment, the Seven Rivers outcrops are extensive but largely intact, with stable slopes showing minimal signs of karstification, whereas within the Pecos River Valley and its vicinity, the slopes are dramatically disturbed by gravitational processes with numerous collapse features, apparently induced by the high degree of karst development in the subsurface. These morphologies indicate intense karstification within the Seven Rivers sequence beneath the migrating and incising valley, induced by rising artesian flow (Fig. 4), in agreement with the general concept of speleogenesis in confined settings (Klimchouk, 2000b; 2003).

Coffee Cave has traditionally been characterized as a maze cave formed by back flooding along the Pecos River associated with the construction of Lake McMillan in the late 19th Century. In this model, flooding produced dissolution along fractures proximal to the scarp. Reports of leakage from Lake McMillan through karst conduits within the Seven Rivers Formation (Cox, 1967) were used as evidence for the origin of Coffee Cave through epigenic, flooding processes (alternatively, this leakage can be perfectly explained by the presence of hypogenic conduit systems). Sediments and organic detritus within Coffee Cave were used as further evidence to support an origin through back flooding. Therefore, any new model for the proposed speleogenesis of Coffee Cave must consider previous, although unpublished, interpretations of cave origin.

Caves exhibiting maze patterns have been shown to form in both epigenic and hypogenic settings; however, the complete morphological feature suite, indicative of rising flow and the role of free convection, observed in Coffee Cave (i.e., feeders, half-tubes, and outlet cupolas) has only been reported from hypogenic caves (Klimchouk, 2003; Frumkin and Fischhendler, 2005). If Coffee Cave had formed by back flooding, as suggested by the presence of allogenic sediments, then the cave should exhibit an average decrease in passage aperture width away from McMillan Escarpment, because high gypsum solubility

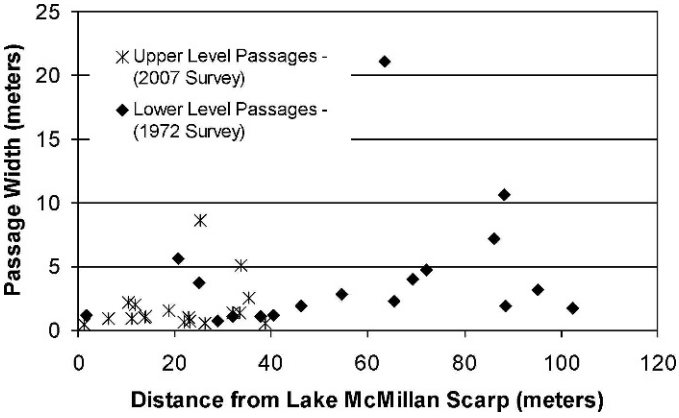

Figure 11. Plot showing relationship between passage width and distance from McMillan Escarpment. Note that the dashed lines in Figure 6A delineate locations where passage widths were measured perpendicular to the McMillan Escarpment.

promotes increased dissolution proximal to the source in epigenic settings (Klimchouk, 2000c). However, mapping in Coffee Cave has revealed that there is no systematic increase in passage width toward the scarp face. Analyses of passage width in relation to distance from the escarpment indicate that passage width actually increases with distance from the scarp (Fig. 11). Because of presence of organic detritus in the cave, it is likely that waters derived from Lake McMillan have modified Coffee Cave to some extent, primarily through sediment infilling, but lake waters do not appear to have significantly modified the cave through dissolution. Most of the overprinting of Coffee Cave's hypogenic origin is the result of scarp failure and retreat, which has produced the complex collapse entrance area along the scarp face, including more than thirty documented entrances (Fig. 6A).

The morphologic feature suite observed in Coffee Cave, as well as the presence of wall pendants and the absence of discernable scallop patterns, strongly supports a model of hypogenic speleogenesis driven by rising cross-formational flow as a significant part of the evolution of karst features in the Lake McMillan area. It is suggested here that the cave was formed under confined conditions, when the floor of the Pecos Valley was at considerably higher elevations than at present. The distribution of feeders and the overall morphology of Coffee Cave are remarkably similar to well-documented hypogenic caves in Miocene gypsum deposits of the Western Ukraine, such as Ozerna Cave (Fig. 12) (Klimchouk, 1991). Coffee Cave and the part of Ozerna Cave on the figure both show a lateral shift in passage development at adjacent levels, where clusters of conduits at the lower level served as a feeding subsystem and rising fluids have migrated laterally through the upper level. Lateral migration results from discordance in distribution of water-bearing zones in the underlying (feeding) aquifer

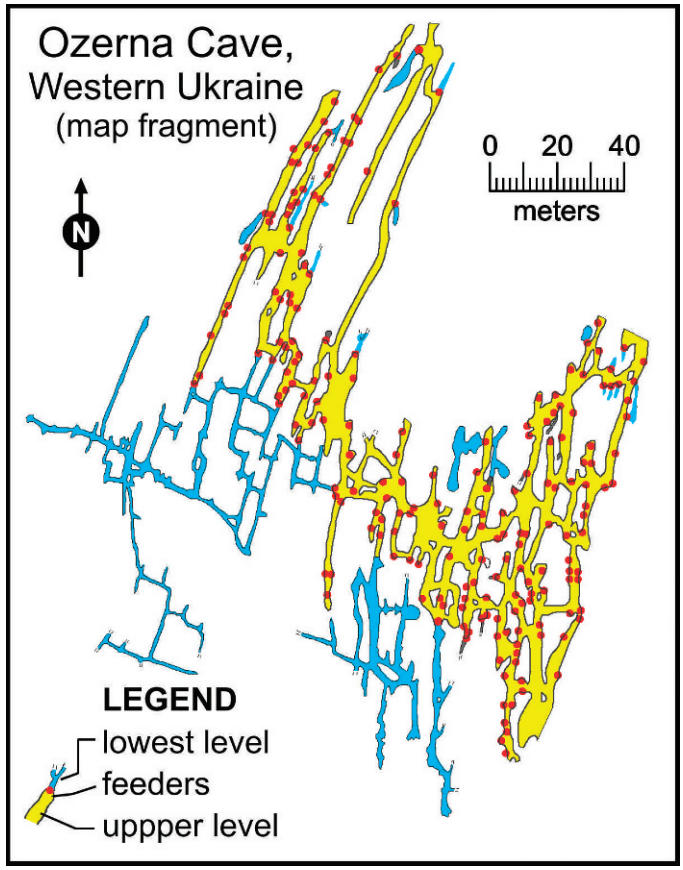

Figure 12. Map fragment from Ozerna Cave, Western Ukraine, showing cave morphology and feeder distribution (Klimchouk, 1991). Note the similarities with Coffee Cave depicted in Figure 6A.

and preferential paths for discharge through the leaky confining units (argillaceous gypsum above the upper dolomite bed in Coffee Cave). In the sluggish flow conditions of the confined system, density differences readily developed when fluids rose from the dolomite beds through gypsum, so that free convection cells operated extensively. This is evidenced by characteristic morphologic imprints of rising buoyant currents (ear-like orifices of feeders, rising wall channels, ceiling channels and cupolas) and characteristic narrowing of feeders to depth due to shielding by sinking convection limbs. The similarity between Coffee Cave and well-documented hypogenic transverse caves elsewhere further supports the role of hypogene processes in the origin of Coffee Cave.

A conceptual model for the speleogenesis of Coffee Cave has been developed (Fig. 13). Prior to karst development, evaporite facies in the Seven Rivers Formation near Lake McMillan provided a leaky seal for confined artesian fluids in the Roswell Basin aquifer (Fig. 13A). Ground water initially flowed downgradient through porous carbonates of the Grayburg and San Andres Formations and rose toward the Pecos River valley. Beneath the valley, karst initiation

began to develop vertical flow paths along fractures in the evaporite facies (Fig. 13B). Highly fractured dolomite layers within the Seven Rivers Formation served as laterally transmissive units to distribute undersaturated, aggressive waters to available fissures in the vertically adjacent gypsum beds. Locally, rising conduits could have developed even without forced flow through guiding fractures in the gypsum, solely by buoyancy-driven dissolution. Controlled by arrangement of fractures within a gypsum-dolomite intercalated sequence, the multi-level maze cave developed (Fig. 13C, D). Eventually, confinement was breached by the entrenching Pecos River Valley, and primary conduits were established for artesian discharge, most likely along a limited number of flow paths (Fig. 13E, F). Base levels within the region lowered and the cave was exposed to epigenic processes. During this final phase, minor vadose overprinting and collapse of thin dolomite beds occurred due to loss of buoyant support (Fig. 10E). Recently, in the 20th Century, flooding of the cave through the construction of Lake McMillan introduced allogenic sediments. Today, continued scarp retreat has created a complex entrance network.

Conclusions

Coffee Cave provides direct evidence for hypogenic transverse speleogenesis driven by cross-formational flow and density convection within the Seven Rivers Formation and more broadly in the Delaware Basin region of southeastern New Mexico. The complex, three-dimensional maze pattern of the cave is suggestive of hypogenic origin where non-competitive confined flow resulted in uniform dissolution along planes of brittle deformation. The complete suite of observed morphological features within the cave provides unequivocal evidence of hypogenic speleogenesis by rising mixed-convection flow, where smooth walls and concave morphologies delineate previous free convection cells. The presence of dolomite interbeds and regional fracturing makes the Seven Rivers Formation ideal for development of hypogenic caves; however, natural heterogeneities in most carbonate and sulfate rocks are sufficient for hypogenic speleogenesis in the proper hydrologic regime. The occurrence of abundant surface fissures beyond the known extent of Coffee Cave suggests that numerous hypogenic, maze caves exist along the same erosional scarp, but most are largely blocked by breakdown. Moreover, clustered highly karstified fields exist beyond the scarp, although still within the broad limits of the Pecos Valley and within the evaporite facies of the Seven Rivers and Rustler Formations. These karstified fields (e.g., Burton Flats, Nash Draw) contain numerous caves lacking genetic relationships with the surface and are likely hypogenic systems that are currently being partially denuded. It is also feasible to assume that the leakage from Lake McMillan through karst conduits within the Seven Rivers Formation was related not to epigenic karst development but the presence of pre-existing hypogenic conduit systems beneath the valley.

Based on current and ongoing studies by the authors of karst development within the New Mexico-West Texas region, the significance of hypogenic speleogenesis appears to be poorly recognized. Karst development in other regional gypsum formations (i.e., Castile, Yeso, Rustler, and San Andres) includes numerous caves that are three dimensional mazes and/or contain complete suites of morphological features indicative of the role of density driven dissolution. However, these features are not limited to gypsum formations but have also been observed in carbonate karst within the region, including, but not limited to, the caves of the Guadalupe Mountains (e.g., Carlsbad Cavern, Lechuguilla Cave, McKittrick Hill caves). Although limestone caves of the Guadalupe Mountains have been attributed to sulfuric acid (H_2SO_4) speleogenesis, they are hypogenic caves, not only by the source of acidity, but also hydrologically. These caves are hypogenic transverse features containing morphologic suites indicative of rising flow and free convection effects. Therefore, the role of hypogenic speleogenesis is likely to be extensive throughout the southwest United States, but is currently not recognized either because of extensive epigenic overprinting, misinterpretation, or because fluid chemistry (e.g., sulfuric acid) is proposed as the primary criterion for distinguishing hypogenic speleogenesis.

The identification of hypogenic speleogenesis within southeastern New Mexico, beyond the caves of the Guadalupe Mountains and breccia pipes within the Delaware Basin, suggests that more studies need to be conducted within the region, including re-evaluation of the origin of many individual caves and karst regions. The implications of an improved understanding of hypogenic speleogenesis within the region will have significant impacts on delineating areas of potential engineering geohazards, investigation of petroleum resources, mineral resources and ground-water behavior associated with karst. Ultimately, recognition of the importance of mixed convection processes related to hypogenic dissolution will enable the development of improved models for the speleogenetic evolution and basin diagenesis of the entire Delaware Basin region.

Acknowledgements

The authors wish to express their appreciation to the numerous individuals involved throughout this project. The resurvey of Coffee Cave was conducted by the authors with help from Stan Allison, Paul Burger, Jon Jasper, Lucas Middleton and Pat Seiser. Dave Belski, Jim Goodbar and Ray Nance provided essential information related to regional cave development and existing cave surveys within the area. Reviewers David Levy and Paul Burger are thanked for their useful comments which helped to improve the manuscript.

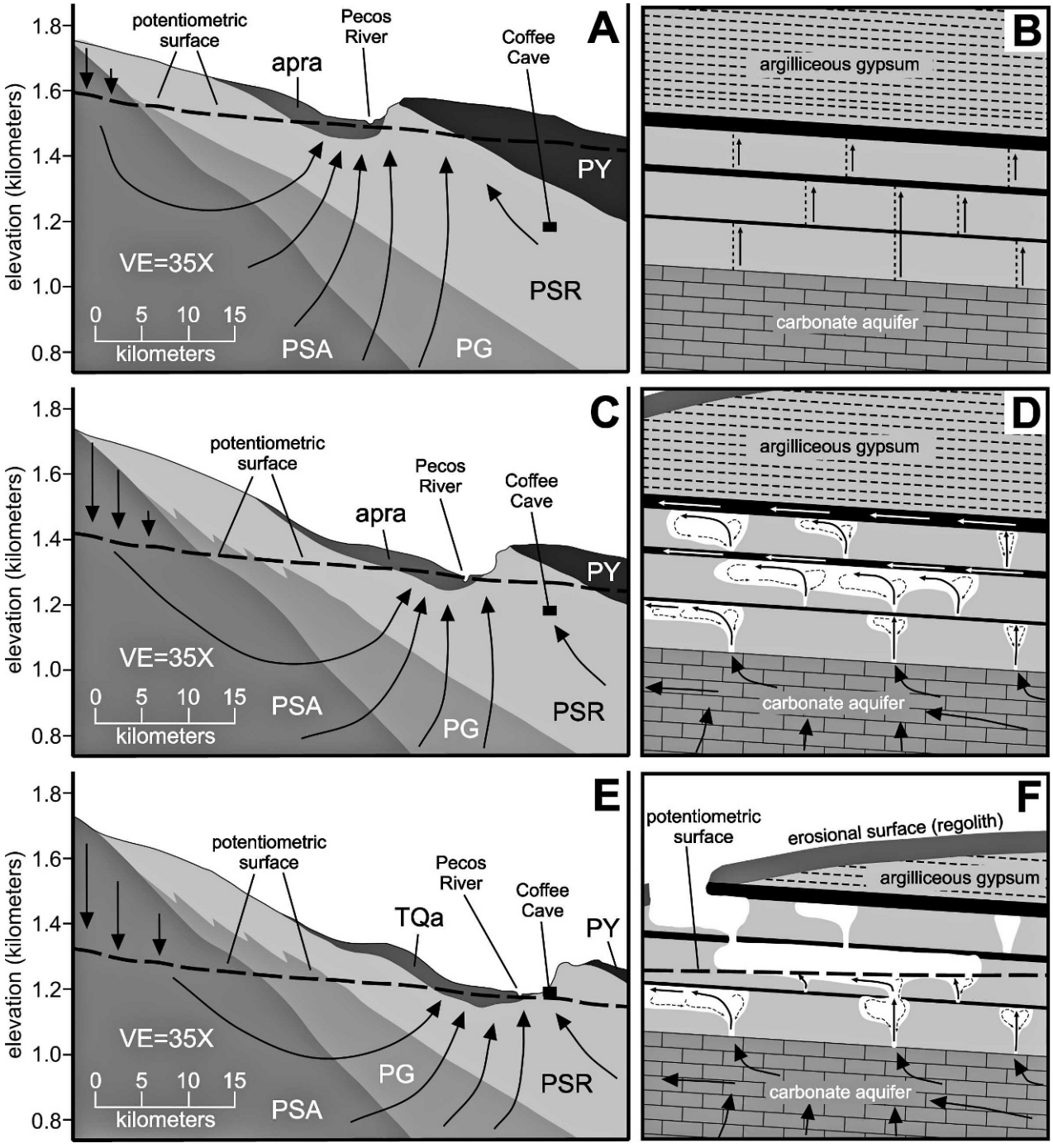

Figure 13. Conceptual model for the speleogenetic evolution of Coffee Cave in relation to the eastward migration of the Pecos River valley, associated surface denudation and evolving ground-water flow paths. A) regional conceptualization of ground-water circulation (solid black lines) in mid-to-late Tertiary time; B) local conceptualization of hydrology in Coffee Cave region, in relation to Figure 13A, showing forced flow (solid black lines) along vertical fractures in the Seven Rivers Formation; C) regional conceptualization of ground-water circulation in mid-to-late Quaternary when Coffee Cave was primarily forming; D) local conceptualization of Coffee Cave in relation to Figure 13C, showing forced convection (solid arrows) and free convection (dashed arrows) circulation involved in speleogenesis; E) current hydrologic regime in the lower Pecos River Valley; and F) conceptualization of the current hydrologic regime of Coffee Cave after surficial breaching, relating to Figure 13E. Note: Figures B, D and F are schematic illustrations that are not drawn to scale, and do not represent the actual levels of cave development, due to the resolution of the figure. PSA=Permian San Andres Fm; PG=Permian Grayburg Fm; PSR=Permian Seven Rivers Fm; PY=Permian Yates Fm; apra = ancestral Pecos River alluvium; TQa= Tertiary and Quaternary alluvium.

References

Anderson, R.Y., and Kirkland, D.W., 1980, Dissolution of salt deposits by brine density flow: Geology, v. 8, p. 66–69.

Bachman, G.O., 1984, Regional geology of Ochoan evaporites, northern part of Delaware Basin: New Mexico Bureau of Mines and Mineral Resources, Circular 184, 22 p.

Belski, D., 1972, Coffee Cave: unpublished map.

Belski, D., ed., 1992, GYPKAP Report Volume #2: Albuquerque, N.M., Southwestern Region of the National Speleological Society, 57 p.

Chapin, C.E., and Cather, S.M., 1994, Tectonic setting of the axial basins of the northern and central Rio Grande Rift, *in* Keller, G.R., and Cather, S.M., eds., Structure, stratigraphy, and tectonic setting: Geological Society of America Special Paper 291, p. 5–25.

Cox, E.R., 1967, Geology and hydrology between Lake McMillan and Carlsbad Springs, Eddy Co., New Mexico: U.S. Geological Survey Water-Supply Paper 1828, 48 p.

Dickenson, W.R., 1981, Plate tectonic evolution of the southern Cordillera: Arizona Geological Society Digest, v. 14, p. 113–135.

Dublyansky, Y.V., 2000, Hydrothermal speleogenesis – its settings and peculiar features, *in* Klimchouk, A., Ford, D.C., Palmer, A.N., and Dreybrodt, W., eds., Speleogenesis: Evolution of Karst Aquifers: Huntsville, Ala., National Speleological Society, Inc., p. 292–297.

Eaton, J., ed., 1987, GYPKAP 1987 Annual Report: Alamogordo, N.M., Southwestern Region of the National Speleological Society, 35 p.

Ford, D.C., 2006, Karst geomorphology, caves and cave deposits: a review of North American Contributions during the past half century, *in* Harmon, R.S., and Wicks, C.W., eds., Perspectives on Karst Geomorphology, Hydrology and Geochemistry: Boulder, Colo., Geological Society of America Special Paper 505, p. 1–14.

Ford, D.C., and Williams, P.W., 1989, Karst Geomorphology and Hydrology: London, Unwin Hymam, 601 p.

Frumkin, A., and Fischhendler, I., 2005, Morphometry and distribution of isolated caves as a guide for phreatic and confined paleohydrological conditions: Geomorphology, v. 67, p. 457–471.

Hendrickson, G.E., and Jones, R.S., 1952, Geology and Ground-Water Resources of Eddy County, New Mexico: Socorro, N.M., New Mexico Bureau of Mines and Mineral Resources, 189 p.

Hill, C.A., 1996, Geology of the Delaware Basin, Guadalupe, Apache and Glass Mountains: New Mexico and West Texas: Midland, Texas, Permian Basin Section – SEPM, 480 p.

Horak, R.L., 1985, Trans-Pecos tectonism and its effects on the Permian Basin, *in* Dickerson, P.W., and Muelberger, eds., Structure and Tectonics of Trans-Pecos Texas: Midland, Texas, West Texas Geological Society, p. 81–87.

Kelley, V.C., 1971, Geology of the Pecos Country, Southeastern New Mexico: Socorro, N.M., New Mexico Bureau of Mines and Mineral Resources, 78 p.

Kempe, S., 1996, Gypsum karst in Germany: International Journal of Speleology, v. 25, no. 3–4, p. 49–60.

Klimchouk, A.B., 1991, Large maze caves in gypsum in the Western Ukraine: speleogenesis under artesian conditions: National Speleological Society Bulletin, v. 53, p. 71–82.

Klimchouk, A., 1996a, The typology of gypsum karst according to its geological and geomorphological evolution: International Journal of Speleology, v. 25, no. 3–4, p. 49–60.

Klimchouk, A., 1996b, Gypsum karst of the western Ukraine: International Journal of Speleology, v. 25, no. 3–4, p. 263–278.

Klimchouk, A., 2000a, Speleogenesis of the great gypsum maze caves in the western Ukraine, *in* Klimchouk, A., Ford, D.C., Palmer, A.N., and Dreybrodt, W., eds., Speleogenesis: Evolution of Karst Aquifers: Huntsville, Ala., National Speleological Society, Inc., p. 431–442.

Klimchouk, A., 2000b, Speleogenesis under deep-seated and confined conditions, *in* Klimchouk, A., Ford, D.C., Palmer, A.N., and Dreybrodt, W., eds., Speleogenesis: Evolution of Karst Aquifers: Huntsville, Ala., National Speleological Society, Inc., p. 244–260.

Klimchouk, A., 2000c, Speleogenesis in gypsum, *in* Klimchouk, A., Ford, D.C., Palmer, A.N., and Dreybrodt, W., eds., Speleogenesis: Evolution of Karst Aquifers: Huntsville, Ala., National Speleological Society, Inc., p. 261–273.

Klimchouk, A., 2003, Conceptualization of speleogenesis in multi-story artesian systems: a model of transverse speleogenesis: Speleogenesis and Evolution of Karst Aquifers, v. 1, no. 2, p. 1–18.

Klimchouk, A., Lowe, D., Cooper, A., and Sauro, U., eds., 1996, Gypsum Karst of the World: International Journal of Speleology, v. 25, no. 3–4, 307 p.

Kohout, F.A., 1967, Ground-water flow and the geothermal regime of the Floridian Plateau: Transactions of the Gulf Coast Association of Geological Societies, v. 17, p. 339–354.

Kohout, F.A., Meisler, H., Meyer, F., Johnston, R., Leve, G., and Wait, R., 1988, Hydrogeology of the Atlantic Continental Margin, *in* Sheridan, R., and Grow, J., eds., The Geology of North America; the Atlantic Continental Margin, U.S.: Boulder, Colo., Geological Society of America, v. I-2, p. 463–480.

Land, L., 2003, Evaporite karst and regional ground water circulation in the lower Pecos Valley, *in* Johnson, K.S., and Neal, J.T., eds., Evaporite Karst and Engineering and Environmental Problems in the United States: Oklahoma Geological Survey Circular 109, p. 227–232.

Land, L., 2005, Evaluation of groundwater residence time in a karstic aquifer using environmental tracers: Roswell Artesian Basin, New Mexico, *in* Proceedings of the Tenth Multidisciplinary Conference on Sinkholes and the Engineering and Environmental Impacts of Karst, San Antonio, Texas, 2005: ASCE Geotechnical Special Publication no. 144, p. 432–440.

Land, L., 2006, Hydrogeology of Bottomless Lakes State Park, *in* Land, L., Lueth, V., Raatz, B., Boston, P., and Love, D., eds., Caves and Karst of Southeastern New Mexico: New Mexico Geological Society, Guidebook 57, p. 95–96.

Land, L., and Newton, B.T., 2007, Seasonal and long-term variations in hydraulic head in a karstic aquifer: Roswell Artesian Basin, New Mexico: Journal of the American Water Resources Association (in press).

Lee, J., ed., 1996, GYPKAP Report Volume 3: Alamogordo, N.M., Southwestern Region of the National Speleological Society, 69 p.

Lowe, D.J., Bottrell, S.H., and Gunn, J., 2000, Some case studies of speleogenesis by sulfuric acid, *in* Klimchouk, A., Ford, D.C., Palmer, A.N., and Dreybrodt, W., eds., Speleogenesis: Evolution of Karst Aquifers: Huntsville, Ala., National Speleological Society, Inc., p. 304–308.

Osborne, R.A.L., 2004, The troubles with cupolas, Acta Carsologica, v. 33, no. 2, p. 9–36.

Palmer, A.N., 1975, The origin of maze caves: National Speleological Society Bulletin, v. 37, no. 3, p. 56–76.

Palmer, A.N., 1991, Origin and morphology of limestone caves: Geological Society of America Bulletin, v. 103, p. 1–21.

Palmer, A.N., 2000, Maze origin by diffuse recharge through overlying formations, *in* Klimchouk, A., Ford, D.C., Palmer, A.N., and Dreybrodt, W., eds., Speleogenesis: Evolution of Karst Aquifers: Huntsville, Ala., National Speleological Society, Inc., p. 387–390.

Quinlan, J.F., Smith, R.A., and Johnson, K.S., 1987, Gypsum karst and salt karst of the United States of America, *in* Atti symposio interntional sul carsimo nelle evaporiti, Le Grotte d'Italia, v. 4, no. XIII, p. 73–92.

Scholle, P.A., Goldstein, R.H., and Ulmer-Scholle, D.S., 2004, Classic Upper Paleozoic Reefs and Bioherms of West Texas and New Mexico: Socorro, N.M., New Mexico Institute of Mining and Technology, 166 p.

Tóth, J., 1999, Groundwater as a geologic agent and overview of the causes, processes, and manifestations: Hydrogeology Journal, v. 7, p. 1–14.

U.S. Geological Survey, 2007, National Water Information System (NWIS): http://nwis.waterdata.usgs.gov.

White, W.B., 1988, Geomorphology and Hydrology of Karst Terrains: Oxford Univ. Press, New York, NY, 464 p.

Welder, G.E., 1983, Geohydrologic framework of the Roswell Ground-Water Basin, Chaves and Eddy Counties, New Mexico: New Mexico State Engineer Technical Report 42, 28 p.

Zeigler, K.E., 2006, Stratigraphic chart, *in* Land, L., Lueth, V., Raatz, B., Boston, P., and Love, D., eds., Caves and Karst of Southeastern New Mexico: New Mexico Geological Society, Guidebook 57, p. inside back cover.

E. Raeisi – Ground-water storage calculation in karst aquifers with alluvium or no-flow boundaries. *Journal of Cave and Karst Studies,* v. 70, no. 1, p. 62–70.

GROUND-WATER STORAGE CALCULATION IN KARST AQUIFERS WITH ALLUVIUM OR NO-FLOW BOUNDARIES

EZATOLLAH RAEISI
Department of Earth Sciences, College of Science, Shiraz University, Shiraz, Iran, e_raeisi@yahoo.com

Abstract: The determination of water-budget parameters, such as change in storage and subsurface inflow and outflow, is costly and unreliable due to heterogeneities of karst aquifers. Some karst aquifers may have one or a combination of boundaries such as impermeable formations, alluvial aquifers, and known ground-water divides. Karst water only discharges through springs or flows to the adjacent alluvium. A new procedure is proposed to estimate volume of storage in region during the dry season in these settings. The subsurface inflow and outflow can be measured in the adjacent alluvium using equipotential and flow lines, cross-sectional area, and transmissivity of the alluvial aquifer. The dry season makes it possible to calculate the karst spring recession coefficient and karst aquifer dynamic volume at the beginning and end of the hydrological year. The change of storage is the difference between the dynamic volumes of the karst aquifer at the beginning and end of the hydrological year. The volume of water which flows to the adjacent alluvium or spring is measured by plotting the discharge as a function of time and estimating the recession coefficient at the beginning (or end) of the hydrological year. Known equations are used to calculate the dynamic volume of springs. A general equation is proposed to calculate the dynamic volume of a karst aquifer when there is a combination of springs, and subsurface inflow and outflow from the karst aquifer. The proposed method is applicable to the Zagros Folded Zone in Iran.

INTRODUCTION

Karst aquifers are classified on a scale that ranges from diffuse, mixed, to conduit (White, 1969). Two extremes can be recognized: a diffuse aquifer which is poorly integrated and has little influence on karst ground-water circulation (Shuster and White, 1971; Atkinson, 1977) and a conduit aquifer, in which ground-water flow is dominated by the conduit system (White, 1988). Most karst aquifers contain both diffuse and conduit regimes in which water flows in conduits as well as fractures and pores. These characteristics of karst aquifers result in extensive variations of hydraulic parameters and water-surface elevations, even over short distances.

The determination of some water-budget parameters, such as storage volume and subsurface inflow and outflow, require the measurement of water levels in boreholes and hydraulic parameters in exploration wells. It is very difficult to obtain reliable ground-water parameters and water-table configurations in a heterogeneous karst system.

The objective of this study is to propose equations for estimating the change of storage in a semi-arid karst system with no-flow boundaries (impermeable or known ground-water divide) in which the karst water discharges only from a karst spring. This method is applied in the Sheshpeer aquifer of Iran. A general equation is proposed to calculate the dynamic volume and change of storage of a karst aquifer when there is a combination of springs, and subsurface inflow and outflow from the karst aquifer to the adjacent alluvial aquifers. The karst subsurface inflow and outflow can be measured in the adjacent alluvium.

WATER BUDGET

A hydrologic budget is a quantitative evaluation of inflow, outflow and the change in storage over a specified time interval, usually a hydrological year. A hydrological year starts and ends when storage is at its minimum. The mass-balance equation for a karstic high mountain aquifer can be simplified as follows

$$I_a + I_s + I_{ss} = O_a + D + E + \Delta V \qquad (1)$$

where I_a is the subsurface inflow from the adjacent aquifer, I_s is the effective recharge, I_{ss} is surface-water seepage which reaches the phreatic ground water, O_a is subsurface outflow to an adjacent aquifer, D is the discharge by pumping wells, springs and qanats (a qanat is a sloped longitudinal channel which is dug below the ground-water surface to intercept ground water and at the end of the qanat, water discharges by gravity into an irrigation channel), E is evaporation from the water table, and ΔV is the change in ground-water storage between the beginning and the end of the hydrological year and may be positive or negative. If the karst aquifer is in direct contact with an adjacent aquifer, the subsurface inflow and outflow can be measured in the adjacent aquifer. This will later be explained in the discussion section.

If the run-off leaves a karst formation, joining the main drainage on a non-karst formation, effective recharge (I_s) is estimated in several typical surface sub-basins by the following equation

$$I_s = P - (R + E_t) \quad (2)$$

where P is precipitation, R is run-off and E_t is actual evapotranspiration or sublimation. If the karst area is covered by snow, then sublimation should be measured instead of evapotranspiration. Runoff (R) is estimated by measuring the flow rates at the outlet of the typical karstic sub-basin. Evapotranspiration (E_t) can be estimated by direct field measurement (soil-water content between two consecutive rainfalls or lysimeters) or by climatological and crop data (Jensen, 1981). Sublimation is measured by lysimeter or calibrated equations.

If a permanent river or channel flows on the surface of a karst aquifer, its seepage (I_{ss}) can be estimated by measuring the discharges at the beginning and end of the reach which traverses the karst aquifer.

Change in Storage

The change in storage can be calculated for a simple karst system if the following conditions are met:

1. The karst aquifer is bounded by impermeable layers (Fig. 1a) and/or a known ground-water divide. The impermeable layers and ground-water divide are no-flow boundaries.
2. The karst water discharges only from a karst spring.
3. There is no precipitation during the dry season, such that the spring recession coefficient can be calculated at the beginning and end of the hydrological year.

The volume of stored water in the saturated zone above the level of the outflow spring is termed the dynamic volume of the spring (Mangin, 1975; Ford and Williams, 1994). If there is no precipitation and base-flow conditions prevail, the dynamic volume gradually discharges from the spring until the spring is completely dry. If the spring discharge is plotted as a function of time, the dynamic volume at any time t is equal to the area under the curve bounded between the time t and the time when discharge reaches zero. On a semi-logarithmic scale, this curve becomes a line with slope $-\alpha$, called the recession coefficient (Fig. 2a). Maillet (1905) proposed the following simple exponential equation for this line

$$Q = Q_0 e^{-\alpha t} \quad (3)$$

where Q is the discharge ($m^3\ s^{-1}$) at time t, Q_o is the discharge at time zero, t is the time elapsed (day) between Q and Q_o, and α is the recession coefficient (day^{-1}). Thus the spring dynamic volume (V), in m^3, is (Milanović, 1981; Ford and Williams, 1994)

$$V = C \int_t^{\infty} Q_0 e^{-\alpha t}\, dt = C \frac{Q}{\alpha} \quad (4)$$

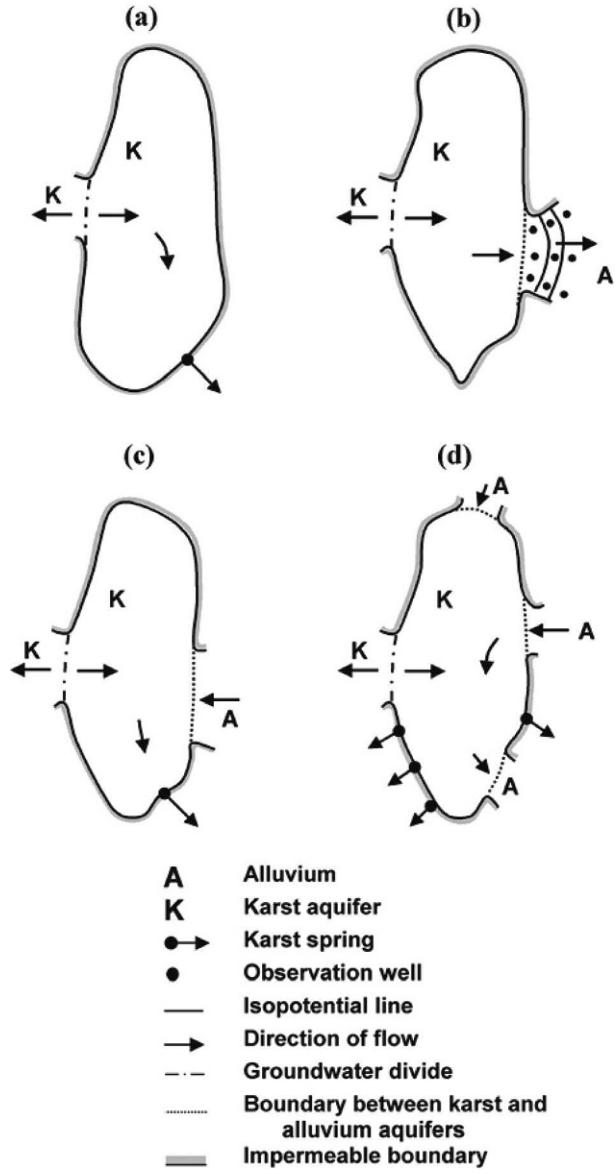

Figure 1. Schematic diagram of the boundary conditions of karst aquifers.

The constant C, equal to 86400, is the unit conversion factor (days to seconds).

The change of storage in the karst aquifer (ΔV) is estimated as the difference between the dynamic volume at the beginning (V_{S1}) and end (V_{S2}) of the hydrological year.

$$\Delta V_S = V_{S1} - V_{S2} \quad (5)$$

The subscript s denotes spring. If there is no change in the recession coefficient after the beginning or end of the hydrologic year, the change of storage may be estimated by a simple combination of Equations (4) and (5).

$$\Delta V_S = C \left[\frac{Q_{S1}}{\alpha_{S1}} - \frac{Q_{S2}}{\alpha_{S2}} \right] \quad (6)$$

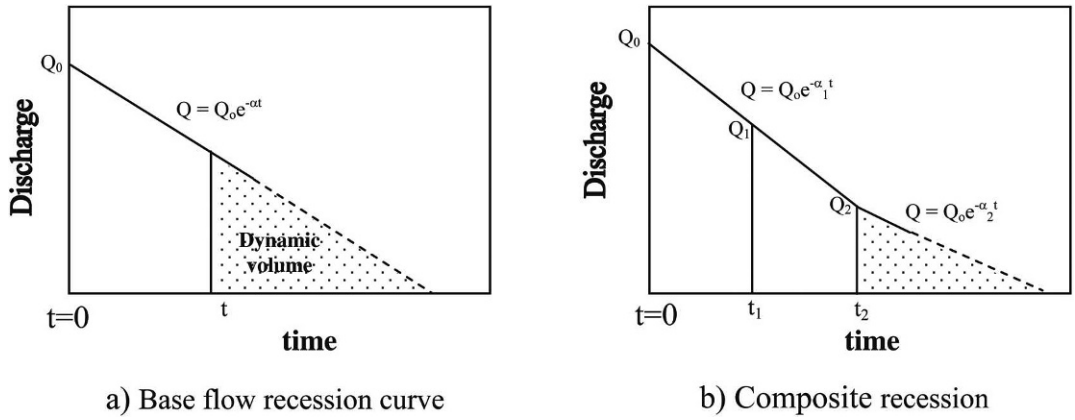

Figure 2. Schematic diagram of recession curves: a) base flow recession curve; b) composite recession curve.

The recession coefficient may change during the recession process (Forkasiewicz and Paloc, 1967). Therefore, if there is a change of recession coefficient (Fig. 2b), the dynamic volume is calculated as follows:

$$V = C\int_{t_1}^{t_2} Q_0 e^{-\alpha_1 t}\,dt + C\int_{t_2}^{\infty} Q_0 e^{-\alpha_2 t}\,dt = C\left(\frac{Q_1 - Q_2}{\alpha_1} + \frac{Q_2}{\alpha_2}\right) \quad (7)$$

in which α_1 and α_2 are the recession coefficients (day^{-1}) of the two slopes respectively, Q_1 is the discharge ($m^3\ s^{-1}$) at the time that dynamic volume is being estimated, Q_2 is the discharge ($m^3\ s^{-1}$) at the point where the slope changes, t_1 is the time (day) when the dynamic volume is being estimated, and t_2 is the time (day) when the slope changes. If several recession coefficients are observed after the time when dynamic volume is being estimated, a similar approach results in the following general equation

$$V = C\left[\frac{Q_1 - Q_2}{\alpha_1} + \frac{Q_2 - Q_3}{\alpha_2} + \frac{Q_3 - Q_4}{\alpha_3} + \cdots + \frac{Q_{n-1} - Q_n}{\alpha_{n-1}} + \frac{Q_n}{\alpha_n}\right] \quad (8)$$

where n is the number of recession coefficients. To estimate the dynamic volume more accurately, it is suggested that discharge be measured very accurately and at least weekly since the dynamic volume is very sensitive to the value of α and the discharge.

SIMPLE CASE STUDY

In the simple case study, the karst water only discharges through a karst spring and there is no inflow from the adjacent alluvium. The study area is located to the west of Shiraz, Iran. Extensive geological, geomorphological, hydrogeological (including dye tracing), hydrochemical and hydrological studies have been carried out in this study area (Pezeshkpoor, 1991; Porhemat, 1993; Raeisi et al., 1993; Raeisi and Karami, 1996; Raeisi and Karami, 1997; Raeisi et al., 1999). The Barm-Firooz and Gar (Mor and Gar Mountains) anticlines extend in the general direction of the Zagros Mountain Range (Fig. 3). The exposed cores of the anticlines dominantly consist of the calcareous Sarvak Formation (Albian-Turonian), underlain and overlain by impermeable shales of the Kazhdumi (Aptian-Cenemonian) and Pabdeh-Gurpi (Cretaceous-Tertiary) Formations, respectively. The tectonic features are a main thrust, and normal and strike-slip faults. The strike-slip fault has produced suitable conditions for extensive karstification. The most important exokarst feature is the presence of 160 sinkholes on the northern flank of Gar Mountain, and 99 sinkholes in Barm-Firooz Mountain (Fig. 3). The Sarvak Formation is present at the highest points of the study area, with a maximum elevation of 3714 m asl. and a minimum of 2110 m asl.

Out of twelve springs emerging from the Sarvak Formation, only Sheshpeer Spring occurs on the northern flank, with a mean annual discharge of 3247 L s^{-1}. One of the springs, Berghan, has a mean annual discharge of 632 L s^{-1}. The mean annual discharge of all the other springs ranges from 1.41 to 68.34 L s^{-1} (Raeisi and Karami, 1997). Precipitation occurs during late fall, winter and early spring. There is no precipitation during the rest of the year. The precipitation in winter is mainly in the form of snow, most of which melts by mid-spring. The average annual precipitation at Berghan station (elevation 2110 m) is 750 mm. Using the regional relationship between elevation and rainfall, the average annual precipitation of the Sheshpeer catchment area is calculated to be 1350 mm (Raeisi et al., 1993 and Porhemat, 1993). Soil cover overlies 35% of the Sarvak Formation. About 95 percent of the soils belong to the regosol and lithosol categories, and the remaining 5 percent are related to the brown soils (Raeisi and Karami, 1996). The study area is a natural pasture.

The 81 km^2 catchment area of the Sheshpeer Spring (Fig. 3) consists primarily of the northern flank of Barm-Firooz and Gar Mountains and a small portion of the

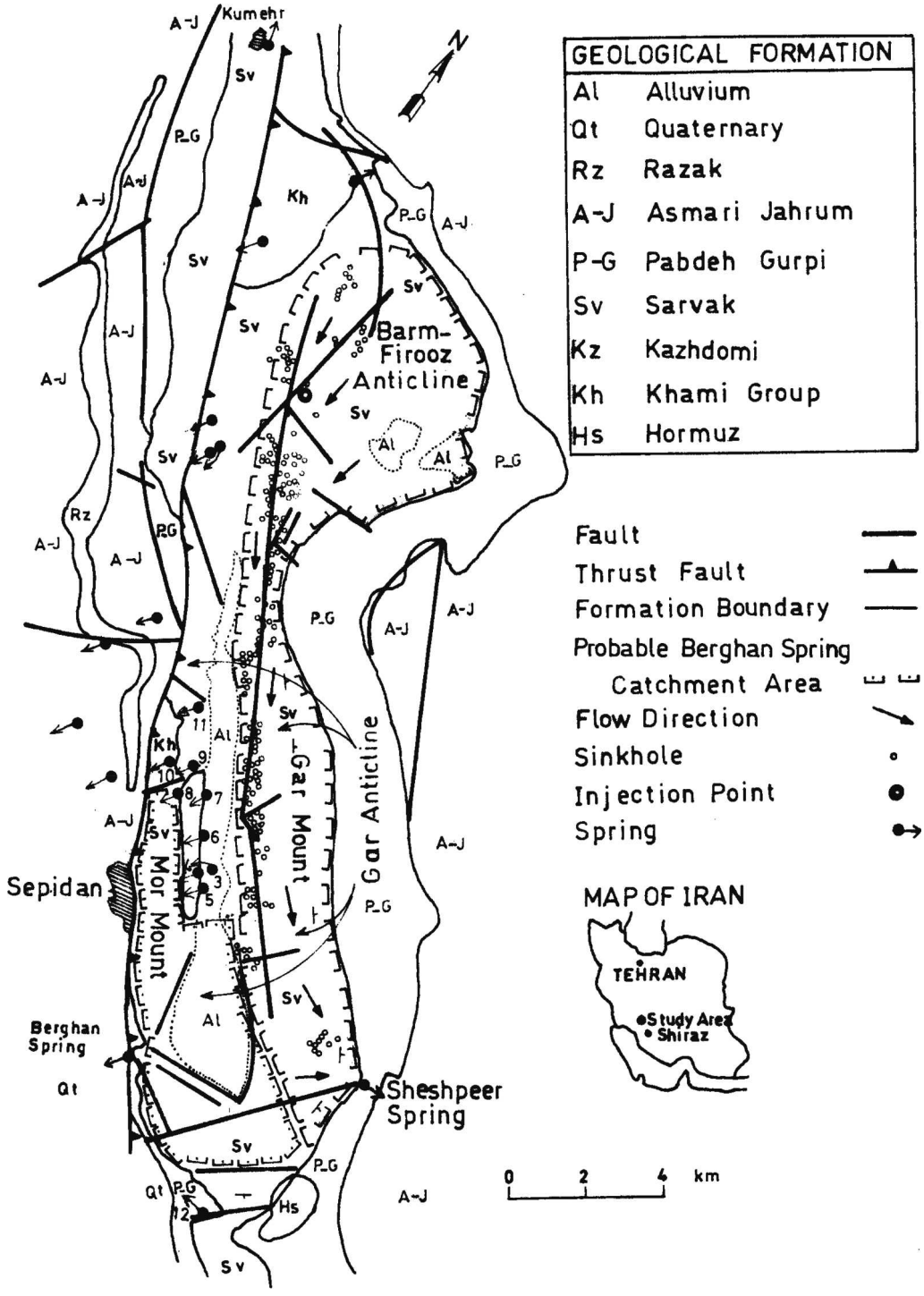

Figure 3. Hydrogeological map of the study area (after Raeisi and Karami, 1996).

southern flank of Barm-Firooz Mountain (Pezeshkpoor, 1991). The indicated boundary for the catchment area is based on:

1. The northern flank of the Gar and Barm-Firooz anticlines have been brought up by tectonic stress, such that the aquifers of the northern and southern flanks have been disconnected and the underlying impermeable Khazdumi Formation is outcropping in a part of the anticline core (Fig. 3). Dye-tracing tests confirm this hydrogeological disconnection between the southern and northern flanks (Raeisi et al., 1999).
2. The northwest and northeast sides of the anticlines are bounded by the impermeable Pabdeh-Gurpi Forma-

tions (Fig. 3 and 4). Water flow under the Pabdeh-Gurpi Formations is not possible because (a) karstification usually does not occur under an 800-meter thick layer of Pabdeh-Gurpi Formations, (b) there are no outcrops of Sarvak Formation in parallel adjacent anticlines, and (c) no dye was detected in the springs of the adjacent anticlines.

3. The sinkholes are only located in the catchment area of Sheshpeer Spring. Sodium fluorescein injected in a sinkhole 18 km away from the Sheshpeer spring (Fig. 3) appeared only in this spring (Raeisi et al., 1999).

It may be concluded that the basin divide of Sheshpeer Spring is a no-flow boundary and all the recharged water emerges only from the Sheshpeer spring.

The hydrographs of Sheshpeer Spring for 1991 and 1992 are presented in Figure 5. The discharge data in the summer of 1991 were measured monthly. Although this reduces the precision of the recession coefficient, it is still accurate enough to describe the proposed method. The recession curves of Sheshpeer Spring for the beginning and end of the hydrological year are presented in Figure 6. The reference time is May 1, so the beginning of the hydrological year (Sep. 21, 1991) is day 144 and the end of the hydrological year is day 509. By fitting the data to Equation (3), the following relation is obtained:

$$Q = 2.9002e^{-0021t} \quad (9)$$

Using Equation (9) for the beginning of the hydrological year (t =144), the discharge is 2.143 $m^3 s^{-1}$. From Equation (4), the dynamic volume at the beginning of the hydrological year is 88.2 $\times 10^6$ m^3.

At the end of the hydrological year (September 21, 1992), the recession equation is as follows (Fig. 6):

$$Q = 19.937e^{-0.0038t} \quad (10)$$

At the end of the hydrological year (t = 509 day) the discharge (Q_1) is 2.88 $m^3 s^{-1}$. In 1992, discharge was only measured up to the end of November (Fig. 5), therefore it is not known if the recession curve continues with the same

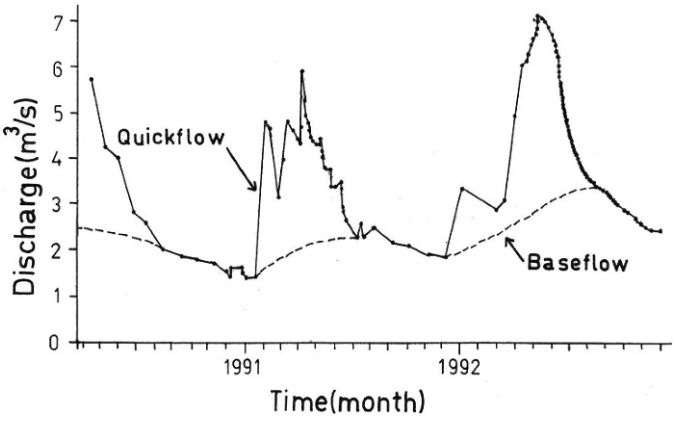

Figure 5. Hydrograph of Sheshpeer spring.

slope or shows a change of slope after this time. In 1991, the recession coefficient changed to 0.0021 at a discharge of 2.5 $m^3 s^{-1}$. Because the recession coefficient is dependent on discharge, a similar coefficient is also expected in 1992 at discharges lower than 2.5 $m^3 s^{-1}$. Taking this into account, the recession curve of 1991 is transferred to 1992 starting at a discharge (Q_2) equal to 2.5 $m^3 s^{-1}$ (dotted line on Fig. 6). The dynamic volume at the end of the hydrological year is calculated to be 111.5 $\times 10^6$ m^3 using Equation (5). The change of storage using Equation (7) is 23.3 $\times 10^6$ m^3.

The subsurface inflow (I_a) and subsurface outflow (O_a), and evaporation from the water table (E) in Equation 1 are zero in the study area. There are neither wells nor qanats in the study area, so the total volume of Sheshpeer spring discharge (D) was 112.2 $\times 10^6$ m^3 during the hydrological year. Applying the above data to Equation (1), a value of 134.7 $\times 10^6$ m^3 is obtained for effective recharge from precipitation and surface water seepage (I_S). Because there are neither rivers nor channels in the catchment area, the volume of precipitation reaching ground water (I_S) is 134.7 $\times 10^6$ m^3. The volume of rainfall was about 146.5 $\times 10^6$ m^3 during the hydrological year. This shows that the infiltration coefficient is 91.9%.

Porhemat (1993) measured runoff and sublimation directly, and estimated snow melt and sublimation by the

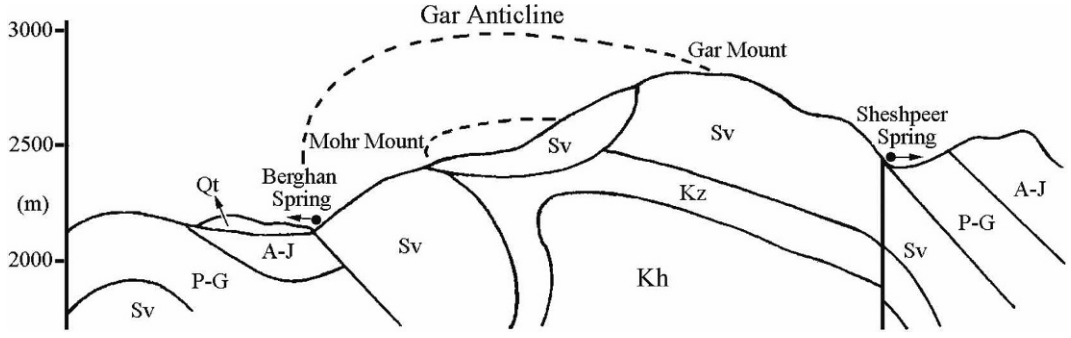

Figure 4. Geological cross section between Berghan and Sheshpeer Springs, The legend is shown on Figure 3 (after Raeisi et al., 1993).

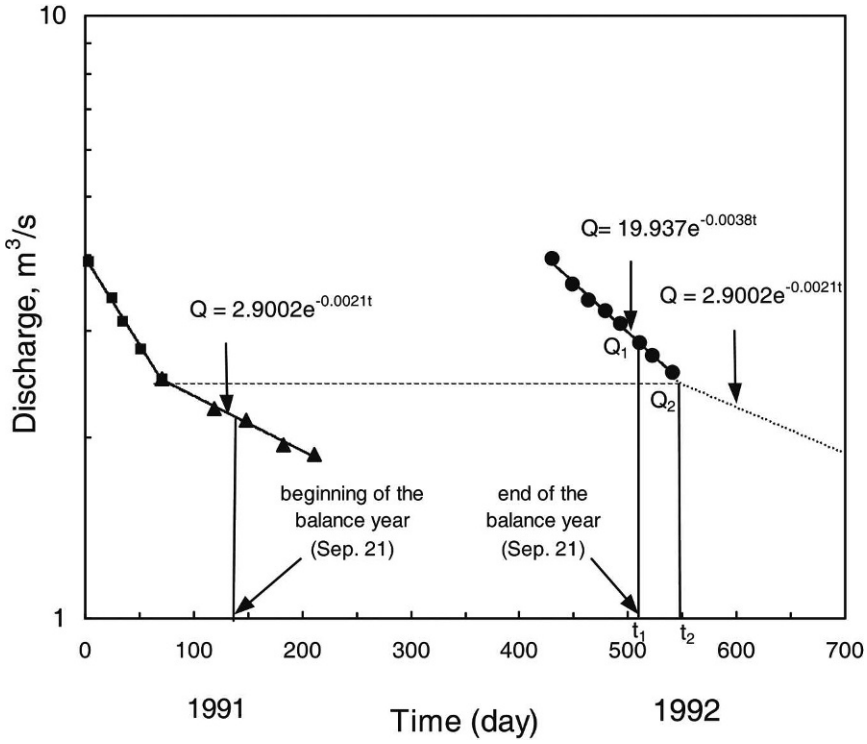

Figure 6. Recession curves of Sheshpeer spring around the beginning and end of the hydrological year.

regionally calibrated equations in three small catchment areas in the Barm-Firooz anticline. The average percentage of sublimation was 5.2%, runoff was 25.3%, and infiltration from melting snow was 69.5%. The catchment of the study area is covered partly by sinkholes; therefore, parts of the runoff flow into the sinkholes, justifying the value of 91.9% for the infiltration coefficient estimated from water-budget equations. Discharge was measured monthly instead of weekly, reducing the accuracy of recession coefficient. This in turn affects the estimated value of change of storage.

Discussion

Boreholes and exploration wells are very small features on the scale of the heterogeneities of a karst aquifer. Values of hydrodynamic parameters obtained from pump tests vary widely over short distances depending on exactly where the wells are drilled (White, 1988). A well that taps a connection with the conduit system can produce very large yields of water with negligible drawdown. A well drilled a few meters away in an unfractured or unkarstified block of limestone may have a very small yield of water. Therefore, it is very difficult to obtain reliable groundwater parameters and water-table configurations in such a heterogeneous system. In addition, the construction of observation and pumping wells is very expensive in the highland karst zone of Iran due to deep water tables and lack of accessible roads.

If the karst aquifer is in direct contact with an adjacent alluvium aquifer overlying an impermeable layer, the subsurface outflow from the karst aquifer can be measured in the adjacent alluvium aquifer, thus avoiding the heterogeneity of the karst aquifer. The outflow from the karst aquifer is equal to subsurface inflow into the adjacent alluvial aquifer. A piezometric network is constructed in the adjacent alluvium. The subsurface outflow can be measured in the adjacent alluvium using the flow net formed by equipotential and flow lines, cross-sectional area, and transmissivity (Todd and Mays, 2005). This is a commonly used method in alluvial aquifers. Three rows of piezometers are constructed in the adjacent alluvium, perpendicular to the direction of flow (Fig. 1b). All the piezometers must reach the top of the impermeable layer beneath the alluvium. The outflow may be measured monthly during the dry season and more frequently during the wet season; therefore, the total annual volume of outflow can be determined. The advantage of this method is that one is no longer confronted with the problems of the high expenses of constructing piezometric networks and pumping wells in a highland karst aquifer, the hydraulic-parameter heterogeneity, and complexity of water-surface configuration.

To overcome the problems of karst heterogeneity, several methods have been proposed in order to avoid the direct measurement of storage coefficients. Milanović (1981) suggested estimating the storage coefficient using the recession coefficient of a spring hydrograph. The

assumptions of homogenous medium, one dimensional and diffuse flow, constant horizontal cross-section of the aquifer and average gradient of the energy potential are not characteristics of karst aquifers. Spatial variations of storage coefficients in an aquifer cannot be detected with this method because the discharge can only be measured at one point. White (1988) suggested estimating the water budget over a sufficiently long time such that the change of storage approaches zero. Unfortunately, long time data are rarely available for many karst regions. In addition, the water budget cannot be determined for a wet, a dry, or a specific year. Milanović (1981) suggested choosing a balance year with negligible change of storage. In this method, the project should be postponed until the occurrence of a year with negligible change of storage.

The simplified case of a karst aquifer with no-flow boundaries having its water discharged only through springs was explained earlier. In addition, the change in storage may be determined while the karst aquifer is partially or totally in direct contact with the alluvium. Two different karst aquifers with simplified boundary conditions are considered for estimating the change in storage, and finally, the general case will be discussed:

CASE 1

The karst aquifer is in direct contact with the impermeable layer, known ground-water divide, and/or alluvial aquifer (Fig. 1b). The adjacent alluvial aquifer is located over an impermeable formation, such that the karst subsurface water flows only to the adjacent alluvium. There is no inflow into the karst aquifer from the adjacent alluvial aquifer. The alluvium dynamic volume is defined as the volume of water stored in a karst aquifer above the impermeable basement which is located beneath the adjacent alluvium. This water is gradually discharged to the adjacent alluvium and decreases to zero under the assumption of no precipitation.

The subsurface outflow from the karst aquifer can be measured in the adjacent alluvium using the method explained in the previous paragraphs. This outflow must be measured at least once a week in the dry season, starting from two to three months before the beginning (and end) of the hydrological year until the first rainfall. The alluvium recession coefficient is then estimated as the slope of the semi-logarithmic plot of outflow versus time using the Maillet (1905) equation. Equations (3) and (4) are used to estimate the alluvium dynamic volume. In this case, the change of storage (ΔV_O) is the difference between the alluvium dynamic volume at the beginning of the hydrological year (V_{O1}) and the alluvium dynamic volume at the end of the hydrological year (V_{O2}):

$$\Delta V_O = V_{O1} - V_{O2} \tag{11}$$

where the subscript o denotes outflow from the karst aquifer. If there is no change in the recession coefficient after the beginning or end of the hydrological year, the change of storage may be estimated by a simple combination of Equations (4) and (11)

$$\Delta V_O = C \left[\frac{Q_{O1}}{\alpha_{O1}} - \frac{Q_{O2}}{\alpha_{O2}} \right] \tag{12}$$

CASE 2

The karst aquifer boundary is similar to Case 1, but there is inflow from the adjacent alluvium into the karst aquifer. Karst water discharges only from a karst spring (Fig. 1c). In this case, water discharging from the spring is a combination of water stored in the karst aquifer and the incoming water from the adjacent alluvium

$$V_S = V_a + V_E \tag{13}$$

where V_S is the total volume of water discharging from the karst spring and can be measured directly, and V_E is the dynamic volume of the adjacent alluvium from which water enters the karst aquifer. V_E is estimated by the same procedure mentioned for the flow of karst water to an adjacent aquifer. V_a is the dynamic volume of the karst aquifer and may be estimated using equation 13. In this case the change of storage is:

$$\Delta V = V_{a1} - V_{a2} = (V_{S1} - V_{E1}) - (V_{S2} - V_{E2}) \tag{14}$$

or

$$\Delta V = (V_{S1} - V_{S2}) - (V_{E1} - V_{E2}) \tag{15}$$

The subscripts 1 and 2 denote the beginning and end of the hydrological year respectively.

GENERAL CASE

A karst aquifer has various springs and inflow and outflow sections (Fig 1d). The general equation is a combination of all the above cases

$$\Delta V = \sum_{j=1}^{n} (V_{S1j} - V_{S2j}) + \sum_{i=1}^{m} (V_{O1i} - V_{O2i}) - \sum_{k}^{p} (V_{E1k} - V_{E2k}) \tag{16}$$

in which V_{S1} and V_{S2} are the spring dynamic volumes, V_{O1} and V_{O2} are the outflow dynamic volumes of the adjacent alluvium, and V_{E1} and V_{E2} are the inflow dynamic volumes of the adjacent alluvium. The subscripts 1 and 2 denote the beginning and end of the hydrological year respectively and n, m, and p are the number of springs, and outflow and inflow sections of the adjacent alluvium respectively. All the above dynamic volumes can be measured using Equations (4), (5) or (6). If there is no change in the recession coefficient after the beginning or end of the hydrological year, the aquifer change of storage may be

estimated by a simple combination of Equations (4) and (16)

$$\Delta V = \sum_{j=1}^{n} \left(\frac{Q_{S1j}}{\alpha_{S1j}} - \frac{Q_{S2j}}{\alpha_{S2j}} \right) + \sum_{i=1}^{m} \left(\frac{Q_{O1i}}{\alpha_{O1i}} - \frac{Q_{O2i}}{\alpha_{O2i}} \right) - \sum_{k}^{p} \left(\frac{Q_{E1k}}{\alpha_{E1k}} - \frac{Q_{E2k}}{\alpha_{E2k}} \right) \quad (17)$$

The changes of storage are calculated in all cases without the necessity of measuring the storage coefficients in exploitation wells, which are not representative of karst aquifers. This increases the accuracy of the proposed method in a complex heterogeneous karst system.

Characteristics of the Zagros Karstic Folded Zone

The proposed method is applicable in a karst aquifer with the special boundary conditions. This type of aquifer is typical in the Zagros Orogenic System, especially in the Folded Zone. The Zagros Highland occupies the borderlands of Iran, from eastern Turkey to the Oman Sea. The Zagros Orogenic System may be divided longitudinally into the folded zone, imbricated zone, and thrust zone. The folded zone, the southwestern half of the orogenic system, is a zone of strong folding produced for the most part by late Pliocene orogeny. This zone is characterized by a repetition of long and regular anticline and syncline folds. The anticlines are normally mountain ridges, mostly composed of limestone, and the synclines are valleys and plains. James and Wynd (1965) and Falcon (1974) described the stratigraphic and structural characteristics of the Zagros sedimentary sequence in detail. Ashjari and Raeisi (2006) showed that most of the aquifers in the Zagros Folded Zone form a broad highland aquifer with the following characteristics:

1. The karstic aquifers are sandwiched between two thick impermeable formations such that the hydrogeological connections between them are disconnected, except in the rare occasions that a major fault juxtaposes the two karstic formations. A cross section at the Kermansh province, west of Iran, shows that the impermeable marly and shaly Pabdeh-Gurpi Formations disconnect the hydrogeological relationship between the karstic Asmari and Illam Formations (Fig. 7). The underlying impermeable Pubdeh-Gurpi Formations inhibit loss of water from the outcropped karstic Asmari Formation to the underlying buried karstic Illam Formation.
2. The outcropped karstic units are present in the high mountains in the Simple Folded Zone. The impermeable overlying formations are eroded from the high elevation parts of the anticlines, and they are mostly exposed at the foot of the anticlines or buried under a thin alluvium (Fig. 7). The impermeable formation surrounds the karstic formation such that each anticline seems to be an independent aquifer unless a major fault changed the normal anticline setting. When the contact of karstic formations with the overlying impermeable formations acts as a local base of erosion, karst water discharges as a spring at the contact zone (Fig. 7). When there is direct connection between the karstic formation and the alluvium, karst water flows to the adjacent alluvial aquifer above the contact zone of karstic formation and the overlying impermeable layer (Fig. 7).
3. Flow from one karstic anticline to the parallel adjacent karstic anticlines is unlikely because a) the karstic formations in synclines are normally buried under very thick overburden. Karstification is usually not significant at greater depths. b) The elevations of the underlying impermeable formations under the crest of parallel anticlines are higher than the ground-water level in adjacent alluvial aquifer, such that the alluvium water cannot flow toward the adjacent anticlines.

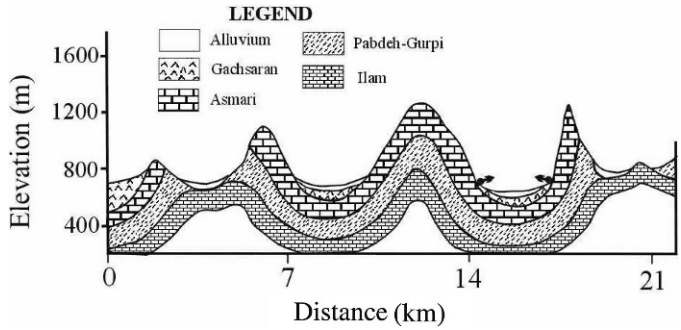

Figure 7. Alvand Basin cross section (after Karimi, 2003).

These characteristics imply that karstic formations in the Zagros anticlines are mostly independent aquifers. The aquifer boundary is limited to the overlying and underlying impermeable formations and/or adjacent alluvium. The general direction of flow is mostly toward the local base of erosion, parallel to the strike. Karst water discharges at springs or flows into the adjacent alluvial aquifer where a direct connection exists between the alluvium and the karst formation.

Examples, such as Case 1, 2, or other complex cases, require a special arrangement of piezometers in the adjacent alluvium (Fig. 1b) to enable the preparation of a reliable flow net. It was not possible to find a piezometric network similar to that of Figure 1b in Iran. In most cases, only one piezometer was found, and the piezometers were often shallow or no hydraulic conductivity data were available. Satisfactory research requires tremendous budgets; it is not possible to construct the piezometers and exploration wells with the limited research budgets of universities. It is our hope that the publication of this paper will encourage research budget support from government offices.

CONCLUSIONS

A new method is proposed to calculate the ground-water storage in karst aquifers with specific boundaries in a semi-arid karst region. These aquifers are delineated by one or more boundaries such as impermeable formations, known ground-water divides or alluvial aquifers. Karst water either discharges as a spring at the foot of the anticlines or flows into adjacent alluvial aquifers. The dry season makes it possible to calculate the recession coefficient and dynamic volume of a karst aquifer. For such conditions, several equations are proposed to estimate the budget parameters of subsurface inflow and outflow of the aquifer, and the change of storage. Subsurface inflow and outflow from the karst aquifer can be measured in the adjacent alluvium instead of the karstic aquifer itself, avoiding the heterogeneities of complex karst systems and the high expenses of constructing accessible roads, deep piezometers, and pumping wells in highlands. The change of storage is estimated as the difference between the dynamic volumes at the beginning and end of the hydrological year. The dynamic volumes of springs are calculated by the known method of plotting discharge as a function of time and using the related equations. The dynamic volume of a karst aquifer which flows to the adjacent alluvium is similarly estimated by plotting the discharge versus time, where the discharge is measured in the adjacent alluvium instead of the karst aquifer. A general equation is presented for estimating dynamic volume for the case where there is a combination of springs and inflow and outflow from adjacent aquifers. The value of the dynamic volume is very sensitive to the values of the recession coefficients, therefore it is highly recommended that the discharge be measured accurately on a weekly basis. The theory was applied for a special case where the karst water discharges only from a spring. It is recommended that the study be extended for a case with the adjacent alluvium boundary.

ACKNOWLEDGEMENTS

This study is the result of a research project on Barm-Firooz and Gar anticlines, which was funded by the Shiraz University Research Council.

REFERENCES

Ashjari, J., and Raeisi, E., 2006, Anticlinal structure influences on regional flow, Zagros, Iran: Journal of Cave and Karst Studies, v. 68, no. 3, p. 119–127.

Atkinson, T.C., 1977, Diffuse flow in limestone terrain in the Mendip Hills, Somerset (Great Britain): Journal of Hydrology, v. 35, p. 93–100.

Falcon, N.L., 1974, Southern Iran: Zagros Mountains in Mesozoic-Cenozoic orogenic belts: Geological Society of London, Special Publication, v. 4, p. 199–211.

Forkasiewicz, J., and Paloc, H., 1967, Le regime de tarissement de la Foux-de-la-Vis. Etude preliminaire: Chronique d'Hydrogeologie, BRGM, v. 3, no. 10, p. 61–73.

Ford, D.C., and Williams, P.W., 1994, Karst geomorphology and hydrology: Winchester, Massachusetts, Unwin Hyman, 601 p.

Jensen, M.E., 1981, Design and operation of farm irrigation systems: The American Society of Agricultural Engineering, Michigan, 829 p.

James, G.A., and Wynd, J.G., 1965, Stratigraphic nomenclature of Iranian Oil Consortium Agreement area: Bulletin of American Association of Petroleum Geologists, v. 49, no. 12, p. 2182–2245.

Karimi, H., 2003, Hydrogeological behavior of Alvand karst aquifers, Kermanshah, [Ph.D. thesis]: Shiraz, Shiraz University, Iran, 282 p.

Mangin, A., 1975, Contribution à lètude hydrodynamique des aquiferes karstiques. DES Thesis: Dijon University, France,

Maillet, E., 1905, Essais dhydraulique souterraine et fluviale, Hermann, Paris,

Milanović, P.T., 1981, Karst Hydrogeology: Fort Collins, Colorado, Water Resources Publications, 434 p.

Pezeshkpoor, P., 1991, Hydrogeological and hydrochemical evaluation of Kuh-e Gar and Barm-Firooz springs [M. Sc. Thesis]: Shiraz, Shiraz University, Iran, 282 p.

Porhemat, J., 1993, Evaluation of hydrological balance parameters in karstic highland catchment area. [M. Sc. Thesis]: Shiraz, Shiraz University, Iran, 427 p.

Raeisi, E., Pezeshkpoor, P., and Moor, F., 1993, Characteristics of karst aquifer as indicated by temporal changes of the springs physico-chemical parameters: Iranian Journal of Science and Technology, v. 17, p. 17–28.

Raeisi, E., and Karami, G., 1996, The governing factors of the physical and hydrochemical characteristics of karst springs: Carbonates and Evaporites, v. 11, no. 2, p. 162–168.

Raeisi, E., and Karami, G., 1997, Hydrodynamics of Berghan karst spring as indicators of aquifer characteristics: Journal of Cave and Karst Studies, v. 59, no. 3, p. 112–118.

Raeisi, E., Zare, M., and Eftekhari, P., 1999, Application of dye tracing for determining characteristics of Sheshpeer karst spring, Iran: Theoretical and Applied Karstology, v. 11–12, p. 109–118.

Shuster, E.T., and White, W.B., 1971, Seasonal fluctuations in the chemistry of limestone springs: A possible means for characterizing aquifers: Journal of Hydrology, v. 14, p. 93–128.

Todd, D.H., and Mays, L.W., 2005, Groundwater Hydrology: John Wiley and Sons, Inc., 636 p.

White, W.B., 1969, Conceptual models for carbonate aquifer: Ground Water, v. 7, no. 3, p. 15–21.

White, W.B., 1988, Geomorphology and hydrology of karst terrains: New York, Oxford University Press, 464 p.

BOOK REVIEW

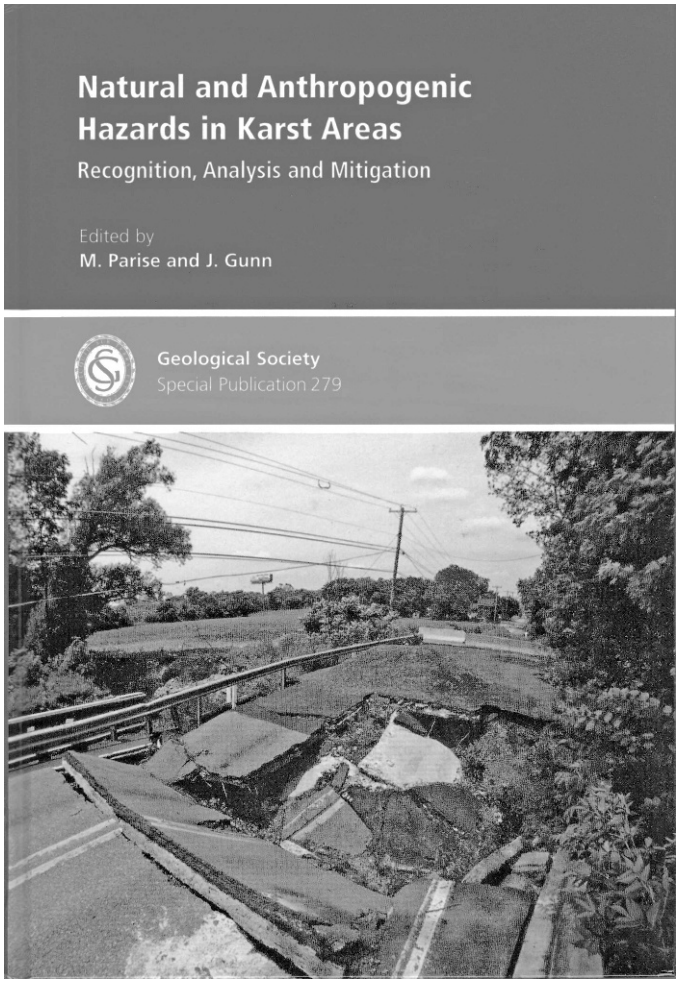

Natural and Anthropogenic Hazards in Karst Areas: Recognition, Analysis and Mitigation

M. Parise and J. Gunn (eds.), 2007. London, The Geological Society, Special Publication 279, 202 p., 6⅞ × 10 inches. ISBN 978-1-86239-224-3, hardbound, £70.00 / $140.00 list, GSL member price £35.00 / $70.00, AAPG/SEPM/GSA/RAS/EFG/PESGB member price £42.00 / $84.00. Available in North America at gsl.orders@aidcvt.com or http://bookstore.aapg.org.

This is a collection of papers presented at the Second General Assembly of the European Geosciences Union in Vienna, Austria April 24–19, 2005. As the title of the book suggests, the emphasis is on natural hazards in karst terranes, which the cover brings home dramatically with a photo of sinkhole subsidence beneath a roadway and bridge caused by dewatering. The book is divided into three sections: Collapse and Subsidence Hazards, Hydrological Hazards, and Managing Karst.

The first paper begins with the only U.S. example, sinkhole distribution in Pinellas County, Florida, which compares pre-development conditions in the urbanized area by examining two sets of aerial photographs (1926 and 1995). Significant features of each photograph were digitized to obtain a baseline (1926) and a post-urbanization distribution of natural sinkholes and man-made depressions (1995). The second paper is a somewhat theoretical assessment of natural and anthropogenic rock collapse over open caves. Most cavers will recognize these events to be relatively rare. However, the rarity of the occurrence is reduced as additional loading is imposed by engineering works directly above caves. This paper should be must reading for geotechnical engineering firms working in karst terranes. The next three papers include (1) an inventory and analysis of sinkholes in Italy, (2) assessment of cover-collapse sinkholes in Sardinia, Italy, (3) assessment of karst processes in the carbonate Apennines of Campania, Italy, and (4) magnetic prospecting for sinkhole detection in northern Spain. I have never been confident of the ability of geophysical methods to detect sinkholes, but the 4th paper in this section makes a convincing case for this somewhat overlooked method.

The section on Hydrological Hazards includes six papers. It begins with a discussion of risk to coastal karst geomorphosites (longshore bar and small backshore lagoon) from severe flooding in Sardinia. It is followed by a discussion of protection of karst aquifer recharge areas and mitigation of karst hazards, which stresses hydrogeologic mapping, hydrologic and hydrochemical observations, and tracer testing, the latter being the most important of the three. The next paper provides an assessment of rapid bypass flow in unsaturated chalk and its significance for contaminant transport. This paper emphasizes the value of tracer testing and modeling of breakthrough curves. Transport through unsaturated chalk can be very rapid and relatively unrestricted, which means that solute retardation and/or decay is minimal. The next paper focuses on stable isotopes in aqueous sulfate as tracers of natural and contaminant sulfate sources, with an emphasis on endemic tracers of various pollutant sulfate sources that are useful for tracing human-influenced releases such as from mining operations. The last two papers in this section address the intrinsic vulnerability of the Alburni karst system (southern Italy), which is another example of the European obsession with karst vulnerability mapping (something only minimally addressed in the U.S.), and an evaluation of the impact of quarrying on karst aquifers in southern Italy. This last paper also addresses karst vulnerability mapping, and, more significantly, it details the terrible concept of using abandoned quarries for landfills, both legal and illegal, into which solid and liquid wastes are repeatedly dumped with serious consequences to the underlying aquifer. (It has been illegal to dump liquids in hazardous waste landfills in the U.S. for over two decades.)

The final section, Managing Karst, includes only two papers, perhaps because the concept seems strange. The first addresses natural and anthropogenic hazards in the karst of Jamaica and documents numerous examples. However, actions such as ecotourism and designation of protected areas are helping to reduce them (e.g., water quality). The last paper addresses biotic and abiotic calcite formation on prehistoric cave paintings in France and the need for protection, particularly because some of the calcite may be a result of human influences.

Overall this book is a highly recommended addition to the library of anyone working on environmental projects in karst terranes. It is printed on high-quality glossy paper and is carefully edited — I found only one typographical error — and with very high quality black and white photos and figures. It also includes an excellent index. However, it is somewhat expensive. The 8-point font size helped cut down the size and cost of the book but makes it a little difficult to read for some.

Reviewed by Malcolm Field, National Center for Environmental Assessment, Office of Research and Development, U.S. Environmental Protection Agency, 1200 Pennsylvania Ave., NW, Washington, DC 20460-0001 (field.malcolm@epa.gov).

ERRATA

It has been brought to the *Journal's* attention that on page 113 in Volume 69 Issue 1 the contribution of Figure 8 by Jim Papadakis was inadvertently omitted from the Acknowledgements section of the manuscript by William Halliday titled Pseudokarst in the 21st Century.

GUIDE TO AUTHORS

The *Journal of Cave and Karst Studies* is a multidisciplinary journal devoted to cave and karst research. The *Journal* is seeking original, unpublished manuscripts concerning the scientific study of caves or other karst features. Authors do not need to be members of the National Speleological Society, but preference is given to manuscripts of importance to North American speleology.

LANGUAGES: The *Journal of Cave and Karst Studies* uses American-style English as its standard language and spelling style, with the exception of allowing a second abstract in another language when room allows. In the case of proper names, the *Journal* tries to accommodate other spellings and punctuation styles. In cases where the Editor-in-Chief finds it appropriate to use non-English words outside of proper names (generally where no equivalent English word exists), the *Journal* italicizes them. However, the common abbreviations i.e., e.g., et al., and etc. should appear in roman text. Authors are encouraged to write for our combined professional and amateur readerships.

CONTENT: Each paper will contain a title with the authors' names and addresses, an abstract, and the text of the paper, including a summary or conclusions section. Acknowledgments and references follow the text.

ABSTRACTS: An abstract stating the essential points and results must accompany all articles. An abstract is a summary, not a promise of what topics are covered in the paper.

STYLE: The *Journal* consults The Chicago Manual of Style on most general style issues.

REFERENCES: In the text, references to previously published work should be followed by the relevant author's name and date (and page number, when appropriate) in parentheses. All cited references are alphabetical at the end of the manuscript with senior author's last name first, followed by date of publication, title, publisher, volume, and page numbers. Geological Society of America format should be used (see http://www.geosociety.org/pubs/geoguid5.htm). Please do not abbreviate periodical titles. Web references are acceptable when deemed appropriate. The references should follow the style of: Author (or publisher), year, Webpage title: Publisher (if a specific author is available), full URL (e.g., http://www.usgs.gov/citguide.html) and date when the web site was accessed in brackets; for example [accessed July 16, 2002]. If there are specific authors given, use their name and list the responsible organization as publisher. Because of the ephemeral nature of websites, please provide the specific date. Citations within the text should read: (Author, Year).

SUBMISSION: Effective July 2007, all manuscripts are to be submitted via AllenTrack, a web-based system for online submission. The web address is http://jcks.allentrack2.net. Instructions are provided at that address. At your first visit, you will be prompted to establish a login and password, after which you will enter information about your manuscript (e.g., authors and addresses, manuscript title, abstract, etc.). You will then enter your manuscript, tables, and figure files separately or all together as part of the manuscript. Manuscript files can be uploaded as DOC, WPD, RTF, TXT, or LaTeX. A DOC template with additional manuscript specifications may be downloaded. (Note: LaTeX files should not use any unusual style files; a LaTeX template and BiBTeX file for the *Journal* may be downloaded or obtained from the Editor-in-Chief.) Table files can be uploaded as DOC, WPD, RTF, TXT, or LaTeX files, and figure files can be uploaded as TIFF, EPS, AI, or CDR files. Alternatively, authors may submit manuscripts as PDF or HTML files, but if the manuscript is accepted for publication, the manuscript will need to be submitted as one of the accepted file types listed above. Manuscripts must be typed, double spaced, and single-sided. Manuscripts should be no longer than 10,000 words plus tables and figures, but exceptions are permitted on a case-by-case basis. Authors of accepted papers exceeding this limit may have to pay a current page charge for the extra pages unless decided otherwise by the Editor-in-Chief. Extensive supporting data will be placed on the *Journal*'s website with a paper copy placed in the NSS archives and library. The data that are used within a paper must be made available. Authors may be required to provide supporting data in a fundamental format, such as ASCII for text data or comma-delimited ASCII for tabular data.

DISCUSSIONS: Critical discussions of papers previously published in the *Journal* are welcome. Authors will be given an opportunity to reply. Discussions and replies must be limited to a maximum of 1000 words and discussions will be subject to review before publication. Discussions must be within 6 months after the original article appears.

MEASUREMENTS: All measurements will be in Systeme Internationale (metric) except when quoting historical references. Other units will be allowed where necessary if placed in parentheses and following the SI units.

FIGURES: Figures and lettering must be neat and legible. Figure captions should be on a separate sheet of paper and not within the figure. Figures should be numbered in sequence and referred to in the text by inserting (Fig. x). Most figures will be reduced, hence the lettering should be large. Photographs must be sharp and high contrast. Color will generally only be printed at author's expense.

TABLES: See http://www.caves.org/pub/journal/PDF/Tables.pdf to get guidelines for table layout.

COPYRIGHT AND AUTHOR'S RESPONSIBILITIES: It is the author's responsibility to clear any copyright or acknowledgement matters concerning text, tables, or figures used. Authors should also ensure adequate attention to sensitive or legal issues such as land owner and land manager concerns or policies.

PROCESS: All submitted manuscripts are sent out to at least two experts in the field. Reviewed manuscripts are then returned to the author for consideration of the referees' remarks and revision, where appropriate. Revised manuscripts are returned to the appropriate Associate Editor who then recommends acceptance or rejection. The Editor-in-Chief makes final decisions regarding publication. Upon acceptance, the senior author will be sent one set of PDF proofs for review. Examine the current issue for more information about the format used.

ELECTRONIC FILES: The *Journal* is printed at high resolution. Illustrations must be a minimum of 300 dpi for acceptance.

Journal of Cave and Karst Studies

Volume 70 Number 1 April 2008

CONTENTS